



2014-05-29

# Aerodynamic Improvements for Auto-Carrying Railcars

Robert Arthur Condie  
*Brigham Young University - Provo*

Follow this and additional works at: <https://scholarsarchive.byu.edu/etd>

 Part of the [Mechanical Engineering Commons](#)

---

## BYU ScholarsArchive Citation

Condie, Robert Arthur, "Aerodynamic Improvements for Auto-Carrying Railcars" (2014). *All Theses and Dissertations*. 4077.  
<https://scholarsarchive.byu.edu/etd/4077>

This Thesis is brought to you for free and open access by BYU ScholarsArchive. It has been accepted for inclusion in All Theses and Dissertations by an authorized administrator of BYU ScholarsArchive. For more information, please contact [scholarsarchive@byu.edu](mailto:scholarsarchive@byu.edu), [ellen\\_amatangelo@byu.edu](mailto:ellen_amatangelo@byu.edu).

Aerodynamic Improvements for Auto-Carrying Railcars

Robert A. Condie

A thesis submitted to the faculty of  
Brigham Young University  
in partial fulfillment of the requirements for the degree of  
Master of Science

R. Daniel Maynes, Chair  
Julie Crockett  
Steven E. Gorrell

Department of Mechanical Engineering  
Brigham Young University  
May 2014

Copyright © 2014 Robert A. Condie  
All Rights Reserved

## ABSTRACT

### Aerodynamic Improvements for Auto-Carrying Railcars

Robert A. Condie  
Department of Mechanical Engineering, BYU  
Master of Science

The railroad industry is responsible for the mass transport of a vast numbers of goods throughout the United States. As needs and capabilities of the railroad industry have changed, the interest in reducing the resistance of locomotives and railcars has increased. This has become paramount as fuel prices have increased in recent years. Resistant forces can result from friction in mechanical components and aerodynamic drag of the moving train. As the average traveling speeds of trains have increased, aerodynamics are contributing a larger fraction of the overall resistance. For this reason, the aerodynamic profiles of trains have become a topic of research. Furthermore, current manufacturing practices of railcars provide an opportunity for research in modifications that reduce the aerodynamic drag.

This thesis reports on research that has been done to reduce aerodynamic drag on automobile-carrying railcars. Data was collected by placing G-scale (1/29) models into a wind tunnel with a  $0.74 \text{ m}^2$  test section. These models were tested for Reynolds Numbers ranging from approximately  $2.05 \times 10^5$  to  $2.79 \times 10^5$ .

Modifications were made to the models with the intention of reducing the drag. The profile features of the auto-carrying railcars were reviewed and three regions were chosen to be the focus of this study. The selected regions are the roof, side panels and structural chassis region. Special attention was given to the regulations of the railroad industry to ensure the tested modifications would be candidates for implementation. From the data, it was determined that drag could be reduced by modifying or covering the roof, side panels and chassis structure by nominally 20%, 5% and 15% respectively.

Keywords: aerodynamics, railcars, train, wind tunnel

## ACKNOWLEDGMENTS

I would like to thank and I offer my deepest gratitude to Dr. Daniel Maynes, Dr. Julie Crockett and Dr. Steven Gorrell for their assistance on this project and help throughout my graduate career. I would also like to thank Wayne Kennedy for his suggestions and guidance throughout this study. His help in finding papers and other resources was invaluable. I openly acknowledge the support of my wife, Amanda, and our children, Jordan, Evelyn, Alexander and Benjamin. Their love and motivation helped me be patient and diligent in completing this work.

## TABLE OF CONTENTS

<b>LIST OF TABLES</b> . . . . .	<b>vi</b>
<b>LIST OF FIGURES</b> . . . . .	<b>vii</b>
<b>NOMENCLATURE</b> . . . . .	<b>x</b>
<b>Chapter 1 Introduction</b> . . . . .	<b>1</b>
1.1 Motivation . . . . .	1
1.2 Literature Review . . . . .	3
1.2.1 Aerodynamics . . . . .	3
1.2.2 Davis Equation . . . . .	8
1.3 Contribution . . . . .	12
1.4 Outline . . . . .	13
<b>Chapter 2 Methodology</b> . . . . .	<b>14</b>
2.1 Wind Tunnel . . . . .	14
2.1.1 Experimental Setup . . . . .	17
2.1.2 Experimental Procedure . . . . .	19
2.2 Uncertainty . . . . .	22
2.3 Models . . . . .	26
<b>Chapter 3 Results and Discussion</b> . . . . .	<b>36</b>
3.1 Testing Results . . . . .	36
3.1.1 Results for Roof Modifications . . . . .	37
3.1.2 Results for Side Panel Modifications . . . . .	39
3.1.3 Results for Chassis Modifications . . . . .	42
3.2 Composite Model . . . . .	44
3.2.1 Results for the Composite Model . . . . .	47
<b>Chapter 4 Energy Analysis</b> . . . . .	<b>51</b>
4.1 Modified Davis Equation . . . . .	51
4.1.1 Term-wise Davis Equation Analysis . . . . .	52
4.1.2 Davis Equation Validation . . . . .	54
4.2 Davis Equation Analysis . . . . .	57
4.3 Davis Equation Results . . . . .	63
<b>Chapter 5 Conclusions</b> . . . . .	<b>67</b>
5.1 Conclusions . . . . .	67
5.2 Future Work . . . . .	68
<b>REFERENCES</b> . . . . .	<b>70</b>

<b>Appendix A</b>	<b>Test Setup Design</b>	<b>74</b>
<b>Appendix B</b>	<b>Side Panel Designs</b>	<b>94</b>
<b>Appendix C</b>	<b>Matlab Analysis Code</b>	<b>107</b>

## LIST OF TABLES

1.1	Empirical Values Used in the Classic Davis Equation (Eqn. 1.1) . . . . .	9
1.2	Definition of Variables Used in the Association of American Railroads Version of the Davis Equation (Eqn. 1.3) . . . . .	10
1.3	Definition of Variables Used in the Canadian National Version of the Davis Equation (Eqn. 1.4) . . . . .	11
1.4	Values for $C_s$ in the Davis Equation Presented by Canadian National . . . . .	12
2.1	Systematic Uncertainty for Mesurands Used to Calculated the Drag Coefficient, $C_d$	25
2.2	Systematic Uncertainty Magnitudes for the Drag Coefficient, $C_d$ . . . . .	25
3.1	Averaged Auto-carrying Railcar Roof Results. . . . .	39
3.2	Averaged Auto-carrying Railcar Side Panel Results . . . . .	41
3.3	Averaged Auto-carrying Railcar Chassis Cover Results . . . . .	44
3.4	Averaged Results for the Composite Model of the Auto-carrying Railcar . . . . .	50
4.1	Values for the General Variables Used in the Modified Davis Equation . . . . .	53
4.2	Values for the Specific Variables Used in the AAR and CN Forms of the Davis Equation . . . . .	55
4.3	Locomotive Data for the General Electric C44AC . . . . .	59
4.4	Values for the Locomotive Variables Used in the Modified Davis Equation . . . . .	59
4.5	Values for the Variables Used in the Total Train Resistance Analysis . . . . .	60
4.6	Force and Fuel Results for Auto-carrying Railcar Roof Modifications . . . . .	64
4.7	Force and Fuel Results for Auto-carrying Railcar Side Panels Modifications . . . . .	65
4.8	Force and Fuel Results for Auto-carrying Railcar Chassis Cover Modifications . . . . .	66

## LIST OF FIGURES

1.1	Weekly averages of retail diesel prices in the United States [3]. . . . .	2
2.1	Image of the wind tunnel test section and a G-scale train model mounted on the track. . . . .	17
2.2	Image of the simulated track using aluminum channel and a foam insert. . . . .	18
2.3	Schematic of the single load cell test rig. . . . .	20
2.4	Schematic of the multiple load cell test rig . . . . .	21
2.5	G-scale model of an auto-carrying railcar. . . . .	27
2.6	Roof modifications for the auto-carrying railcars: (a) corrugated, (b) detail of the corrugated roof, (c) smooth roof without leading and trailing lip, (d) detail of the smooth roof without lips, (e) smooth roof with leading and trailing lip and (f) detail of the smooth roof with lips. . . . .	29
2.7	Side panel modifications for auto-carrying railcars: (a) ribbed without holes, (b) smooth without holes, (c) typical industry replica, (d) large holes, grouped patten, (e) slots and (f) large holes, distributed pattern. . . . .	30
2.8	Detailed schematics of the hole patterns used on the model railcars: (a) industry replica, (b) four times larger holes, grouped pattern, (c) slots and (d) four times larger holes, spaced pattern. Dimensions given in millimeters. . . . .	32
2.9	Image of the bottom structure of the auto-carrying railcar: (a) without a covering and the structure exposed, (b) with a cover. . . . .	33
2.10	Chassis covers for the auto-carrying railcars: (a) standard chassis, no cover, (b) chassis covered, (c) full length skirt and (d) partial skirt. . . . .	35
3.1	$C_d$ as a function of $Re$ for a standard model with three different roofs: ● corrugated roof (baseline), ▲ smooth roof with leading and trailing lip and ■ smooth roof without leading and trailing lip. . . . .	38
3.2	$C_d$ as a function of $Re$ for a hollow model with different side panels: ● industry replica panels, ■ smooth panels, ▲ ribbed panel without holes, ◀ panels with $4\times$ larger venting holes in a grouped pattern, ▼ slotted panels and ▶ panels with $4\times$ larger venting holes in a spaced pattern. . . . .	40
3.3	$C_d$ as a function of $Re$ for a standard model with different chassis coverings: ▲ standard uncovered chassis, ■ full length chassis cover, ▼ full length skirts and ● partial length skirts. . . . .	43
3.4	Replica scaled model of the auto-carrying railcar. . . . .	44
3.5	Roof modifications for the auto-carrying railcar replica model: (a) corrugated roof and (b) smooth roof. . . . .	46
3.6	Bottom modifications for the auto-carrying railcar replica model: (a) uncovered baseline bottom and (b) covered bottom. . . . .	47
3.7	Side modifications for the auto-carrying railcar replica model: (a) 9.5% void fraction side panels and (b) modified side panels. . . . .	48



3.8	$C_d$ as a function of $Re$ for a replica model with different composite modifications: ▼ baseline model with a corrugated roof, uncovered chassis and 9.5% void fraction side panels, ■ smooth roof, ◀ side panels with four times larger venting holes in a spaced pattern, ▲ side panels with four times larger venting holes in a spaced pattern and a smooth roof, ● side panels with 4× larger venting holes in a spaced pattern, smooth roof and full length bottom cover with V-fairing and ▶ side panels with four times larger venting holes in a spaced pattern, smooth roof and full length bottom cover without V-fairing. . . . .	49
4.1	Term-wise contribution of the Davis Equation for the baseline model: ● A term, ● B term and ● C term. . . . .	54
4.2	Comparison of the modified Davis Equation to the published analyses. (a) Comparison to the Association of American Railroads version of the Davis Equation and (b) comparison to the Canadian National Railway Company version of the Davis Equation. . . . .	56
4.3	Tractive force curve for the GE C44AC locomotive. . . . .	58
4.4	Tractive force curve for the locomotives and resistive force results of the corrugated and modified roof analyses, also showing vertical lines used when assuming constant velocity in the analysis (B Included). (a) Tractive and resistive force results and (b) tractive and resistive force results detail, zoomed in on the interestion point at the seventh and eighth throttle settings. . . . .	62
A.1	Test setup assembly page 1. . . . .	75
A.2	Test setup assembly page 2. . . . .	76
A.3	Test setup assembly page 3. . . . .	77
A.4	Test setup assembly page 4. . . . .	78
A.5	Base plate assembly for the test setup assembly. . . . .	79
A.6	Right-hand tower for the test setup assembly. . . . .	80
A.7	Left-hand tower for the test setup assembly. . . . .	81
A.8	Shaft used to carry the bearings for the test setup assembly. . . . .	82
A.9	Channel section used as the track for the test setup assembly. . . . .	83
A.10	Top mount for the single load cell configuration of the test setup assembly. . . . .	84
A.11	Track aligner for the test setup assembly. . . . .	85
A.12	Spacer used on the shaft to position the bearing for the test setup assembly. . . . .	86
A.13	Bottom mount weldment of the bottom mount for the test setup assembly. . . . .	87
A.14	Bracket section of the bottom mount for the test setup assembly. . . . .	88
A.15	Wind screen section of the bottom mount for the test setup assembly. . . . .	89
A.16	Single load cell assembly used in the multi load cell test setup. . . . .	90
A.17	Double load cell assembly used in the multi load cell test setup. . . . .	91
A.18	Bottom bracket for the multi load cell test setup. . . . .	92
A.19	Top bracket for the multi load cell test setup. . . . .	93
B.1	Large smooth side panels . . . . .	95
B.2	Small smooth side panels . . . . .	96
B.3	Large replica side panels page 1 . . . . .	97

B.4	Large replica side panels page 2 . . . . .	98
B.5	Small replica side panels page 1 . . . . .	99
B.6	Small replica side panels page 2 . . . . .	100
B.7	Large slotted side panels . . . . .	101
B.8	Small slotted side panels . . . . .	102
B.9	Large spaced side panels with larger holes . . . . .	103
B.10	Small spaced side panels with larger holes . . . . .	104
B.11	Large grouped side panels with larger holes . . . . .	105
B.12	Small grouped side panels with larger holes . . . . .	106

## NOMENCLATURE

$A$	Constant resistance term
$A_c$	Cross-sectional area in $ft^2$
$A_{holes}$	Area of holes in the side panels
$A_{total}$	Total panel area
$B$	Mechanical friction resistance term
$C$	Aerodynamic resistance term
$c$	Confidence level for the Student's $t$ score
$C_{CN}$	Canadian National Railroad Company's Drag Coefficient
$C_{DA}$	American Association of Railroads' area drag coefficient in $ft^2$
$C_d$	Drag Coefficient
$C_s$	Streamlining coefficient
$e$	Element of error term
$F$	Force in <i>pounds</i>
$F_d$	Drag force
$f_{void}$	Void fraction
$h$	Fuel usage
$j$	Number of datasets for a given test case
$K$	Number of elements of error
$L$	Width of the railcar
$M$	Number of a type of vehicle
$N$	Number of axles on a vehicle
$n$	Number of datasets
$P$	Atmospheric air pressure
$P_{total}$	Total air pressure
$P_{static}$	Static air pressure
$R$	Resistive force in <i>pounds</i>
$Re$	Reynolds Number
$R_i$	Ideal gas constant
$R_t$	Resistive force in <i>lbs/ton</i>
$R_{Total}$	Total resistive force in <i>pounds</i>
$S$	Number of measurands needed to calculate a result
$T$	Air temperature in $K$
$t$	Time fraction
$t_{v,c}$	Student's $t$ score
$u$	Uncertainty
$u_r$	Random uncertainty
$u_s$	Systematic uncertainty
$V$	Velocity
$W$	Weight of a vehicle in <i>tons</i>
$w$	Weight per axle
$x$	Measurand used to calculate result $Z$
$Z$	Result calculated from measurand values
$\alpha$	Force Ratio

$\Theta$	Partial differential of $Z$ with respect to $x$
$\mu$	Dynamic viscosity in $lb_f s/ft^2$
$\nu$	Degrees of freedom for the Student's $t$ score
$\rho$	Air density in $slugs/ft^3$
$\sigma$	Standard deviation
$\Phi$	Percent force reduction
$\psi$	Percent fuel reduction

### Subscripts, superscripts, and other indicators

$[ ]_{CN}$	indicates $[ ]$ is specific to the Canadian National Davis Equation
$[ ]_l$	indicates $[ ]$ is specific to locomotives
$[ ]_r$	indicates $[ ]$ is specific to railcars
$[ ]_{single}$	indicates $[ ]$ is specific to a single vehicle
$[ ]_{base}$	indicates $[ ]$ is specific to baseline test case
$[ ]_{modified}$	indicates $[ ]$ is specific to modified test case
$[ ]_{reduced}$	indicates $[ ]$ is specific to value that has been reduced by a given ratio
$\overline{[ ]}$	indicates $[ ]$ is a weighted average or mean of a set of values

## **CHAPTER 1. INTRODUCTION**

This thesis describes research conducted to reduce the aerodynamic drag on auto rack style railcars. Previous work has studied many aspects of vehicle and train aerodynamics. This chapter will review these studies and seeks to develop a connection between them and the work presented here.

### **1.1 Motivation**

Our society requires the transportation of goods. As communities have grown and expanded, moving large quantities of goods to previously remote locations has led to the development of a complex network of trains, trucks and highways. In the United States and many other countries, goods that are imported to the coast need to be moved long distances inland. Natural resources like coal need to be moved from mines to power plants where they can be utilized. Industrial and agricultural products, automobiles, intermodal containers and energy resources are all moved throughout the United States by rail.

Locomotives and railcars have seen great improvements since they were first implemented in the early 19th century. From the first steam engine in 1804 to the current day, trains have changed the way we move goods and resources [1]. Not surprisingly, people have sought to make transporting goods as efficient as possible.

Many things contribute to the speed and cost at which resources and products can be moved from one location to another and some of them are easier to influence than others. Loading and unloading methods have been developed, refined and automated to minimize the time and cost required to handle goods. Locomotive engines have evolved from being powered with a coal fired boiler to diesel generators which power electric motors. This has lead to locomotives that have the capacity to move larger tonnages in fewer trips at faster speeds.

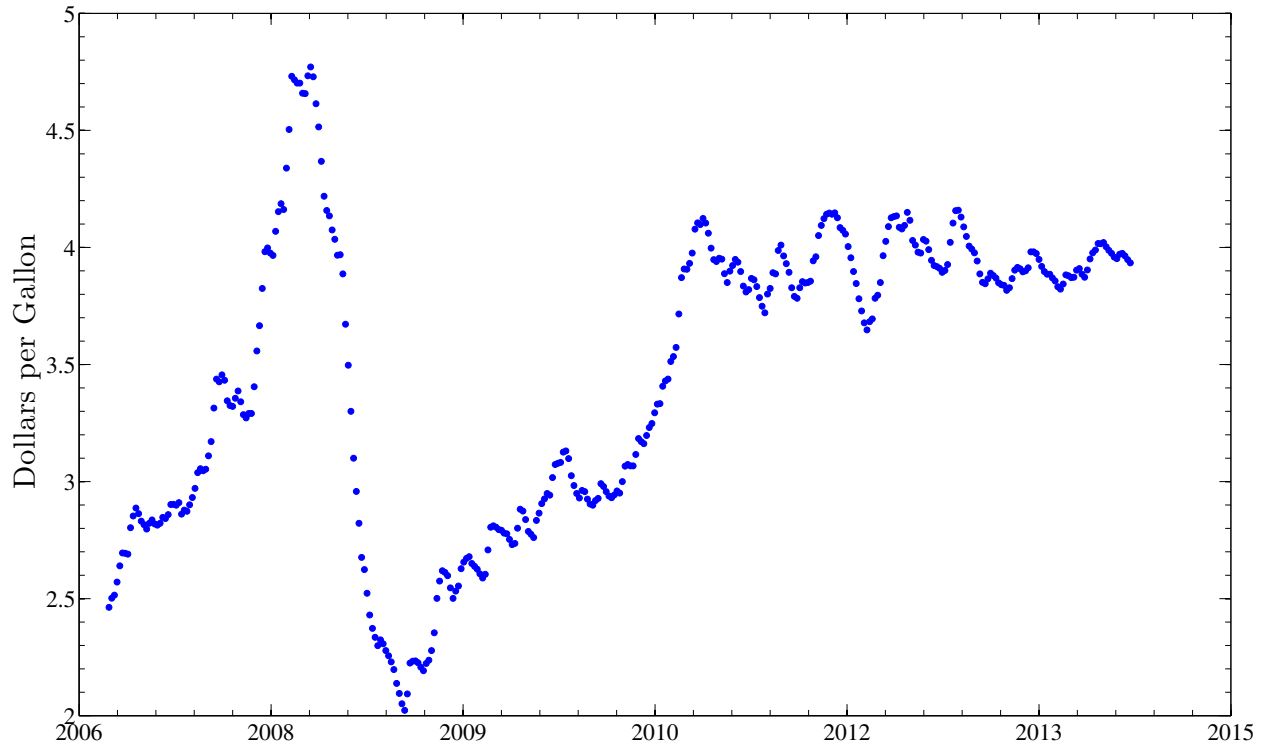


Figure 1.1: Weekly averages of retail diesel prices in the United States [3].

Rising fuel prices have impacted the transportation industry. The trend of retail diesel fuel prices can be seen in Fig. 1.1. As diesel fuel costs have increased, the railroad industry has been impacted with higher operating costs. As a result, great effort is being taken to reduce the resistant forces that act on trains which directly reduces energy required to operate them. Some of this resistance can be attributed to the interaction of mechanical parts. There is friction between wheel and rail which also contributes to the sum of the resistant forces. As the train travels at greater average speeds, the aerodynamic profile of the train begins to contribute significantly to the resistant forces in the form of aerodynamic drag. Aerodynamic drag increases proportional to the velocity squared, and this relationship leads to large drag at high velocity. Studies have reported that the resistance to the tractive effort of the locomotives can be as much as 90% aerodynamic resistance for trains running at high speeds [2].

To reduce the resistive forces, railcar construction methods are being reviewed and modifications are being studied with the goal of ultimately reducing fuel consumption. One area of research is focused on modifications to the aerodynamic profile of the locomotives and railcars.

## 1.2 Literature Review

### 1.2.1 Aerodynamics

Aerodynamics is the study of fluid flow, more especially when the fluid is interacting with a solid body or surface. This fluid/body interaction produces forces that act on the body as the fluid moves over and around the surface of the body. In the case of trains, the most prominent aerodynamic force is drag and needs to be overcome as the train travels through the fluid (air). The effect of aerodynamic drag is to resist the forward motion of the train. It becomes apparent that by reducing the aerodynamic drag, the total resistance on the train will also be reduced. Ultimately, the force and fuel needed to propel the train forward will also be reduced. The amount of aerodynamic drag reduction needed to make a significant contribution to fuel conservation will be explored later.

Aerodynamic drag is comprised of two components, namely pressure and friction drag. The sum of these is the total aerodynamic drag that must be overcome to move a body through a fluid. In the case of vehicles and trains the working fluid is air. Friction drag is induced by the viscous effects in the boundary layer on the surface of the solid body, or more simply said the shear stress on the surface of the body. The pressure drag is caused by the pressure distribution over the surface of the body, and is greatly increased by flow separation from the surface of the body [4,5]. An understanding of these components of drag leads to the conclusion that the drag on a body depends on the profile or geometry of the body as well and the speed at which the fluid is moving past the body.

As a train travels on a track, there are several resistive forces that must be overcome. The tractive force generated by the locomotives has to be greater than or equal to the total resistive force for the train to move. Although drag is not always the most dominant resistive force, as the train increases speed the contribution of each resistive component changes. At high speed, the aerodynamics will become the dominant resistive component in the summation of resistive forces. This is largely due to the aerodynamic term being a function of the velocity squared. At speeds above this critical speed the total resistive force will be dominated by the aerodynamic drag.

The geometry of the train largely influences the drag of the train. The physical size, and more specifically the surface area, influences the friction drag while the profile largely determines

the pressure drag. Ideally the train profile will minimize the aerodynamic drag. Such a profile is said to be streamlined. A streamline shape has a profile that has low resistance to motion in a fluid. An example of a streamlined shape is a teardrop profile. The gradually curved leading surface and the tapered tail reduces or eliminates flow separation on the lee side of the shape and reduces drag.

Prior to the advent of high speed trains, which have had considerable aerodynamic work performed on them, trains have historically fit into the class of aerodynamic shapes called bluff bodies. Bluff bodies are typically characterized by having sharp corners, blocky geometry and generally are the opposite of a streamlined profile. A principal phenomenon of this class of aerodynamic profiles is that sharp edges or steep angles along their profile create regions of separated flow which in turn become sources of vortex shedding [6–8] and the vortices induce pressure drag. Although there is a pressure component felt across the entire surface of the train, flow separation creates regions of low pressure which results in high pressure drag. The main strategy to reduce aerodynamic drag on ground vehicles is to eliminate or reduce the flow dynamics causing the high drag [9]. Pressure drag is typically the largest contributor to the total drag for bluff bodies.

There has been much learned in the areas of aerodynamics and aerospace through testing on airfoils and fuselage shaped bodies, yet direct application of that knowledge is less accurate when applied to ground based vehicles. The three-dimensionality of the flow and proximity to the ground make the flow dynamics of ground vehicles quite different when compared to other vehicles that are typically aerodynamically studied like rockets and aircraft [10]. Although the streamlining principles used on aircraft will be applicable to some extent, the profile of the train has limited options because the functionality of the train must be maintained. The interest in aerodynamics on ground vehicles has lead to many studies being performed on truck-trailer vehicles [11–15], which offer a closer comparison to trains than studies focused on aerospace applications.

The differences between truck/trailer combinations and trains make the quantitative comparison between results difficult. One obvious difference between trucks and trains is the overall length of each. This length greatly influences the flow dynamics surrounding these vehicle geometries. A unit train is a train that has all the same type railcars. An example of this is a coal train. Studies on these types of trains are most often performed because the variables can be controlled. The center most railcars are studied to isolate modifications and determine their influence on the aerodynamics. These center most cars are different from semitrailers in several different ways.



Semitrailers rear surface is directly exposed to the surrounding flow. The center railcars have gaps between the railcars before and aft. These gaps have different dynamics than the open trailing edge of semitrailers. Another difference is the surfaces these vehicles travel on. Truck and trailers travel on a relatively smooth interstate. Trains are restricted to tracks. This difference not only manifests itself in flow dynamics between the undercarriage and ground, but also between the vehicle and its surroundings. Semitrailers travel close to other vehicles which means they are influenced by other vehicles' slipstreams. Trains travel through more tunnels which also presents different flow dynamics. Although this means that the drag is not distributed the same on the two vehicles, the studies for reducing drag on trucks have been reviewed and relevant methods have been applied in an effort to glean knowledge from studies already completed.

The design of railcars is based largely on structural requirements. This frequently leads to aerodynamic penalties because structural members are often left exposed to the air flow. For example, corrugated material is often used on railcars because it is inexpensive and resists bending. In the case of auto rack railcars, the roof is made with corrugated material with the corrugations aligned perpendicular to the direction of travel. Aerodynamically, the corrugated material appears like a rough plate and ultimately the air flow behaves like it is interacting with small, connected bluff bodies in series. The total drag will be the summation over the series of small bluff bodies [4]. By looking at the designs and materials like this, changes and modifications to the current railcar profile can be proposed and the drag on railcars can be reduced.

Studies have investigated many aspects of ground vehicle aerodynamics with the goal of reducing the aerodynamic drag [15–19]. In general, the studies break the vehicles into four basic areas, namely the front, nose or leading surface of the vehicle, the base or trailing surface, the roof and the undercarriage. These areas have received attention individually and in some cases collectively.

Starting with the leading surface of the vehicles, research has been done on both trucks and trains. Regarding truck/trailer combinations, often the studies focus on the gap and height change between the truck and trailer. One modification implements a series of fences on the leading surface of the trailer that conditions the flow and reduces drag. One study states this type of modification can provide a 16.6% drag reduction [15] and another claims a 21.3% drag reduction [16]. Although the nominal drag reduction values vary, the method of studying the leading surfaces of the vehicle

and modifying it to reduce drag has shown to be beneficial. In a study on intermodal transportation of semitrailers transported on flat well-type intermodal railcars, streamlining the shape of trailers by rounding the edges was observed to reduce the drag by as much as 20% [20]. Extrapolation of this research suggests that modifying the leading surface of the railcars and rounding the edges of the railcars will result in a drag reduction. This conclusion is further supported by a study that investigated the trailing section of an Ahmed model. An Ahmed model is a model where the back edge sloped down from the roof at some angle, similar to the way a rear window of a car slopes away from the roof. This study shows that by rounding the edge between the roof and the sloped tail, the flow separation region was reduced which resulted in a drag reduction [21].

Studies that worked on the trailing section of trucks/trailers proposed that by reducing the area of the trailing surface of the trailer may reduce the drag as much as 19% in an experimental study [22] and 15% in a Computational Fluid Dynamics model that employed flaps to reduce the area [23]. Although quantitatively these results do not correspond to train sets, qualitatively reducing the area of the trailing locomotive/railcar should reduce the drag. Reducing the trailing area and streamlining the trailing profile will not only reduce the drag, but also will decrease the slipstream behind the train. The slipstream becomes particularly important when the train is passing other trains or moving through a station. Large slipstream regions can cause damage to hardware or injure individuals standing close to the tracks. For this reason, a small slipstream is favorable and streamlining is one way to achieve it.

Trailing surface results, coupled with those from leading surface studies, are promising for trains. Train specific studies have proposed general streamlining of the leading and trailing locomotive/railcar [24–26]. One way to do this is to reduce the flat region on the leading and trailing locomotive/railcar and giving it a more wedge-like or bullet-like shape. A study that thoroughly reviewed this streamlining method determined that this indeed reduced the drag on a train, especially in the case of shorter trains [27]. An important point is that as the length of the train increases due to the addition of more railcars, the increased aerodynamic drag that is generated by the leading and trailing railcars becomes a smaller percentage of the overall drag. Furthermore, as the length of the train increases, the flow dynamics along the length of the train becomes more important to the aerodynamics and ultimately to the fuel consumption of the train.

Other research has focused on the area underneath the train [24,28,29]. This region exhibits complex flow dynamics due to the structural members, wheel assemblies and the interaction that occurs between the train and the ground. One study suggests that wheel assemblies, known as trucks, might be covered in order to reduce drag [28]. Another study suggests that the addition of bottom covers to the railcars will reduce the air resistance by as much as 50% [24]. This large reduction is surely dependent on the railcar being modified. Results for studies on trucks are more conservative with skirts that prevent the air from entering underneath the trailer yielding a drag reduction of 13% at a 0° yaw angle [30]. Another similar undercarriage study on trucks suggests that by adding full length side skirts, the drag reduction is nominally 9% [12]. Although the results for modifying underneath ground vehicles vary, the prospect of drag reduction by covering or modifying the region underneath the railcars is worth investigating.

Focused studies on differently shaped trains have yielded good results. This success has led to an investigation of how to apply these similar principles to auto rack style railcars. Some of these positive results come from simply changing loading practices. One study reviewed the practices of loading intermodal railcars. By developing an algorithm to place the intermodal containers so the gaps between railcars was minimized, the drag on the train could be reduced [31]. Although the loading practices of auto rack railcars is rather straight forward, research like the study cited does call the the gap between railcars into question and although not studied here, further research may yield positive results. Another study investigated coal carrying railcars, which are similar to gondola type railcars with a geometry similar to a rectangular box with an open top. This open top design leaves these railcars highly susceptible to aerodynamic drag generation, and when full of coal the load creates a very rough surface which also generates drag. Reducing the drag of these cars by covering them has been studied with positive results [18]. One particular study performed on gondola type cars suggested many types of covers, and the drag reduction ranged from a few percent for some covers to as much as 48.7% for a fully covered railcar [32]. As discussed earlier, the auto rack railcars have a corrugated roof with ridges which are a source of pressure drag. The studies cited above suggest covering a rough section with a smooth cover can reduce drag. Another study regarding coal cars involved streamlining the bottom of the car by changing the unloading mechanism to the more aerodynamic shape of bomb-bay doors. This modification gave 10-15% lower drag and emphasizes the importance of the structure underneath railcars [33]. Although the

coal carrying railcar is functionally and geometrically different from the auto rack railcars, the principles regarding the drag reduction of a smooth roof or cover and covering the undercarriage structure should hold for both railcar types. These types of modifications will be explored in this study.

### 1.2.2 Davis Equation

Resistive force opposes the tractive effort of the locomotive and must be overcome for the train to move. The ability to calculate the total resistive force of a train allows engineers and operators to make fuel conserving predictions about loading practices and modifications to the vehicle geometry. This is not a trivial calculation due to parameters involved. To calculate the total resistance of the train the mechanical friction, friction associated with interactions between the wheels and tracks and aerodynamic forces must be considered. The Davis Equation has been used by the railroad industry to approximate the resistance of a train traveling at a given speed [34]. The Davis Equation is a summation of resistive forces. A run-down test is a method used to determine these resistive forces on a full-size train and the Davis Equation is a quadratic approximation of such tests [35]. The most general form of the equation is Eqn. 1.1.

$$R_t = A + B V + C V^2 \quad (1.1)$$

where  $R_t$  is the resistive force,  $V$  is the total velocity and  $A$ ,  $B$  and  $C$  are coefficients that consider different resistive components which will be further discussed. The units of Eqn. 1.1 are dependent on the version of the equation being used and shall be discussed further. The summary presented here of the development of the Davis equation is by no means all inclusive. Other versions and methods are described by Rochard and Schmid [35].

As seen in Eqn. 1.1, the first term on the right hand side of the equation is not a function of velocity. The static resistance phenomena that the  $A$  term traditionally includes are rolling and journal bearing resistances. The  $B$  term involves interactions between the wheels and the tracks. As a train travels, the trucks of the railcars undergo a side to side motions known as hunting. As the flanges on the wheels touch the rails, it causes the axles to move from one side extreme to the other. This motion is a large contributor to the resistance represented by second term in the Davis

Table 1.1: Empirical Values Used in the Classic Davis Equation (Eqn. 1.1)

$R_t$	train resistance in $\frac{\text{lb}}{\text{ton}}$
$A$	$1.3 + \frac{29}{w}$
$B$	0.03 for locomotives or 0.045 for freight railcars in $\frac{\text{lbs hour}}{\text{ton mile}}$
$C$	$\frac{C_s A_c}{wN}$

where:

$w$	axle weight of locomotive/railcar in $\frac{\text{tons}}{\text{axle}}$
$N$	number of axles of vehicle of interest
$A_c$	cross-sectional area of the locomotive/railcar ( $\text{ft}^2$ )
$C_s$	streamlining coefficient
$V$	velocity of the train ( $\frac{\text{miles}}{\text{hour}}$ )

Equation. Considering all factors, the  $B$  term consists of the flange friction and impact, rolling resistance between the wheel and the rail and the flexing action of the rails under the weight of the train. This second term is a linear function of velocity. Finally, the last term is the aerodynamic term. The  $CV^2$  is the representation of the aerodynamic drag on the locomotive/railcar, where  $C$  accounts for the geometry of the train and properties of the air with which the train is interacting. Noting that the aerodynamic term is also a function of  $V^2$ , the total aerodynamic drag experienced by the train will increase rapidly as the train accelerates and becomes the largest fraction of the overall resistive force as the train travels at higher velocities.

The actual values for each of these coefficients have varied over the years due to improvements to locomotives and railcars. These improvements have caused the resistant forces to be reduced. In 1926, W.J. Davis proposed values for these coefficients, assuming that the train traveled on a straight, level track [36]. His empirical values are given in Table 1.1.

As noted in Table 1.1, the constant values that contribute to the  $A$  term account first for a speed-independent rolling resistance of 1.3 lbs/ton and second for the bearing resistance that is a function of axle weight,  $w$ . This version of the Davis Equation assumes the bearing resistance to be  $29/w$  (lbs/ton) [37]. The  $B$  term, which largely considers the interaction between wheels and tracks, is 0.03 for locomotives or 0.045 for freight cars. The  $C$  term is also given to be  $C_s A_c/wN$ , the aerodynamic term [36]. Recasting the Davis equation with the above values specific to freight

Table 1.2: Definition of Variables Used in the Association of American Railroads Version of the Davis Equation (Eqn. 1.3)

$R_t$	rolling resistance of single locomotive/railcar in $\frac{\text{lb}}{\text{ton}}$
$w$	axle weight of locomotive/railcar in $\frac{\text{ton}}{\text{axle}}$
$\rho$	local air density $\left(\frac{\text{slug}}{\text{ft}^3}\right)$
$C_{DA}$	the drag area coefficient measured by the AAR in $(\text{ft}^2)$
$N$	number of axles
$V$	Velocity of train in $\frac{\text{ft}}{\text{s}}$

railcars gives

$$R_t = 1.3 + \frac{29}{w} + 0.045 V + \frac{C_s A_c}{w N} V^2. \quad (1.2)$$

Equation 1.2 has become a foundational form of the Davis Equation. This equation has been manipulated by others to create a more precise method for calculating resistant forces.

Two versions of the Davis Equation have been published by large groups with much foundational work. One was published in 1988 by the Association of American Railroads (AAR) [38] and the other was published in 1990 by the Canadian National Railway Company (CN) [36]. Each of these versions of the Davis Equation have thoroughly developed approaches and experimental backing. These studies are supported by both large scale wind tunnel testing as well as full scale testing using roll down tests and dynamometer railcars. They will be discussed and compared to the data from this study.

The AAR version of the Davis Equation changed the coefficients to match data gathered from scaled model wind tunnel testing and full size train testing. The second component of the  $A$  term that includes the bearing resistance has previously been given as 29 lbs/axle, but more modern roller bearings have resistances of 16-18 lbs/axle and this value has been updated to reflect this improvement [36]. This AAR version neglects the  $B$  term of the Davis equation based on the assumption that for operation on high quality track this second term is generally very small [38]. With this term removed and the other terms redefined to match the data gathered by the AAR, the Davis equation becomes

$$R_t = 1.3 + \frac{18}{w} + \frac{0.5 \rho C_{DA}}{w N} V^2 \quad (1.3)$$

Table 1.3: Definition of Variables Used in the Canadian National Version of the Davis Equation (Eqn. 1.4)

$R_t$	rolling resistance of single locomotive/railcar in $\frac{\text{lbs}}{\text{ton}}$
$N$	Number of axles of vehicle of interest
$W$	Total weight in tons of single locomotive or car
$V$	Velocity of train in $\frac{\text{miles}}{\text{hour}}$
$C_{CN}$	CN streamlining coefficient for locomotive/railcar of interest
$A_{c,CN}$	cross-sectional area of the locomotive or railcar ( $\text{ft}^2$ )

The speed-independent rolling resistance ( $A$  term) of 1.3 lbs/ton was kept the same in the AAR version of the equation from Eqn. 1.2. It should be noted that this value can vary from 1.77 lbs/ton (empty car) to 2.13 lbs/ton (loaded car) without rail lubrication down to 0.7 lbs/ton to 0.8 lbs/ton with lubrication. Intermediate values are also possible, depending on trucks and track design. This updated information was presented in the the current version of the AAR publication Manual for Railway Engineering [36]. The coefficients that the AAR version of the Davis Equation (Eqn. 1.3) uses were determined and presented in the AAR Report R-685 [38]. For the auto rack style railcars the value of  $C_D A$  is given as 39.6. If the density of the local air is available, enough information is known to utilize the AAR version of the Davis Equation to calculate the resistive force for an auto rack railcar. Equation 1.3 will be used to fully implement the results of this study.

The CN version of the Davis Equation was largely developed using dynamometer railcar tests. The coefficients for the foundational Davis Equation (Eqn. 1.2) have been adjusted to reflect the results of these tests. Note that the CN version includes the  $B$  term in the Davis Equation. The information for the CN version of the Davis Equation is presented in the AAR publication Manual for Railway Engineering [36].

$$R_t = 1.5 + \frac{18 N}{W} + 0.045 V + \frac{C_{CN} A_{c,CN}}{10000 W} V^2 \quad (1.4)$$

The determined values for the aerodynamic term and cross sectional area for use with the CN formula (Eqn. 1.4) are presented in Table 1.4. From the data obtained in the CN study, the

Table 1.4: Values for  $C_s$  in the Davis Equation Presented by Canadian National

Type of Equipment	$C_{CN}$	Cross-sectional Area ( $A_{CN}$ ) in ft <sup>2</sup>
Box Car	4.9	140
Coal Gondola (loaded)	4.2	105
Coal Gondola (empty)	12.0	105
Covered Hopper	7.1	125
Tank Car	5.5	95
Standard Flat Car (without trailers)	5.0	25
Standard Flat Car (with trailers)	5.0	125
Leading Freight Locomotive	24.0	160
Multi-level Auto Transporter (open)	12.3	150
Multi-level Auto Transporter (closed)	7.1	170

value in the  $A$  term varied slightly, but maintained good agreement with the values that have been presented above.

It can be easily noted from the values in Table 1.4 that that drag term varies significantly depending on the geometry of the railcar of interest. For this particular study, the Multi-level Auto Transporter (closed) will be compared to data gathered during wind tunnel testing. With this data, the CN version is able to be used to calculate the resistive force. Both the AAR and CN analyses have assumed that the train is traveling on flat ground and straight track. It was also assumed there were no crosswinds, or in other words the yaw angle of the train is zero. The aerodynamic term of the equation must be determined experimentally or through computational fluid dynamic (CFD) software analysis. This study measures the drag coefficients of auto rack style railcars, and modifications made to them using wind tunnel testing. The wind tunnel tests mimic the same conditions stated above, namely zero yaw angle and travel on a flat straight track.

### 1.3 Contribution

The contribution of this research will be to determine the fuel conserved by reducing the aerodynamic drag on auto rack style railcars. To accomplish this, the aerodynamic drag on model railcars will be measured. The aerodynamic contribution will be quantified by determining an average drag coefficient for each railcar modification. These drag coefficients can then be used in a form of the Davis Equation to determine an expected total resistance. The form of the Davis Equation to be used will be discussed in detail later. With information regarding the tractive force



and fuel consumption of the locomotives of interest, the total resistive force from each modification can be used to determine the fuel consumption for the train set and the fuel conservation for a given modification.

#### **1.4 Outline**

The remainder of this thesis will explain the details of the experiments performed and present the results of the testing. The experimental methods used to collect the wind tunnel data will be explained in detail, along with a description of the models used. The modifications implemented on the models will be reviewed, and the results of the wind tunnel testing will be tabulated. Using these results, the Davis Equation will be utilized to calculate the resistive force regarding an auto rack unit train. The modifications and the validation of the Davis Equation used in this analysis will also be discussed. With knowledge of a selected locomotive, the fuel conserved by railcar modifications will be presented. Following this analysis, the results will be summarized and conclusions discussed.

## CHAPTER 2. METHODOLOGY

### 2.1 Wind Tunnel

Wind tunnels have been used to study the aerodynamics of ground vehicles for many years [39–43]. The study of train aerodynamics is no exception. Wind tunnels provide a controlled environment to perform tests. Data in this study was acquired using the large wind tunnel on the BYU campus. The test section of this wind tunnel has a height of 0.61 m, a width of 1.22 m and an overall length of nominally 5.1 m. Due to the size constraints of wind tunnels, scaled models are typically employed and the results extrapolated to full scaled scenarios. The accuracy of these comparisons vary. One study on railcars performed using 1/76, 1/40 and 1/20 scale models claimed that the difference in the drag parameters between scale models and full scale scenario can be as high as 30% [39]. Another study employing 1/10 scale models, compared results to the full scale railcars and determined the difference between the model drag parameters and the full scale to be less than 10% [40]. The disagreement of these studies regarding the amount of difference between full scale and model size testing is evidence that care must taken to compare and validate results before they can be directly applied to full scale operations.

The wind tunnel used in this study operates at nine discrete settings in both a high and low gear. This allows for 18 velocity settings. To limit the difference between full scale values and test data, only the top 7 speeds were used in this study. The air speed generated by the wind tunnel at these settings ranges nominally between 38 m/s and 52 m/s. From the velocity, the nondimensional Reynolds number can be calculated using Eqn. 2.1.

$$Re = \frac{\rho VL}{\mu} \quad (2.1)$$

The viscosity,  $\mu$ , was determined by a second order polynomial curve fit to tabulated values as a function of temperature [44]. The characteristic length,  $L$ , was taken to be the width of the

railcar or model under consideration. These velocities translate to a range of Reynolds numbers of approximately  $2.08 \times 10^5$  to  $2.85 \times 10^5$ . The full scale Reynolds number has a nominal upper threshold of  $5.3 \times 10^6$  for auto-carrying railcars traveling at 75 mph. The closer the model Reynolds numbers match the full scale Reynolds numbers, the better the model testing will be expected to approximate the full scale case. A difference between full scale and model Reynolds numbers like this is not uncommon in aerodynamic testing and although this situation is not the ideal case, it can be overcome. This difference is certainly a concern regarding the applicability of the model values to the full scale case. The difference between speeds and scales does cause different flow dynamics especially at the leading edge [45]. A flow field surrounding the leading and trailing sections of a train do not necessarily behave the same at different scales. This is largely the reason why the locomotives and railcars at the front and back ends of the train will not be studied here. Although the difference in Reynolds numbers should be considered, the basis for the comparison between model testing and full scale application in this study is founded in the fact the the percent change of the the aerodynamic drag due to a given modification is expected to hold regardless of whether is it at a model or full scale. Also, comparison to full scale testing would help validate the wind tunnel analysis. Such a comparison of the wind tunnel data from this study will be achieved using the analyses done by the the Association of American Railroads and Canadian National, which used full scale testing to determine the drag parameters for selected railcars [36].

The measurements used in this study, along with force data, were acquired by a National Instruments data acquisition (Model: SCXI - 1000) system and then manipulated with the software package Labview. Commercial load cells were used during testing to measure the drag force. The auto-carrying railcars were attached to the simulated track using thin wire. Any effects from these wires are assumed to be negligible. The output from the load cells was read into Labview and saved.

The wind tunnel was instrumented with a thermocouple to measure air temperature and a pitot probe connected to a differential pressure transducer. The local atmospheric pressure was obtained from a weather station at the Brigham Young University campus. The temperature and local atmospheric pressure data were used to determine local air density, which was calculated using Eqn. (2.2).

$$\rho = \frac{P}{R_i T} \quad (2.2)$$

where the ideal gas constant,  $R_i$ , used for air was 287.04 J/kg · K. The free stream velocity in the wind tunnel was calculated from

$$V = \sqrt{\frac{2\Delta P}{\rho}} \quad (2.3)$$

where  $\Delta P = P_{total} - P_{static}$ , the pressure difference between the total pressure,  $P_{total}$ , and the static pressure,  $P_{static}$ . This was measured by the pressure transducer connected to the pitot probe. The air density,  $\rho$ , is the result obtained from Eqn. 2.2. Again, models for this study were tested at air velocities ranging from 38 m/s to 53 m/s.

The locomotive and railcar models used are G-scale models; 1:29 scaled replica models of their full-scale counterparts. All testing was done on a unit train. This means that all the railcars were of the same type. Care was taken to align the locomotives and railcars horizontally and vertically so they appeared as they would in normal operating conditions. The force measuring system was calibrated using a weight and pulley system for forces ranging between 0 N to 6.9 N. This calibration covered the range of forces that was measured during the tests. The calibration method will be discussed in detail later.

Two G-scale model locomotives and a single auto-carrying railcar were placed in front of the test railcar and a single auto-carrying railcars followed the test railcar to simulate actual operating conditions. Multiple locomotives at the either or both ends of a train are not uncommon in industry and the placement of similar railcars before and aft of the test railcar creates a simulated train where the measurements for the test railcar will represent the drag of railcars in the center-most region of the train. The railcars in the center region of the train were the focus of the study. To clarify, the auto-carrying railcar model was located directly behind the locomotives was a placeholder to condition the flow. The drag on this railcar was not measured. Following this railcar the instrumented test section of the track was installed. Following the test section, another auto-carrying railcar was placed in alignment with the others to serve as a place-holding trailing railcar. This setup is illustrated in Fig. 2.1. It should be noted that a simulated train bed was built and used in the auto-carrying railcar tests to allow space for the instrumentation and to aid in negating the boundary layer effects developing from the bottom of the wind tunnel.

All configurations were tested at least four times and the results were averaged. The force, temperature and velocity data were sampled at 1000 Hz and averaged over a 30 second interval

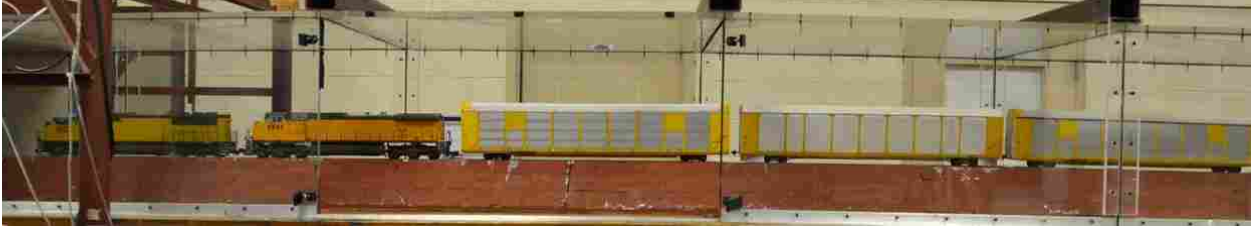


Figure 2.1: Image of the wind tunnel test section and a G-scale train model mounted on the track.

for each wind tunnel speed tested. The atmospheric pressure was assumed to be constant during the course of any single test set. After all the data had been collected, the drag coefficient and Reynolds number were computed as defined in Eqns. 2.4 and 2.1.

$$C_d = \frac{2 F_d}{\rho V^2 A_c} \quad (2.4)$$

$F_d$  is the drag force measured on the auto-carrying railcar model and  $A_c$  is the projected frontal area of the railcar model. Although the drag coefficient varies with velocity, for some regions of Reynolds numbers the drag coefficient can be nearly constant. If such a region exists across the Reynolds Numbers of interest, an average drag coefficient can also be calculated across that range of Reynolds numbers for the model configuration being tested. This provides a single drag coefficient value for each model configuration that can be compared against the results of other model configurations at the same experimental conditions. This can be done when the drag coefficient is independent of  $Re$ . From these averaged results, a percentage difference from the baseline model behavior can be determined.

### 2.1.1 Experimental Setup

The locomotive and railcar models were mounted to the track base as was discussed earlier and is shown in Fig. 2.1. The base allowed instrumentation to be fastened to the bottom of the wind tunnel and provided a mounting surface for the models. Aluminum channel was used to simulate a track. The aluminum channel was fitted with a foam insert to fill extra space. This reduced the distance between the model and the test track surface which better imitated the distance between full scale railcars and the track bed they travel on. This is shown in Fig. 2.2.

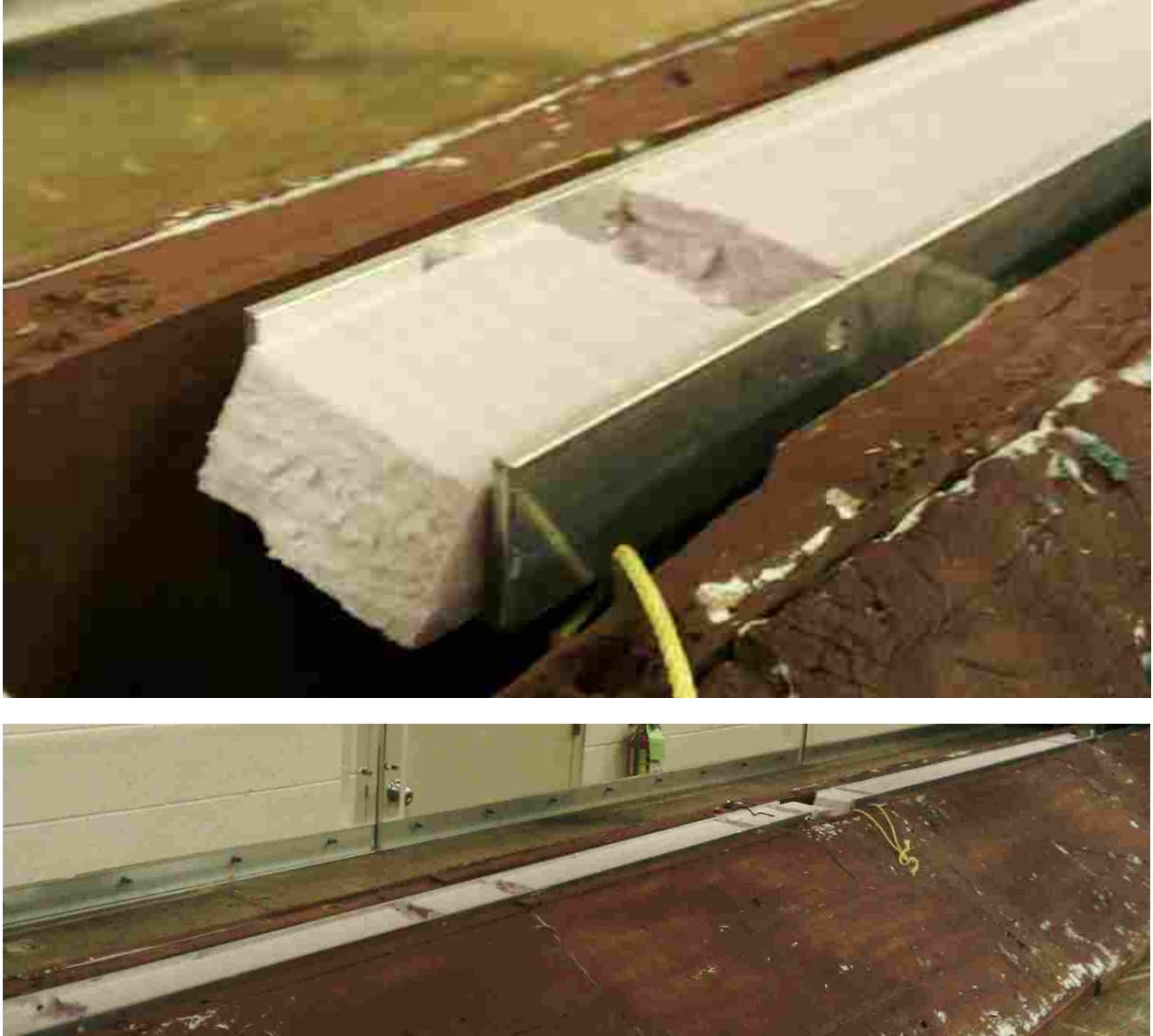


Figure 2.2: Image of the simulated track using aluminum channel and a foam insert.

A first test apparatus was constructed using a single load cell (Interface MBP-5-19) aligned parallel to the direction of travel of the train. Due to limitations of the load cell, the designed test rig needed to support the vertical load of the models. This was accomplished by using vertical supports and ceramic bearings which carried the weight of the simulated track and models while still allowing the track to float freely in the horizontal direction. This design is shown in Fig. 2.3b. Another feature of this test rig was the wind shield that was included on the load cell mount to negate aerodynamic loading that may occur from the air entering the hollow middle section below the simulated track of the track base.

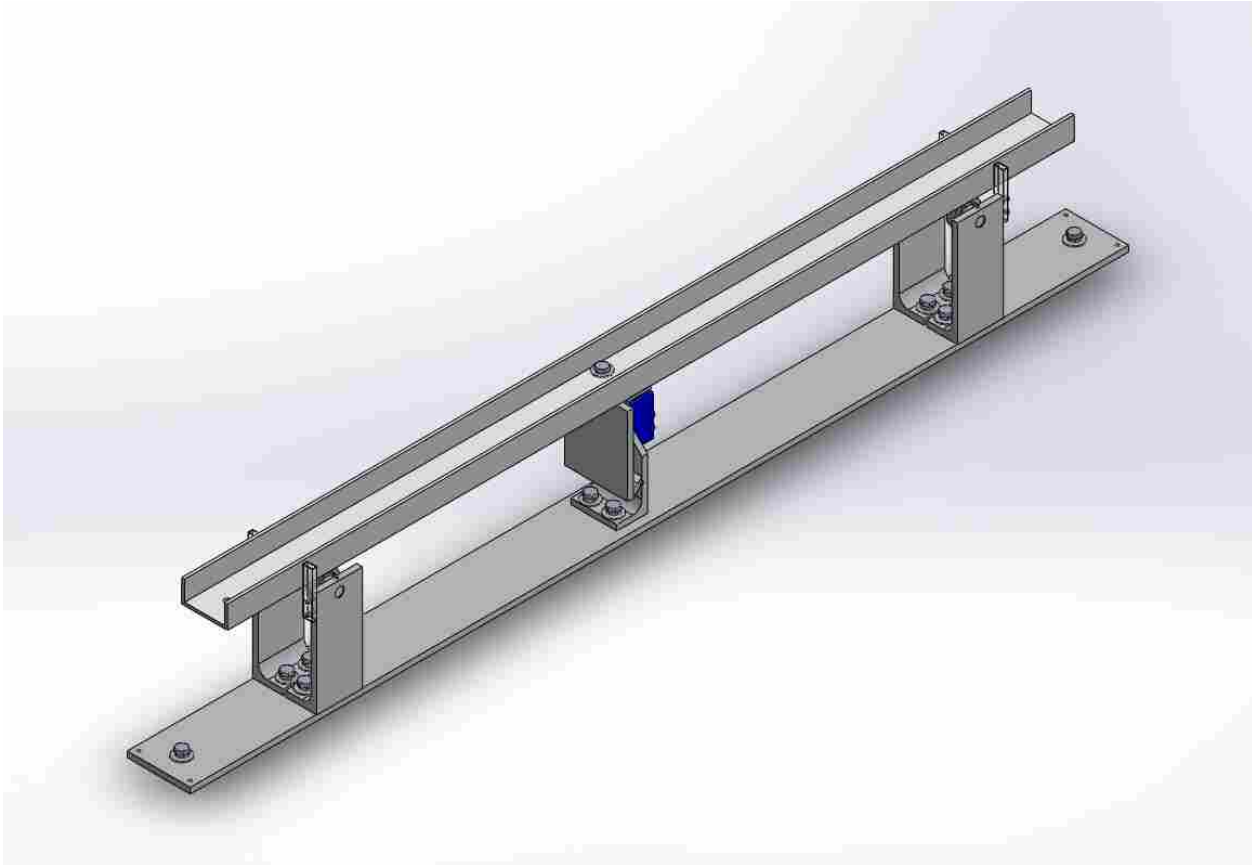
This setup was used and the data collected was considered acceptable as long as the calibration of the load cell remained consistent over the course of the entire test. There were tests when the zero point would not remain constant. This was attributed to the variability of the bearings. To remove any unpredictability, the test rig was calibrated before every test and verified following the test. If the difference between the calibration and the verification exceeded a threshold of nominally 2.5%, the dataset was discarded and the data was reacquired. This process was continued until a more robust test rig design was built and tested. The new test rig is shown in Fig. 2.4.

The new test rig employed different load cells (Transducer Techniques LSP-2) which were able to support the weight of the track and models. This allowed the bearings to be removed from the apparatus. The new test rig was subjected to the same calibration procedure as the first design and fluctuations in the zero point were not observed. The measured drag between the two test rigs was nominally identical, so the second test rig was used to complete acquisition of the data.

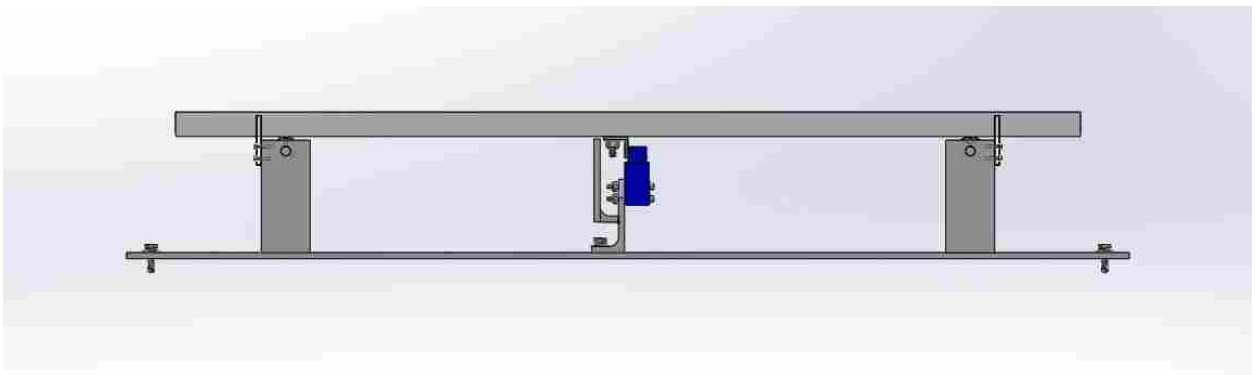
### **2.1.2 Experimental Procedure**

Locomotive and railcar models were attached to the simulated track using small gauge wire. Great care was taken to ensure the models aligned horizontally and vertically, more especially at the gaps of the leading and trailing ends of the test model. A level was used to ensure that the roofs of the models aligned horizontally. The models were checked optically by the experimenter to ensure that they didn't roll to one side or the other. If necessary, shims were added to ensure the models were as close to parallel as possible. The gap between the railcars was maintained at 3.97 cm (1.56 inches).

As discussed previously, the load cells were calibrated often to ensure the data was consistent. The calibration process consisted of subjecting the load cell to a series of known weights and measuring the resulting sensor voltage output. The resulting force-voltage data was fit to a linear curve with an average  $R^2$  value of 0.99. This curve fit provided the constants used to scale output data during testing. Weights ranging from 0 g to 700 g in 100 g increments were used, and this range of weights exceeded the range that was measured during testing, ensuring the voltage output during testing was scaled accurately. Calibration was performed in both an increasing and decreasing manner to explore hysteresis. The calibration results revealed no hysteresis in the loading.



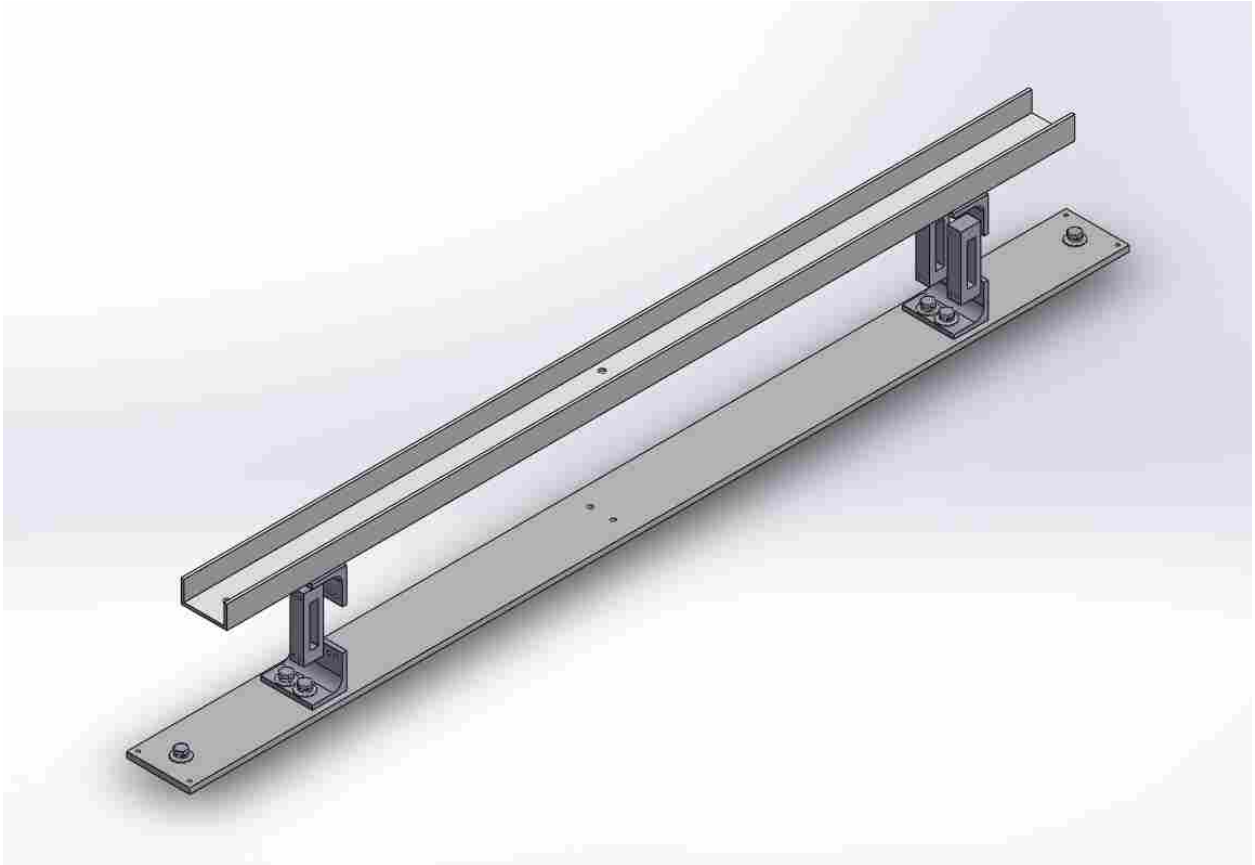
(a)



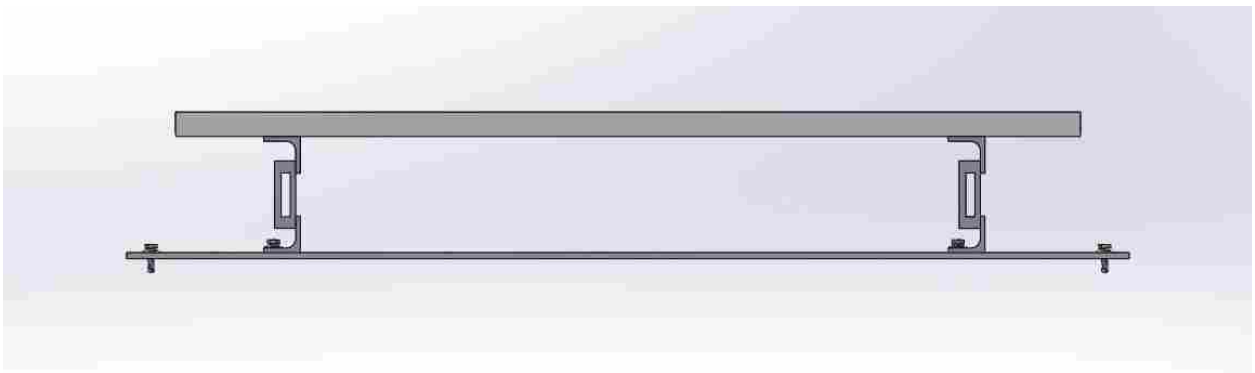
(b)

Figure 2.3: Schematic of the single load cell test rig.





(a)



(b)

Figure 2.4: Schematic of the multiple load cell test rig

After the test section was closed and the air velocity measurement was zeroed a test would begin. All seven wind tunnel speed settings were used in every test run, but the sequence was randomized to ensure the independent variable (i.e. the modification of the model) was unbiased. A random number generator was used to determine a number 1-7, which corresponded to the seven different speeds used in this study. The tests were initially done on each type of modification or configuration independently of others. The goal of this was to determine the influence of single independent variables on the aerodynamics of the railcar models. Testing was also done to measure a collective drag coefficient after optimal configurations were determined. Each modification was tested a minimum of four times. As stated before, all measurements were sampled at 1000 Hz for 30 seconds and the averaged data was saved. This allowed final averaging of a minimum of four independent tests to give final values for baseline and modified cases.

## 2.2 Uncertainty

Experimental uncertainty is a combination of systematic error and random error [46, 47]. The systematic error is introduced by the instruments used to take the measurements and their inability to measure the true value of a parameter. All instruments have some variability when measuring a parameter, which are manifest in the form of elemental errors like non-linearity, hysteresis, non-repeatability [47]. Using statistical methods, these error terms can be combined using the root-sum-squares or RSS method. For elemental errors, the RSS method is presented as Eqn. 2.5.

$$\begin{aligned}
 u_s &= \pm \sqrt{e_1^2 + e_2^2 + \dots + e_K^2} \\
 &= \pm \sqrt{\sum_{k=1}^K e_k^2} \quad \text{for } k = 1, 2, \dots, K
 \end{aligned}
 \tag{2.5}$$

where  $u_s$  is the combined systematic uncertainty associated with the systematic error from an instrument,  $e_k$  are the elements of error and  $K$  is the number of elements.

The random error is introduced into an experiment in the form of data scatter. Random error caused by environment conditions, measurement procedure and techniques, and general repeatability of the experiment [47]. Although random error can be difficult to avoid, the influence it has

can be reduced by averaging over many data points and furthermore by acquiring multiple datasets for a given experimental case. The random error for a single dataset is accounted for by finding the random uncertainty,  $u_r$ , which is the standard deviation of that dataset,  $\sigma_x$  and multiplied by the Student's  $t$  score which is based on the degrees of freedom,  $\nu$  and the desired confidence level,  $c$ . Typically,  $c$  is desired to be 95% which is the case for this study [46]. This method is presented in Eqn. 2.6.

$$u_r = \pm t_{\nu,c} \sigma_x \quad (2.6)$$

where

$$\nu = j - 1 \quad (2.7)$$

and  $j$  is the number of data points acquired in the dataset.

The RSS method can then be used to find a total uncertainty for a measurement,  $u_x$ , by combining the  $u_s$  and  $u_r$  for that measurement. This is shown by Eqn. 2.8.

$$u_x = \pm \sqrt{u_s^2 + u_r^2} \quad (2.8)$$

The goal of this study was to measure the drag coefficient for auto-carrying railcars. The drag coefficient can not be measured directly, as shown previously. The drag coefficient is calculated using Eqn. 2.4, however if Eqn. 2.3 is substituted into Eqn. 2.4 for  $V$ , a simplified equation for  $C_d$  is obtained in terms of measurands that can be measured directly. This resulting equation for  $C_d$  is presented as Eqn. 2.9.

$$C_d = \frac{F_d}{\Delta P A_c} \quad (2.9)$$

When the result of an equation has multiple measurands contributing to its calculation, determining the uncertainty of the result becomes more involved. The systematic uncertainty for each individual instrument needs to be calculated per Eqn. 2.5. The absolute sensitivity coefficient for each measurand must also be determined. The absolute sensitivity coefficient,  $\Theta_x$ , is the partial derivative of the result,  $Z$ , with respect to a given measurand  $x$ , as shown by Eqn. 2.10.

$$\Theta_x = \frac{\partial Z}{\partial x} \quad (2.10)$$

where  $Z$  is the result which in this case is  $C_d$  and  $x$  represents each of the measurands used to calculate  $Z$  which are  $F_d$ ,  $\Delta P$  and  $A_c$  for this  $C_d$ .

The systematic measurand uncertainties can be combined into a single systematic uncertainty for the result using a method similar to the RSS method. This is accomplished using Eqn. 2.11. This equation is a simplified version which assumes no covariance between the measurands [46].

$$u_{s,Z} = \pm \sqrt{\sum_{i=1}^S (\Theta_x u_{s,x})^2} \quad \text{for } i = 1, 2, \dots, S \quad (2.11)$$

where  $S$  is the number of measurands needed to compute the result.

The random error for a result after acquisition of multiple datasets can be calculated by modifying Eqn. 2.6 to calculate the random error for multiple datasets instead of just a single collection of points. This is done by using  $n$  number of datasets and calculating the mean,  $\bar{x}$ , for each. The standard deviation,  $\sigma_{\bar{x}_n}$  of the means is also obtained. The random error for the result is then calculated using Eqn. 2.12.

$$u_{r,Z} = \pm t_{v,c} \frac{\sigma_{\bar{x}_n}}{\sqrt{n}} \quad (2.12)$$

where

$$v = n - 1 \quad (2.13)$$

and the Student's  $t$  is again based on the degrees of freedom  $v$  and the desired confidence level which was taken here to be 95%.

The total uncertainty,  $u_Z$  of the result can now be calculated modifying Eqn. 2.8 to calculate the random error of the result. This is done by substituting  $u_{s,Z}$  in for  $u_s$  and  $u_{r,Z}$  for  $u_r$ . The equation then becomes Eqn. 2.14.

$$u_Z = \pm \sqrt{u_{s,Z}^2 + u_{r,Z}^2} \quad (2.14)$$

Applying this method to Eqn. 2.9 will yield a series of equations that can be used to determine the uncertainty for  $C_d$ . This is accomplished by first calculating the systematic uncertainties for the instruments used to acquire the measurements. These values are presented in Table 2.1. Using these values of  $u_s$  and substituting Eqn. 2.10 for  $\Theta_x$  into Eqn. 2.11 by taking the partial

Table 2.1: Systematic Uncertainty for Mesurands Used to Calculated the Drag Coefficient,  $C_d$

Instrument	Parameter Measured	Systematic Uncertainty, $u_s$
Load Cell	$F_d$	$8.83 \times 10^{-3}$ N
Pressure Transducer	$\Delta P$	6.16 Pa
Calipers	$A_c$	$3.59 \times 10^{-6}$ m

Table 2.2: Systematic Uncertainty Magnitudes for the Drag Coefficient,  $C_d$

$\Theta_x u_{s,x}$	Magnitude
$\Theta_{F_c} u_{s,F_c}$	$\times 10^{-4}$
$\Theta_{\Delta P} u_{s,\Delta P}$	$\times 10^{-3}$
$\Theta_{A_c} u_{s,A_c}$	$\times 10^{-5}$

derivatives of Eqn. 2.9 with respect to each measurand, Eqn. 2.11 becomes Eqn. 2.15 which can be used to calculate the systematic uncertainty,  $u_{s,C_d}$ , of  $C_d$ .

$$u_{s,C_d} = \pm \sqrt{\left(\frac{\partial C_d}{\partial F_c} u_{s,F_c}\right)^2 + \left(\frac{\partial C_d}{\partial \Delta P} u_{s,\Delta P}\right)^2 + \left(\frac{\partial C_d}{\partial A_c} u_{s,A_c}\right)^2} \quad (2.15)$$

For each modification tested, multiple datasets were obtained. Each of these datasets yielded a mean  $C_d$  value from raw data for each of the wind tunnel speeds utilized. These mean  $C_d$  values were then averaged to produce an absolute mean  $C_d$ . The random error is the variation between the mean  $C_d$  values of the datasets based on the absolute mean  $C_d$  value, which is quantified by the random uncertainty,  $u_{r,C_d}$ , for each experimental case. Each railcar modification yielded seven standard deviations of the mean  $C_d$  values,  $\sigma_{C_{dn}}$ , which corresponds to the seven wind tunnel speed settings used during testing.  $\sigma_{C_{dn}}$  was then divided by the square root of the number of tests,  $n$ , completed for that modification which was a minimum of four. The appropriate Student's  $t$ , based on  $\nu$  and  $c = 95\%$ , was then multiplied to find the value of  $u_{r,C_d}$ . This method can be seen as the second term on the right-hand side of Eqn. 2.16.

$$u_{C_d} = \pm \sqrt{u_{s,C_d}^2 + \left(t_{N-1,95\%} \frac{\sigma_{C_{dn}}}{\sqrt{n}}\right)^2} \quad (2.16)$$

An analysis of the terms in Eqn. 2.15 shows the pressure uncertainty to be the largest contributor to  $u_{s,C_d}$ , as shown in Table 2.2. This could have been reduced with a more accurate pressure transducer. However, an investigation of the difference between  $u_{s,C_d}$ , of which pressure uncertainty is only a part, and  $u_{r,C_d}$  showed that the values were not only on the same order of magnitude, but  $u_{r,C_d}$  was typically slightly higher than  $u_{s,C_d}$ . This comparison suggests that random error to be the largest contributor to the uncertainty and if more accurate results were desired, effort should be made to reduce the random error. This can be accomplished by taking more datasets. Ultimately, the uncertainty analysis showed that the uncertainty of many of  $C_d$  values to be nominally  $\pm 2.0\%$ . This was considered acceptable for this study.

### 2.3 Models

The current manufacturing practices of railcars focus largely on the structural demands of the railcar. As a result, there are areas of the design that are completed without considering the railcar aerodynamics. This study on auto rack railcars focuses on three general areas, namely the roof, side panels and the chassis/under body region.

The standard profile of an auto carrying railcar has a corrugated roof, holed side panels and structural chassis region. For this study, all of the features, including those listed here, have been scaled down to 1:29 scale of the full size railcars. An image of a scaled model is shown in Fig. 2.5. The overall body dimensions of this model are nominally 94.6 cm long, 10.3 cm wide and 16.8 cm high. The distance from the bottom of the wheels to the top of the model is nominally 20 cm.

As noted earlier, the roof of auto carrying railcars is currently constructed using corrugated material, primarily for structural reasons. For the models, the grooves of the corrugated material are nominally 0.263 cm at the base, 0.216 cm wide at the top, and 0.082 cm deep. The nominal dimensions of the grooves are 0.274 cm at the root and 0.315 cm at the top. The roughness then is  $\varepsilon/\ell = 8.68 \times 10^{-4}$  where  $\varepsilon$  is the depth of the corrugation and  $\ell$  is the length of a single model railcar. The corrugated material runs the entire length of the full size railcars with the corrugations being aligned transverse or normal to the direction of travel of the train. These corrugations significantly affect the flow by creating regions of separated flow which result in increased pressure drag on the railcar.

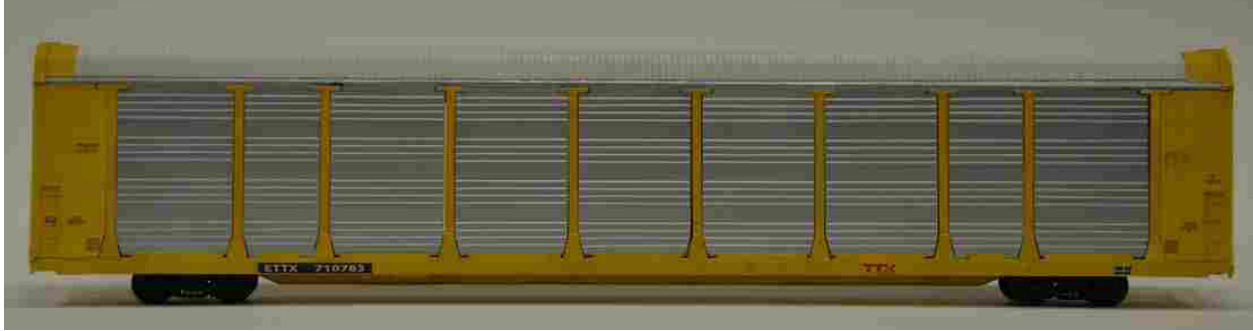


Figure 2.5: G-scale model of an auto-carrying railcar.

The pattern of the holes in the side panels is not defined and varies considerably across the industry. However, the side panel must have a void fraction of at least 5% to meet railroad industry standards. This void fraction was calculated using Eqn. 2.17.

$$f_{void} = \frac{A_{holes}}{A_{total}} \times 100 \quad (2.17)$$

where  $A_{total}$  is the total area of a single side panel without holes and  $A_{holes}$  is the total area of all of the holes in the side panel. This void space allows exhaust gases to escape while loading and unloading vehicles and also allow light to enter the railcars for the crews who load and unload vehicles. Although there is a requirement to maintain a 5% void space, a standard for the size, shape and orientation of the holes does not exist. There does seem to be some consistency throughout the patterns currently used in that most patterns use holes that are nominally 1.6 cm in diameter.

The under body of the auto carrying railcars is typically left completely uncovered. The trucks are mounted before and aft of the middle section. This middle section includes structural members that are aligned transverse to the direction of travel of the train. Other components underneath the auto carrying railcars include but are not limited to air handling hoses and equipment for braking, electrical lines and other mechanical systems. Some of these systems are checked visually by crew members. This limits some of the possible modifications that could be made on the under structure of the railcars.

## Roof

As noted earlier, the current roof structure of auto carrying railcars is made of corrugated material, typically a galvanized metal. The corrugations are aligned transverse to the direction of flow. To reduce the aerodynamic drag, changing or covering the corrugated section with a flat profile was expected to yield an aerodynamic drag reduction.

The baseline rough roof models that were tested in this study had a lip at both ends of the railcar with a height of 0.22 cm and a width of 0.81 cm, as illustrated in Fig. 2.6b. For this reason, the influence of this lip was studied and this lip was replicated on the smooth roof case (Fig. 2.6f). Figure 2.6c shows a case where the lip was removed from the smooth roof model. Testing was done on all three of these cases to measure the influence of both the smooth roof and the leading/trailing lip. The smooth roof profiles were made of painted wood sanded smooth, and attached to the model using magnetic strips. The entire roof section was removable for a more modular construction. This allowed for quick roof changes and a streamlined testing process.

## Side Panels

The side panels for the auto carrying railcars vary considerably throughout the railroad industry. Although there is a requirement to maintain a 5% void space, a standard for the size, shape and orientation of the holes does not exist. There does seem to be some consistency throughout the patterns currently used in that many patterns use holes that are nominally 1.6 cm in diameter.

The existing hole patterns range widely. One pattern may evenly distribute the holes across the surface of the panel when another may group them. For this study, one such panel was chosen to serve as the baseline case and the general pattern is shown in Fig. 2.8a. The scaled holes are 0.055 cm diameter nominally, and correspond to the industry typical 1.6 cm after being scaled down to the scale of the models. The pattern was chosen because it is often observed on current full scale auto carrying railcars. This pattern is shown on the model railcar in Fig. 2.7c. The scaling of the panels did not yield themselves well to a normal machining processes. For this reason, the panels were created using a 1.5 mm thick acrylic that was cut using a laser cutting table. There were two widths of panels, here referred to as large panels and small panels. This width variation can be easily seen in Fig. 2.5. There are seven large panels and two small panels per side of the





(a)



(b)



(c)



(d)



(e)



(f)

Figure 2.6: Roof modifications for the auto-carrying railcars: (a) corrugated, (b) detail of the corrugated roof, (c) smooth roof without leading and trailing lip, (d) detail of the smooth roof without lips, (e) smooth roof with leading and trailing lip and (f) detail of the smooth roof with lips.



(a)



(b)



(c)



(d)



(e)



(f)

Figure 2.7: Side panel modifications for auto-carrying railcars: (a) ribbed without holes, (b) smooth without holes, (c) typical industry replica, (d) large holes, grouped patten, (e) slots and (f) large holes, distributed pattern.

railcar model. These meant fourteen large panels and four small panels were created to form a full set of panel models for each modification tested. The detailed drawings of all manufactured panels are included in Appendix B. The panels were attached to the models using magnets.

From an aerodynamic viewpoint, smooth, flat plates that are aligned parallel to the flow direction are considered to be the optimal case. For this reason, smooth panels were also tested as an aerodynamic optimal. Although in industry smooth panels likely won't be used due to the 5% void fraction regulation, this case establishes the ideal. There were two types of panels considered that were smooth and had no holes. The first of these is shown in Fig. 2.7a. This panel does not have any holes, but does have ridges that are nominally 0.072 cm high and run the length of the panels, parallel to the direction of the train. These ridges are representative of the corrugated material that is often used to build these side panels. These ridges are typically stamped into the material to add structural strength to the panel. This profile was tested in an effort to determine if the ridges were significant to the aerodynamics of the railcars. The second smooth panel tested was simply flat with no structure or texture, (Fig. 2.7b).

The holes are a prominent feature on the side panels. The holes allow the flow to enter and leave the railcars and in so doing increase the drag on the railcar. Therefore the size of the holes are considered a key parameter. For two sets of panels, the holes were increased to four times larger than the typical hole diameter. The scaled diameter of these holes is 0.22 cm. Increasing the hole diameter effectively reduces the number of holes needed to achieve the 5% void fraction. By reducing the number of holes needed, the pattern of the holes can be modified in such a way to localize the holes and create areas of localized smooth surface area which is uninterrupted by void space, i.e. the holes. This localization of smooth space is expected to result in a drag reduction for the railcar.

The holes were configured in two different orientations. One orientation was based on the idea that grouping the holes together will offer the largest drag reduction by increasing the overall amount of smooth space. This configuration is diagrammed in Fig. 2.8b. Auto carrying railcars are typically split into two or three levels. This motivated grouping the pattern as shown on the model railcar in Fig. 2.7d. The holes are aligned into two sections. The two groups of holes are intended to align with the upper and lower levels on the inside of the auto carrying railcars. The single rows aim to assist with gas ventilation.

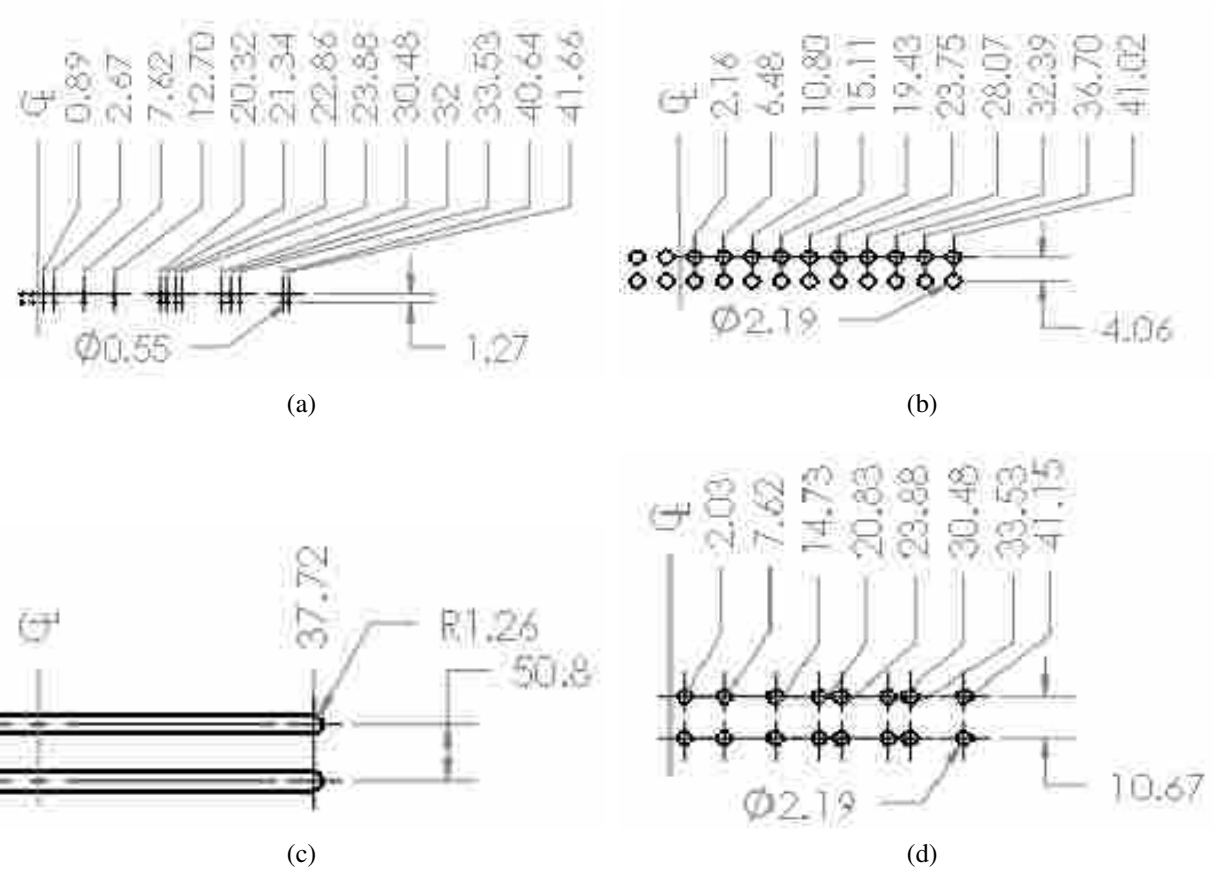


Figure 2.8: Detailed schematics of the hole patterns used on the model railcars: (a) industry replica, (b) four times larger holes, grouped pattern, (c) slots and (d) four times larger holes, spaced pattern. Dimensions given in millimeters.

The other orientation studied, which employed the larger holes, implemented a more distributed pattern. It is similar to the pattern chosen from industry, as diagrammed in Fig. 2.8d. The pattern needed to be adjusted to maintain the 5% void fraction with the larger holes, but effort was made to maintain the horizontal and vertical placement. This orientation can be seen on the model in Fig. 2.7f.

The last panel design tested attempted to maximize the amount of smooth space so the void space was enlarged and localized. This was done by using slots that run longitudinally with the direction of the train. Three slots were used. The geometry of the slot is shown on in Fig. 2.8c. They are spaced to provide light and ventilation for a three level auto carrying railcar. The 5% void fraction was maintained. The configuration is shown on the model in Fig. 2.7e.



(a)



(b)

Figure 2.9: Image of the bottom structure of the auto-carrying railcar: (a) without a covering and the structure exposed, (b) with a cover.

## Chassis

Currently, the structure underneath the auto carrying railcars are left largely exposed to the ambient conditions, as shown in Fig. 2.9. The railcars have a truck assembly at either end with a series of truss-like cross members which run transverse to the direction of flow and span the center of the railcar. The baseline case left all of the structure underneath the railcar exposed. As previously mentioned, there are mechanical systems and air handling equipment underneath the railcars as shown in Fig. 2.9a. For the baseline cases, these were also left uncovered. To reduce the aerodynamic drag, the first modification covered the truss structure, shown in Fig. 2.9b. A fairing was also added at the front and rear of the train before the leading truck and aft of the trailing truck (Fig. 2.10b). This particular cover was designed to cover everything underneath the railcar including the air handling equipment. This design was used to establish the ideal case of all structure being covered underneath the railcar.

The next modifications to the chassis area of the railcars was designed to simply divert the flow around this section of the railcar. To do this, skirts were used to move the air around the lower section of the railcar. The first of these was to attach a skirt that would extend vertically from the

base of the railcar down to just above the top of the tracks. The skirts ran horizontally the full length of the railcar without any large gaps or removed sections and tapered into the center of the railcar at the leading and trailing end. The modeled skirt is shown in Fig. 2.10c. The bottom of the skirts extended to within 0.25 cm of the top of the model track to simulate the height needed to avoid interference with other systems along the tracks. This height effectively reduced the ground clearance of the vehicle. One study suggests that by decreasing the ground clearance, when the undercarriage surface is rough, the aerodynamic drag will be reduced [48].

As was previously mentioned, the undercarriage is often inspected by railroad personnel. There are also optical and thermal sensors that have been implemented to detect wear of components and other issues. For this reason, as shown in Fig. 2.10c, there were holes cut in the full skirt panels to allow visibility to the bearings of the trucks. These holes were cut to a minimum size while assuming that all these sensors would be on straight track. This allows the holes to be a minimum width, with the height being slightly larger to accommodate the vertical travel of the railcar suspension.

The second skirt design is one that left the area around the trucks exposed, (Fig. 2.10d). This partial skirt configuration was introduced because the trucks may be more easily examined by crew members. Aside from the gap exposing the trucks, the partial length skirt was the same height and followed the same profile as the full skirt. When the skirts were attached, the structure underneath the railcar was open and exposed to the atmosphere. The full length bottom covers and the skirts were made of a flexible polystyrene material for the models.



(a)



(b)



(c)



(d)

Figure 2.10: Chassis covers for the auto-carrying railcars: (a) standard chassis, no cover, (b) chassis covered, (c) full length skirt and (d) partial skirt.

## CHAPTER 3. RESULTS AND DISCUSSION

### 3.1 Testing Results

This chapter presents and discusses the results of the wind tunnel testing. Each of the modifications discussed in Chap. 2 have been tested in a wind tunnel to obtain an independent contribution to the overall drag of the railcar. The results will be presented in the following order: roof modification results, side panel modification results and chassis modification results. The results for each region will be analyzed and discussed. Following these results, the model design for composite testing will be discussed and results from composite testing presented.

Due to the construction of the scaled models, not all modifications could be tested on a single scaled model. During roof, side panel and chassis modification testing, two different baseline models were used depending on the region being studied. For roof and chassis modifications, a scaled model had been constructed using a solid core model body. This allowed a solid base to which the roof and chassis modifications could be fastened. The side panel tests were completed using a hollow scaled model. The hollow model allowed more realistic flow dynamics by allowing the air to pass in and out of the railcar through the holes in the side panels. The composite testing was done using a more detailed scaled model than the two already discussed. This composite model is explained in more detail later.

The data obtained from wind tunnel testing for each railcar modification was used to calculate the Reynolds number,  $Re$  and an accompanying drag coefficient,  $C_d$  at each wind speed tested. The equations to calculate these are Eqn. 2.1 and Eqn. 2.4, respectively. These equations have been restated here for ease of reference.  $C_d$  versus  $Re$  values have been plotted for each modification tested. The values of  $Re$  represent the speed and air conditions when a test was performed and the  $C_d$  values represent the geometry and forces measured for the model.

$$Re = \frac{\rho VL}{\mu} \quad (2.1)$$



$$C_d = \frac{2 F_d}{\rho V^2 A_c} \quad (2.4)$$

For each region of testing, a baseline model was evaluated and all modifications were then compared to the baseline line model chosen for each respective region. For each scenario, the percent drag reduction from the baseline was quantified.

### 3.1.1 Results for Roof Modifications

Three roof cases were tested on the railcar models. The first of which was the baseline corrugated case, as shown in Fig. 2.6a. The other two roof cases tested were modifications to the baseline case. The first of which was a smooth roof with a lip on the leading and trailing edges and the second modification was a smooth roof without the lip on either end of the railcar. The models of these cases are presented in Fig. 2.6.

The measured drag coefficients,  $C_d$  for the roof cases are shown in Fig. 3.1 as a function of the Reynolds Number,  $Re$ . The error bars have been included on this figure. They are representative of the uncertainty of the results from wind tunnel testing. In following figures, the error bars will be omitted to avoid excessive markings that make the figures difficult to read, however the uncertainty will be given with tabulated data. The results show significant changes of the aerodynamic drag between the models tested. The largest drag coefficients correspond to the corrugated roof. This was expected as a result of the corrugated material acting like a rough plate on top of the model, which increases drag as discussed earlier. The data also suggests that changing the corrugated roof to a smooth roof greatly reduces the drag on the auto-carrying railcars. Regardless of the leading and trailing lip being included or removed, changing from the corrugated roof to the smooth roof decreased the drag on the railcar models.

The figure also shows that for increasing  $Re$ , the  $C_d$  curves for all roof cases exhibit very little variation with  $Re$ . This characteristic of the  $C_d$  curves suggest that the  $C_d$  can be assumed constant over the range of  $Re$  tested. Under this assumption, an average drag coefficient can be calculated across the range of  $Re$ . This average  $C_d$  can then be used to compare various railcar modifications to the baseline case.

The average  $C_d$  values for the roof cases are presented in Table 3.1. With all other variables controlled, these results reveal that compared to the baseline corrugated roof result, the smooth

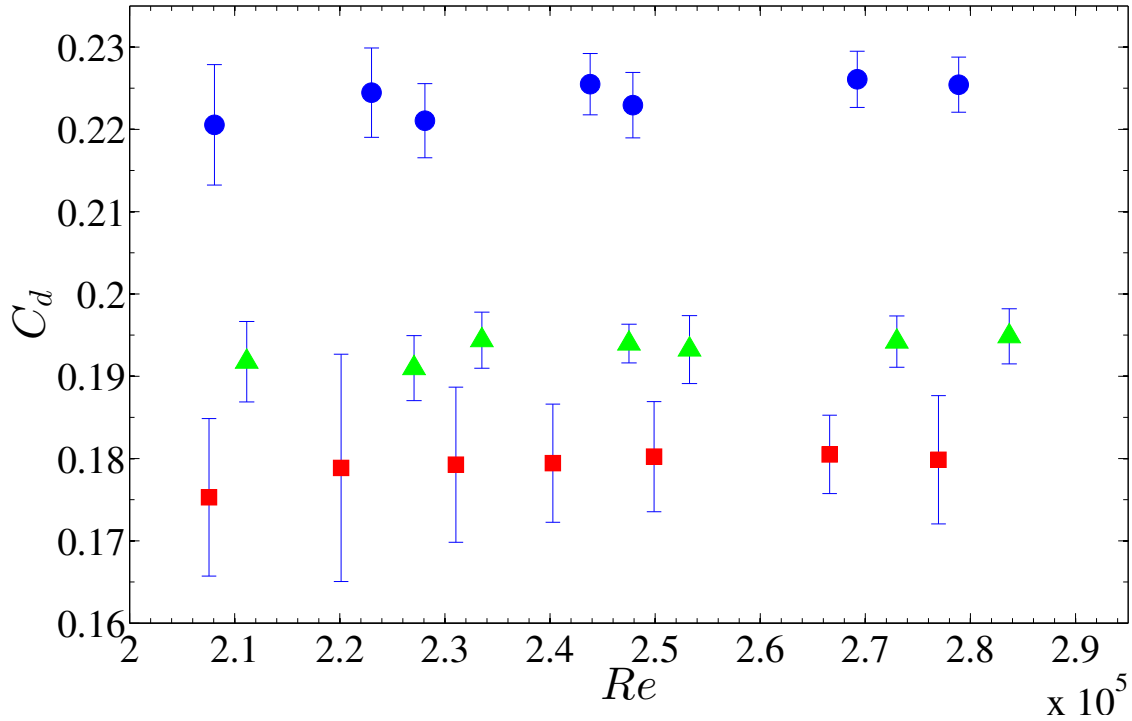


Figure 3.1:  $C_d$  as a function of  $Re$  for a standard model with three different roofs: ● corrugated roof (baseline), ▲ smooth roof with leading and trailing lip and ■ smooth roof without leading and trailing lip.

roof with a lip on both the leading and trailing edges yields a drag reduction of nominally 13.6%. This large drag reduction is solely due to the change from the use of a corrugated materials to a smooth roof material. This change from a corrugated to a smooth roof eliminates flow separation as a result of the corrugated material acting like bluff bodies in series and thereby eliminating the pressure drag associated with the separation.

The smooth roof model without the lip, when compared to the corrugated roof with a lip, yields a drag reduction of nominally 20.0%. The difference here suggests that the lips on the ends of the railcar are adding 6.4% drag to the railcar. This significant increase emphasizes the importance to remove or at least minimize the amount of structural members exposed to the flow around the railcar. These structural members protruding from the surface of the train often have sharp edges which encourage flow separation. When the flow separates from the body, the pressure drag increases which likewise increases the resistance on the train. Ultimately, any uncovered geometry which promotes flow separation is going to add turbulence to the flow and may promote flow separation from the surface of the railcar, which increases the drag on the railcar.

Table 3.1: Averaged Auto-carrying Railcar Roof Results.

Model Type	Drag Coefficient	Percent Reduction
Corrugated Roof (Baseline)	$0.224 \pm 2.0\%$	-
Smooth Roof without Lip	$0.179 \pm 4.7\%$	20.0%
Smooth Roof with Lip	$0.193 \pm 1.9\%$	13.6%

### 3.1.2 Results for Side Panel Modifications

The investigation of the side panels was based around the hole pattern that is often observed in practice. This pattern replicated from the railroad industry served as the baseline model and the model with side panels with this pattern is shown in Fig. 2.7c. In total, six panel models were tested; the baseline industry replica panels and five modifications. Two of these modifications were smooth with no holes. Although these panels did not fulfill the requisite 5% void fraction, aerodynamic theory suggests that the minimal amount of drag will result from a smooth continuous plate. For this reason, these panels were tested to determine a theoretical best case scenario for drag reduction from side panels. The difference between the two smooth panels is that one panel had corrugation-like ridges running parallel to the direction of travel of the train (Fig. 2.7a) and the other was simply smooth (Fig. 2.7b). These ridges represent corrugations that appear on the full scale model and are tested to determine if they influence the drag on the railcar.

The three other side panel modifications are variants of the industry hole patterned panels. Two of these modifications employ holes that are four times larger than those on the baseline pattern. The first of these panels with larger holes attempts to group the holes together horizontally in an effort to increase the amount of surface area that is interrupted by void space. These side panels were shown in Fig. 2.7d. The other side panels with the larger holes follow a layout similar to the industry replica hole pattern. The horizontal placement of the holes emulates the same spacing as the baseline panels. The vertical placement of the holes on these panels are simply spaced evenly to achieve the 5% void fraction as shown in Fig. 2.7f. The last modification is the side panels with slots. The slots were oriented horizontally to create bands of uninterrupted smooth surface area along the sides of the railcar. These panels have been shown in Fig. 2.7e.

The wind tunnel results for the side panel modifications are shown in Fig. 3.2. The data from the baseline side panels yielded a high drag coefficient when compared to most of the other

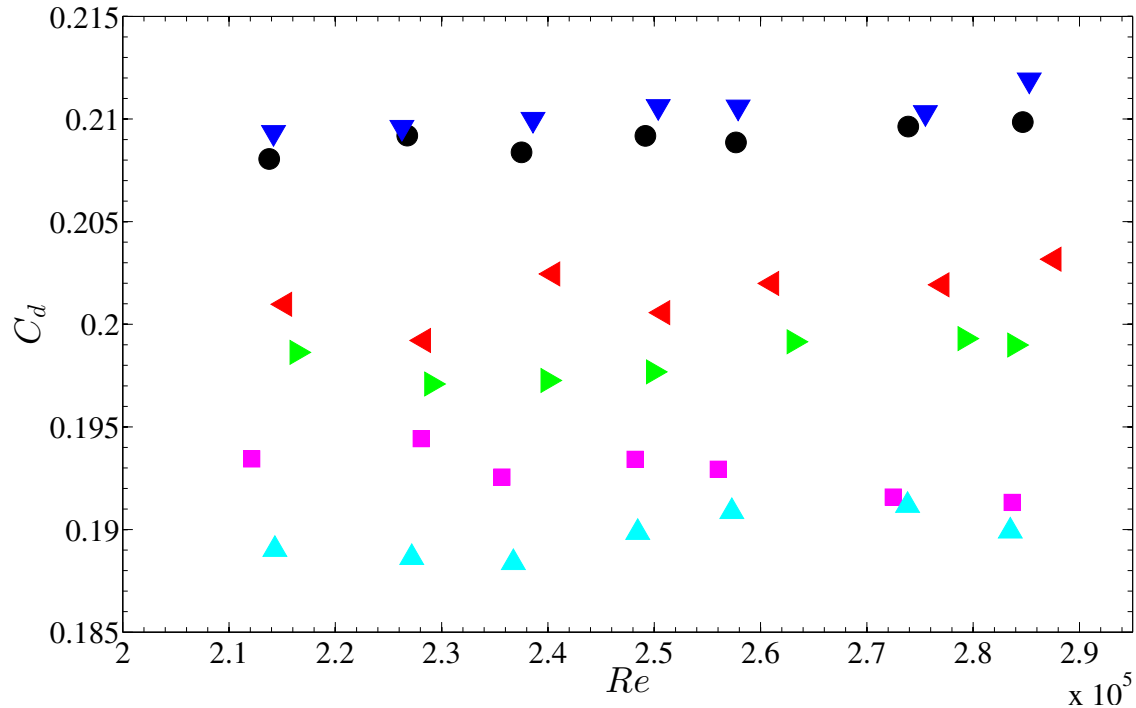


Figure 3.2:  $C_d$  as a function of  $Re$  for a hollow model with different side panels: ● industry replica panels, ■ smooth panels, ▲ ribbed panel without holes, ◄ panels with  $4\times$  larger venting holes in a grouped pattern, ▼ slotted panels and ► panels with  $4\times$  larger venting holes in a spaced pattern.

panels tested. This was expected as a result of the many holes causing numerous locations for flow separation to occur. Also, with the close proximity of the holes, little space is available for the flow to reattach before flow separation is probable to happen again due to another row of holes. Conversely, the smooth panel design, both with and without the ridges, gave the lowest drag coefficients tested. These results were expected due to the dynamics explained earlier, namely the absence of holes which cause flow separation. Although the results indicate that the smooth surface would be the most aerodynamically efficient, they do not meet the necessary 5% void fraction. This means the other modifications must be considered. The panels with slots produced a higher drag coefficient than that of the baseline panels. This result was counterintuitive. A drag reduction was expected from this panel modification. Explanation for this may lie in the orientation of the slots. Further investigation would be needed to validate this theory. The data for the panels with four times larger holes indicate that these panels achieved the largest drag reduction while still maintaining the 5% void fraction.

Table 3.2: Averaged Auto-carrying Railcar Side Panel Results

Model Type	Drag Coefficient	Percent Reduction
Ribbed (No Holes)	$0.190 \pm 2.3\%$	9.2%
Smooth Panels	$0.193 \pm 2.0\%$	7.8%
Industry Replica	$0.209 \pm 2.8\%$	-
4x Larger, Blocked	$0.201 \pm 1.2\%$	3.6%
Slotted	$0.210 \pm 1.4\%$	-0.6%
4x Larger, Spaced	$0.198 \pm 1.2\%$	5.1%

To quantify the drag reduction, the previously discussed method of assuming  $C_d$  to be constant for the range of tested  $Re$  appears valid for the data and was implemented to acquire average  $C_d$  values. These values are presented in Table 3.2. The data shows several important differences that will be discussed. The first of these is to note the drag increase of the slotted panels. Although the increase was within experimental uncertainty, the possibility that slotted panels could actually be causing a drag increase illustrates that simply increasing the amount of undistributed flow by increasing the smooth space on the side panels doesn't necessarily guarantee a drag reduction will result.

The data also suggests that the ridges on the smooth panels have little influence on the drag of the railcar. The comparison between the smooth panels with ridges and the smooth panel without ridges is within the experimental uncertainty, however if the difference of the side panels is real, the ridges show slightly higher drag reduction. The difference may be attributed to the ridges assisting in directing the flow and thereby helping to reduce the drag slightly more than the plain smooth panels. The spacing and number of ridges may influence these results.

The side panels with holes that were four times larger than those on the baseline model are the most promising. The results show a modest drag reduction while still maintaining the 5% void fraction required by the industry standards. The panel that emulated the horizontal spacing of the industry replica pattern exhibited to larger drag reduction at nominally 5.1%. An explanation for the superior result, compared to the other panel that implemented these larger holes, may be explained by the hole spacing. By spacing the holes out, the flow is expected to have a chance to reattach to the surface of the railcar and in so doing minimizing the amount of drag induced by the necessary void space.

### 3.1.3 Results for Chassis Modifications

The chassis modification results are shown in Fig. 2.10. The baseline for testing chassis modifications is the same as used for the roof modification testing. The baseline left the chassis exposed to the atmosphere. By leaving the chassis exposed, the air will be expected to become highly turbulent as it passes through the trucks. As air passes around the structural members underneath the railcar, the flow will stagnate on the front side of the members and separate on the back side, causing regions of increased drag. The modifications involved covering the chassis region underneath the railcar and thus covering the areas where high drag behavior can develop. This was accomplished in two ways. The first of these methods was to add a covering plate to the bottom of the railcar to cover the structure that is typically left exposed to the air flow underneath the railcar. This covering ran the length of the railcar starting behind the leading set of trucks and stopping in front of the trailing set as shown in Fig. 2.9. This chassis cover also implements a V-fairing at either end of the railcar that starts at the coupler and extends outward to the edges of the railcar ending in front of the trucks. The intent of these V-fairings is to deflect the air around the trucks.

The other modifications employ a skirt to block air from entering the region underneath the railcar. The full length skirt runs the full length of the railcar. They start and end the same as the V-fairing used in the previous covering. Starting at the coupler on the leading end of the railcar, the skirt extends on either side of the railcar back to the trailing end of the railcar, terminating at the opposite coupler. Holes have been cut in this skirt over the bearings of the wheels to allow for inspection. The other skirt is identical to the full length skirt except in the region directly around the trucks. This region has been cut out of the skirts to allow for ease of inspection and maintenance to the trucks of the railcar.

Results from wind tunnel testing for the chassis covers are presented in Fig. 3.3. The data show that each of the modifications implemented resulted in a drag reduction compared to leaving the chassis exposed. The figure also suggests that the full length skirt and the partial skirt are nominally the same. Again, the  $C_d$  is assumed to be constant for the range of  $Re$  tested and average drag coefficients are calculated.

The average chassis cover results are presented in Table 3.3. The data shows that the influence of the structure underneath the railcar can be considerable. Simply covering the structure

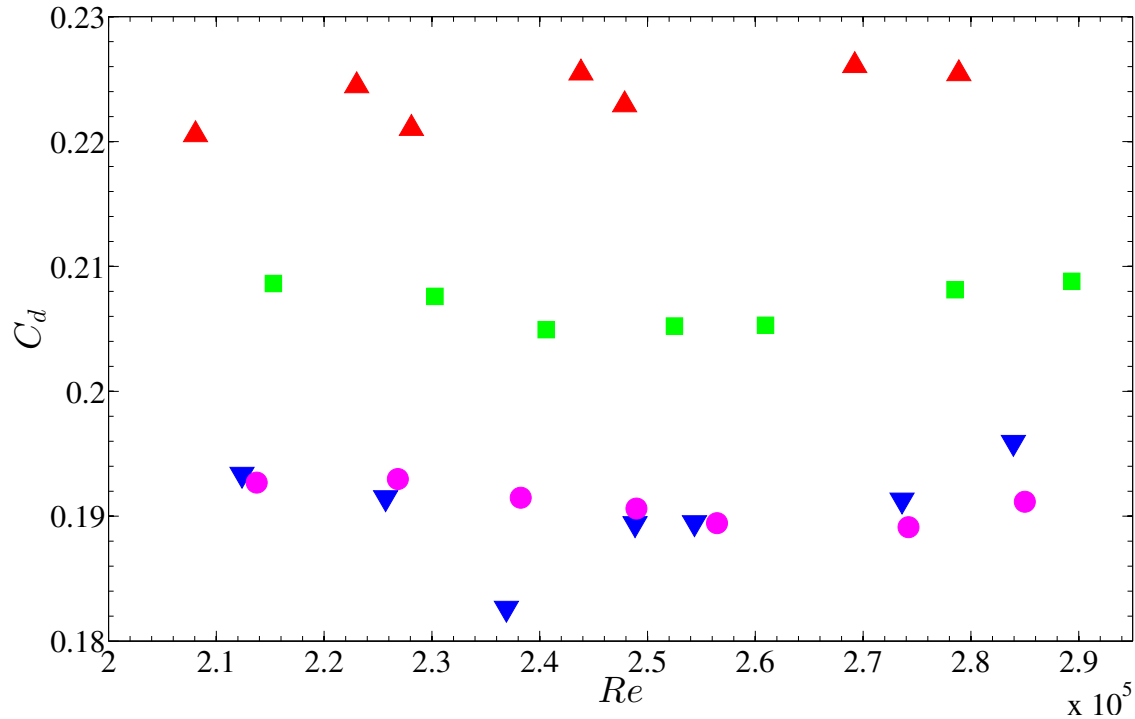


Figure 3.3:  $C_d$  as a function of  $Re$  for a standard model with different chassis coverings:  $\blacktriangle$  standard uncovered chassis,  $\blacksquare$  full length chassis cover,  $\blacktriangledown$  full length skirts and  $\bullet$  partial length skirts.

underneath the railcar and adding a V-fairing reduced the drag by nominally 7.5%. This cover prevented the air from stagnating on the front and separating off the back of the structural members. This is a very favorable result when covering the entire region underneath the railcar is not an option. However, these results are for a case where all of the structure underneath the railcar was covered. If any of mechanical components are left uncovered out of the necessity for inspection and maintenance, this drag reduction would be expected to be less.

For the cases where the skirts are implemented, the drag reduction is considerable. By comparing the  $C_d$  values, the observation regarding the results from full length skirt and the partial skirt being nominally the same appears to be valid. This outcome is helpful in proposing potential design changes because it shows that a less invasive design like the partial skirts may exhibit the same results as designs that are more difficult to implement. Although the result from the skirt testing yield a nominally 15% drag reduction, the execution of such a design is still difficult at the full scale level. Further iterations may be necessary to refine the model into a usable design.

Table 3.3: Averaged Auto-carrying Railcar Chassis Cover Results

Model Type	Drag Coefficient	Percent Reduction
Standard Chassis	$0.224 \pm 2.0\%$	-
Chassis Cover	$0.207 \pm 2.2\%$	7.5%
Full Length Skirt	$0.191 \pm 4.8\%$	14.8%
Partial Skirt	$0.191 \pm 2.1 \%$	14.6%

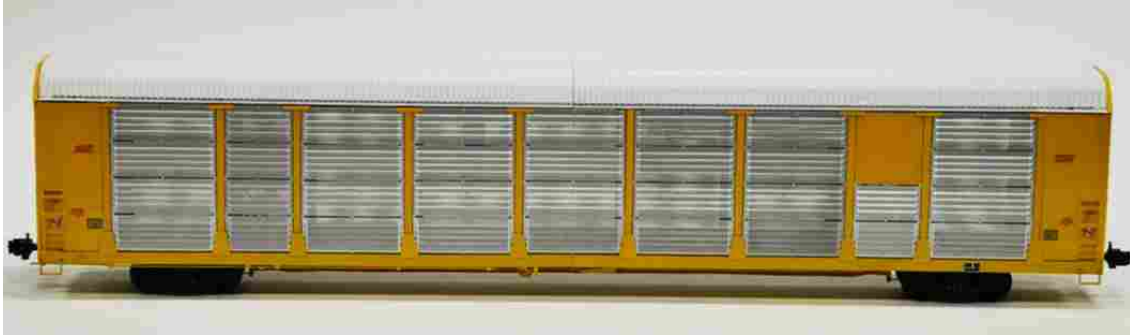


Figure 3.4: Replica scaled model of the auto-carrying railcar.

### 3.2 Composite Model

Following single modification testing, the best modifications were chosen based on aerodynamic drag reduction and the ability to apply them in industry. These modifications were tested collectively to determine an absolute drag reduction. Implementing multiple modifications would be expected to be additive. This means that each modification should increase the drag reduction by the percentage it would have if independently applied.

A new model was used for the collective study which is shown in Fig. 3.4. The new model was an updated version of the scaled models used previously and will be referred to as the replica model. The replica model focused largely on the undercarriage of the model and detailed attention was given to the components underneath the railcar. Connecting lines were included in the replica model as well as components that represent braking assemblies. Also, the corrugations on the roof extended to the either end of the model. The lips on the roof were also omitted. This better replicated the full scale railcars. The undercarriage differences can be seen by comparing Fig. 2.9a and Fig. 3.6a. The roof differences can be observed by reviewing Fig. 2.6 and comparing those images to Fig. 3.5.

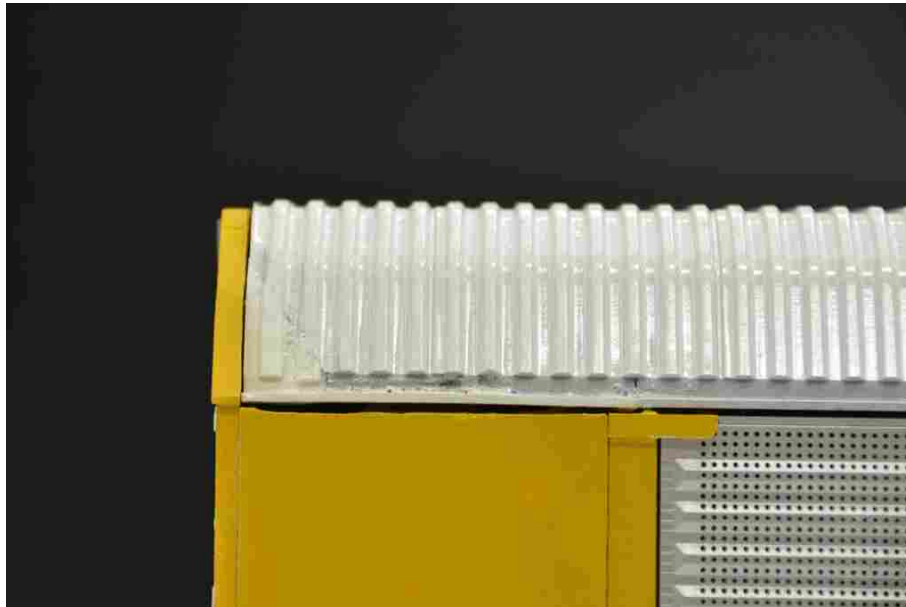


For the roof and the side panels, the modification that showed the largest drag reduction during independent testing were implemented in the composite study. The modification selected for the chassis section used different criteria to determine which modification would be best to implement. The chassis section needs to be accessible to railroad workers. This area is normally checked visually by workers and there are many mechanical systems that require routine maintenance underneath the railcar. For this reason the skirts, which showed the largest drag reduction, were not employed in the composite test. Due to stated requirements, the full length undercarriage covers were favored.

The covers themselves were also modified to make the mechanical and pneumatic systems that are underneath the railcar more accessible. The previous studies on the undercarriage employed a modification that covered the entire section between the trucks as shown in Fig. 2.9b. The cover was changed to leave sections of the undercarriage exposed to allow accessibility to critical systems. These changes are shown in Fig. 3.6b. The chassis was also tested with and without the V-fairing before and aft of the center-most section of the railcar, similar to the one used in previous testing (shown in Fig. 2.10b). This was performed to see what influence this V-fairing had on the overall drag.

The roof had to be modified differently in this study because the smooth wooden roofs used in the previous tests did not fit on the new model. To create a roof with a similarly smooth surface, stiff paper and tape were used to create a smooth surface by covering the corrugated region. Two layers of paper were adhered and covered with tape to ensure a surface thick and rigid enough to simulate a solid surface. This covering is shown in Fig. 3.5b. Great care was taken to ensure that the tape was flat and smooth. All edges of the tape were aligned parallel to the direction of flow of the wind tunnel to ensure that any influence they might have on the drag was negligible.

The side panels implemented were those that had four times larger holes which were in a distributed pattern similar to the industry pattern used previously as the baseline. The replica model came from the model builder with panels that were not representative of anything tested thus far. The new panels, shown in Fig. 3.7a, had holes that were much larger than others that had been tested. The hole diameter of the replica models is 0.71 mm (0.028 inches). This hole diameter yielded a void fraction of 9.5% instead of the desired 5%. Testing this case created another modification that could be compared against the other data collected.

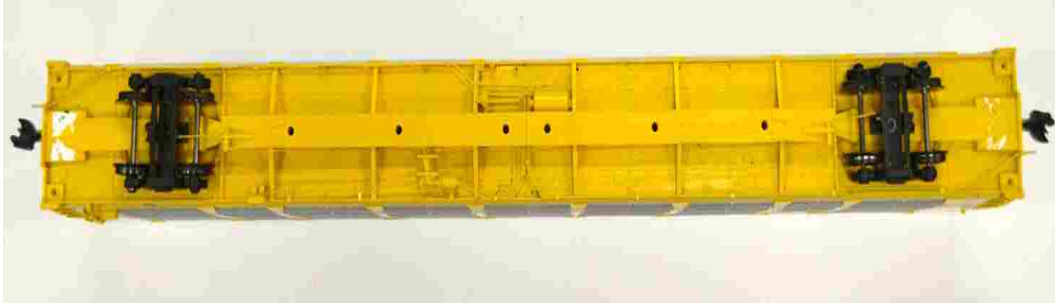


(a)

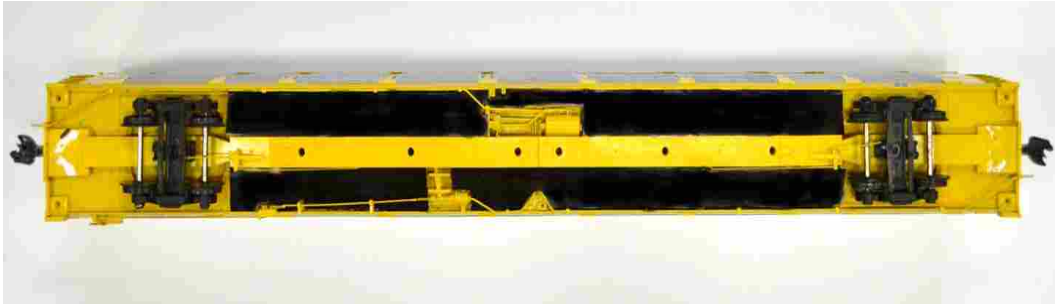


(b)

Figure 3.5: Roof modifications for the auto-carrying railcar replica model: (a) corrugated roof and (b) smooth roof.



(a)



(b)

Figure 3.6: Bottom modifications for the auto-carrying railcar replica model: (a) uncovered baseline bottom and (b) covered bottom.

### 3.2.1 Results for the Composite Model

The results of the composite tests are presented in Fig. 3.8. From these results, much can be determined about the nature of the interaction between the different modifications tested. Testing the different cases on the chassis cover revealed that the V-fairing increases the drag. Removing the V-fairing yielded a lower  $C_d$  than when it was implemented. The difference in drag between the side panel variations was significant. From the data, it can be seen that the increased void fraction of the replica model side panels had a large effect on the drag on the model. This validated the behavior seen earlier with the smooth side panels, namely that minimizing the void fraction also minimizes the drag and conversely increasing the void fraction increases the drag.

The assumption of having constant  $C_d$  over the  $Re$  ranging again holds for the composite modification testing and the averaged data is presented in Table 3.4. The drag reductions for the composite cases are expectantly large. The first thing to note is that these comparisons are made against the replica model with 9.5% void fraction panels. This means the reductions will be higher



(a)



(b)

Figure 3.7: Side modifications for the auto-carrying railcar replica model: (a) 9.5% void fraction side panels and (b) modified side panels.

than if they were compared to the industry replica panels. Although this is not the ideal situation, much can still be learned from these cases.

The results from testing the smooth roof reflected the same drag reduction as presented previously. This suggests that changing the model didn't have any affect on the drag reduction obtained when implementing a smooth roof modification. Comparing the 9.5% void fraction side panels to the modified 5% void fraction side panels yielded a nominally 30% drag reduction. This

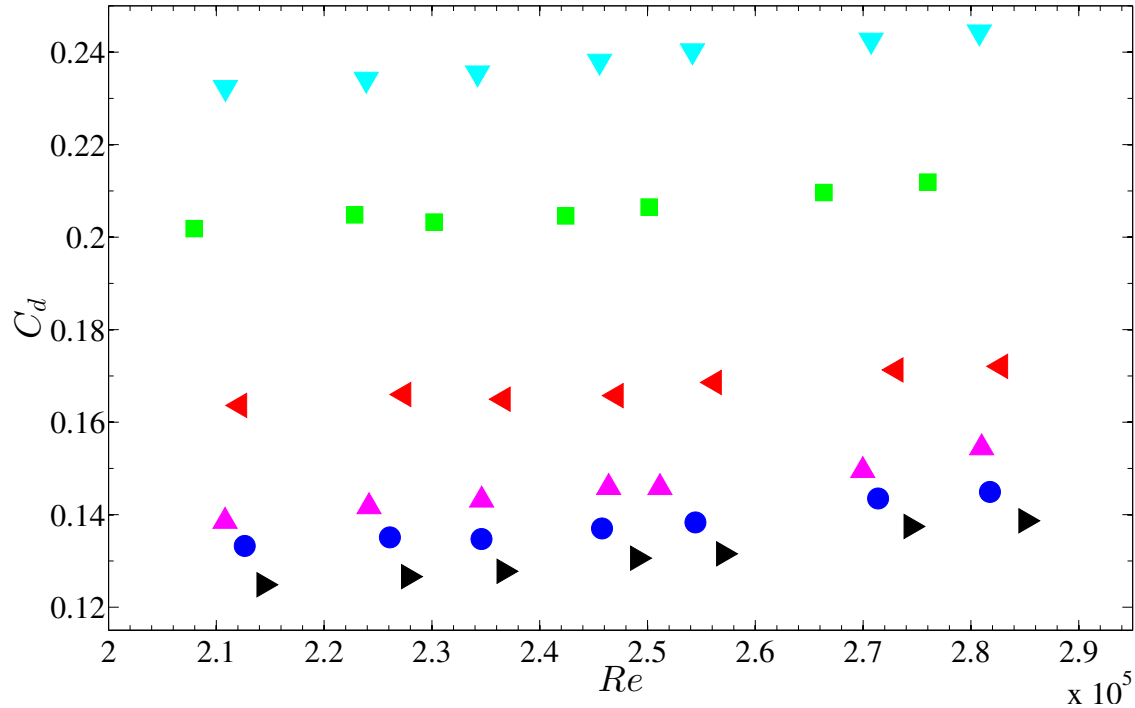


Figure 3.8:  $C_d$  as a function of  $Re$  for a replica model with different composite modifications:  $\blacktriangledown$  baseline model with a corrugated roof, uncovered chassis and 9.5% void fraction side panels,  $\blacksquare$  smooth roof,  $\blacktriangleleft$  side panels with four times larger venting holes in a spaced pattern,  $\blacktriangle$  side panels with four times larger venting holes in a spaced pattern and a smooth roof,  $\bullet$  side panels with  $4\times$  larger venting holes in a spaced pattern, smooth roof and full length bottom cover with V-fairing and  $\blacktriangleright$  side panels with four times larger venting holes in a spaced pattern, smooth roof and full length bottom cover without V-fairing.

large difference is attributed to the increased surface area that is experiencing separated flow due to the increased void space.

As noted from Fig. 3.8 earlier, the V-fairing on the undercarriage of the railcar adversely affected the drag. Compared against the baseline case where no undercarriage covering was implemented, the addition of the bottom covering added nominally 3% drag reduction when implemented with the V-fairing. This reduction increased to 6% when the V-fairing was removed. Explanation for this may lie in the fact that by adding the V-fairing, the effective frontal area has been increased. Also, as the flow reaches the back of the V-fairing, the flow will separate and create a large region of pressure drag. Ultimately, this result illustrates that adding fairings and air diverters is not always the optimal solution when aerodynamics are concerned.

Table 3.4: Averaged Results for the Composite Model of the Auto-carrying Railcar

Model Type	Drag Coefficient	Percent Reduction
Baseline	$0.238 \pm 1.4\%$	-
Smooth Roof	$0.206 \pm 2.5\%$	13.5%
Side Panels	$0.167 \pm 3.9\%$	29.7%
Side Panels and Smooth Roof	$0.146 \pm 2.3\%$	38.9%
Bottom Cover with V-fairing, Side Panels and Smooth Roof	$0.138 \pm 2.2\%$	42.0%
Bottom Cover without V-fairing, Side Panels and Smooth Roof	$0.131 \pm 3.5\%$	45.0%

The results suggest that the combining of modifications does not result in perfectly additive drag reduction percentages as previously thought. When the roof was the only modification implemented on the replica model, a drag reduction of nominally 13.5% was measured. This value agrees with the testing done during single modification implementation on other auto-carrying railcar models. However, when the smooth roof was added to the replica model which was already experiencing a drag reduction due to the implementation of modified side panels, only an additional 9.1% nominal drag reduction was seen due to the smooth roof implementation. Similar behavior was seen when the chassis covers were added. When a chassis cover with V-fairings was the only modification added to a baseline uncovered model a nominal 7.5% drag reduction was measured. When the chassis cover and V-fairings were added to a model which already has the side panels and roof modifications implemented, only an additional 3.1% nominal drag reduction is realized. Although the chassis cover on the replica model doesn't perfectly replicate the cover used in individual modification testing in that it has been cut out to allow access to mechanical and pneumatic components, the results still differ by more than a factor of two. These results suggest that the regions may be negatively interfering with the drag reduction modifications in the other regions. This might account for the reduced drag reduction being realized in each region. Although this topic should be further investigated, no such efforts were attempted during this study.

## CHAPTER 4. ENERGY ANALYSIS

### 4.1 Modified Davis Equation

As previously discussed, the Davis Equation is the accepted way of calculating the total resistance on a train. With the use of Davis Equation, the drag coefficients acquired from wind tunnel testing can be used to determine the total resistance expected on a full train. This is accomplished by summing all the non-negligible resistant force terms. The foundational form of the Davis Equation is Eqn. 1.2. Modifications to Eqn. 1.2 allow the resistive force to be calculated using modern, more accurate values for each respective coefficient. The terms of the Davis Equation, as presented in Eqn. 1.1, are  $A$ ,  $B$  and  $C$ . Each of these terms represent different resistive forces. This nomenclature will be used further in this chapter. The aerodynamic drag is represented by the  $C$  term of the Davis Equation. The focus of this study was to reduce the aerodynamic drag on auto-carrying railcars. No effort was made to validate the coefficient values of the  $A$  and  $B$  terms. They are accepted to be the values given in the literature [36, 37].

The  $A$  and  $B$  terms of Eqn. 1.2 have been altered to reflect the improvements discussed previously in Chap. 1. Equation 2.4 was also substituted into the Davis Equation for the  $C$  term. After these modifications, the Davis Equation becomes Eqn. 4.1a, which is used to calculate the resistive force of a single railcar. Similarly, Eqn. 4.1b is given for the resistance on a single locomotive. The results from these equations will be used to develop an equation to calculate the total resistance for the train.

$$R_{t,r} = \overbrace{1.3 + \frac{18}{w_r}}^A + \overbrace{0.045 V}^B + \overbrace{\frac{0.5 \rho A_{c,r} C_{d,r}}{w_r N_r} \left( \frac{1}{1.4667} \right)^2 V^2}_C \quad (4.1a)$$

$$R_{t,l} = 1.3 + \frac{18}{w_l} + 0.030 V + \frac{0.5 \rho A_{c,l} C_{d,l}}{w_l N_l} \left( \frac{1}{1.4667} \right)^2 V^2 \quad (4.1b)$$

where

$$w_r = \frac{W_r}{N_r} \quad \text{and} \quad w_l = \frac{W_l}{N_l} \quad (4.2)$$

for a single railcar or locomotive, respectively. Note that the velocity,  $V$  used in this form of the Davis Equation is taken in miles/hour. For this reason, a conversion factor appears in the  $C$  term of both equations to convert the between ft/s needed in the  $C$  term and miles/hour which are the given units of  $V$  ( $1/1.4667$ ). In calculating the resistive force for a locomotive, the  $B$  coefficient has been changed from 0.045 to 0.03, as discussed in Chap 1. This change is reflected in Eqn. 4.1b. The drag coefficient ( $C_d$ ) in the  $C$  term was also changed to reflect the forces on a locomotive. These forms of the Davis Equation are the basis for the energy analysis in this study. Equation 4.1a and Eqn. 4.1b give results in force per unit weight (lbs/ton) and only calculate the resistive force for a single railcar or locomotive, respectively. These equations will be use later to find the total resistance on a full train.

#### 4.1.1 Term-wise Davis Equation Analysis

With the terms in the Davis Equation now defined, a term-wise analysis of the resistances represented by the Davis Equation for the auto-carrying railcars can be performed. Each term in the modified Davis Equation was calculated separately, namely  $A$ ,  $B$  and  $C$  with respective dependence on  $V$ . This is done to better understand the influence of the different resistance terms, particularly how the aerodynamics influences the sum of the resistive forces on a railcar. The term-wise analysis is subject to the variation of several variables, therefore a simplified case will be outlined to isolate  $A$ ,  $B$  and  $C$ .

Equation 4.1a was implemented using the values presented in Table 4.1. The drag coefficient,  $C_d$ , used here was taken from the baseline model in the roof study (see Table 3.1). Although the analysis will vary if a different  $C_d$  were used, this analysis will offer a general approach to analyzing the terms of the Davis Equation. To simplify the analysis and observe the isolated influence of the  $A$ ,  $B$  and  $C$  terms, a constant density was assumed for this term-wise study. The velocity range was from 0 - 82 miles/hour.

As noted earlier, the  $A$  term is constant with respect to  $V$ . The  $B$  term increases linearly as a function of  $V$  while the  $C$  term increases as a function of  $V^2$ . The  $A$ ,  $B$  and  $C$  terms were each



Table 4.1: Values for the General Variables Used in the Modified Davis Equation

Variable	Value	Units
Number of Railcar Axles, $N_r$	4	axles
Weight of a Railcar, $W_r$	73	tons
Air Density, $\rho$	0.00238	$\frac{\text{slugs}}{\text{ft}^3}$
Cross-sectional Area, $A_{c,r}$	157.2	$\text{ft}^2$
Drag Coefficient, $C_{d,r}$	0.224	nondimensional

calculated individually and divided by the total calculated resistance. The results are presented in Fig. 4.1. The plot shows the contribution of each resistant term as it relates to the total resistance as a function of velocity,  $V$ . Note that this analysis includes the  $B$  term.

As the velocity of the train increases, the fraction of the total force that each term contributes changes. When the train begins from rest, all resistance is a result of the  $A$  term. The independence of the  $A$  with respect to  $V$  results in the influence of the  $A$  term on the total resistance decreasing quickly as the train accelerates. When the train reaches approximately 30 miles/hour, the  $A$  term is less than 50% of the total resistance. Trains traveling at speeds lower than 30 miles/hour will benefit greatly from modifications that reduce the  $A$  term. Above 30 miles/hour the combination of  $B$  and  $C$  terms will begin to contribute the majority of the resistance.

It is difficult to specify a speed when one might suggest the  $B$  and  $C$  term becomes significant. As the train continues to accelerate, the influences of  $B$  and  $C$  continue to grow. The growth of both terms is continuous until approximately 47 miles/hour. At this point, dependence upon  $V$  of each of these terms becomes apparent.  $C$ , as a function of  $V^2$ , increases much faster than the linear  $B$  term and as a result the influence of  $B$  peaks at approximately 47 miles/hour and then begins to decrease as the influence of  $C$  continues to grow. Ultimately,  $C$  will be the dominate term in the summation of resistance terms.

This analysis, in showing the contribution of each of these terms, illustrates the velocity ranges where modification may be most beneficial. However, it is important to note that these trend lines are variable. For example, as the drag coefficient changes dependent on modifications made to the profile of the train, the trend lines will shift. Even with this variability, this analysis fundamentally shows that modifications to the railcar, whether mechanical or aerodynamic in

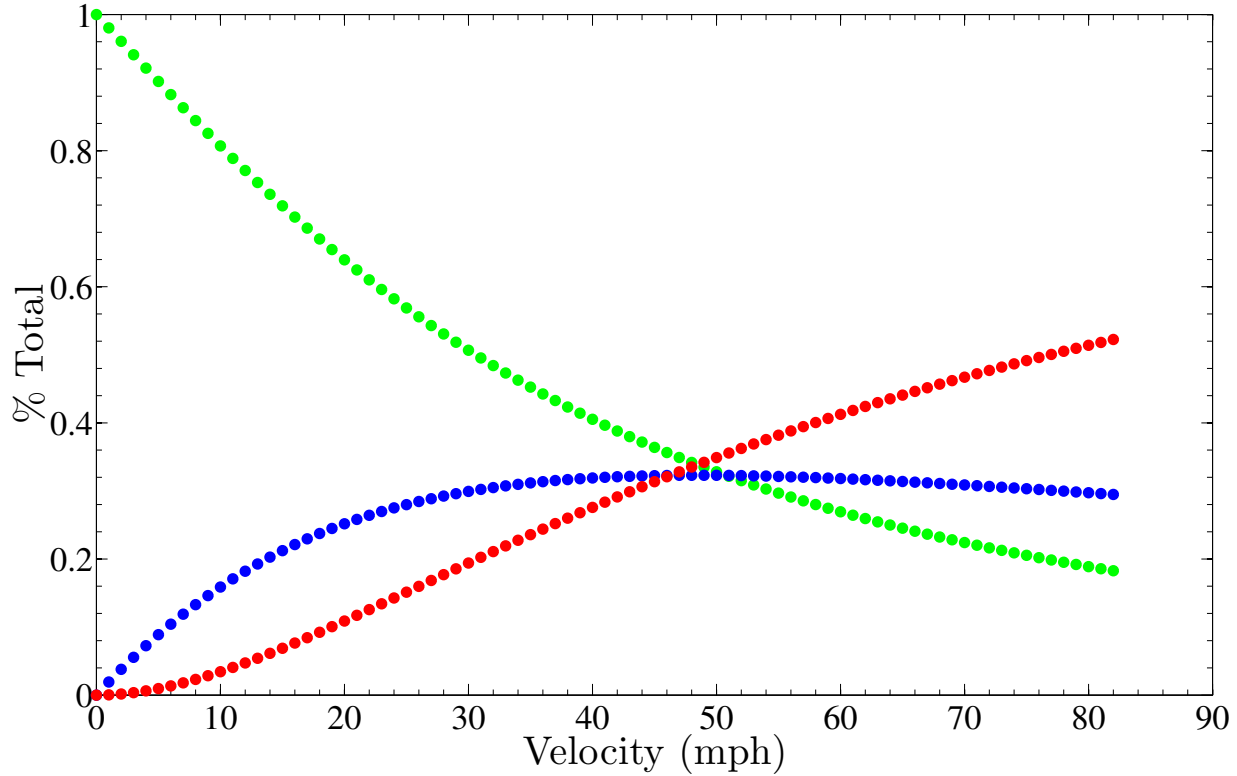


Figure 4.1: Term-wise contribution of the Davis Equation for the baseline model: ● A term, ● B term and ● C term.

nature, will affect the total resistance on the train based on which term in the Davis Equation the modification affects and the speed at which the train is traveling.

#### 4.1.2 Davis Equation Validation

The Association of American Railroads (AAR) and the Canadian National Railroad Company (CN) models of the Davis Equation can be used to validate the modified form of the Davis Equation (Eqn. 4.1a). To reiterate the details that were presented in Chap. 1, the AAR form of the Davis Equation (Eq. 1.3) neglects the  $B$  term and the CN form (Eq. 1.4) retains the  $B$  term in the Davis Equation. These equations have been restated here for the convenience of the reader. In both the CN and AAR forms of the Davis Equation the  $A$  term is split into two parts. The values used in the speed-independent  $A$  term vary slightly between these two models. In the CN form of the Davis Equation the first part of the  $A$  term is 1.5 lbs/ton and the AAR gives it to be 1.3 lbs/ton [36]. Although this difference is a constant and offers only a slight variation it is necessary to consider

Table 4.2: Values for the Specific Variables Used in the AAR and CN Forms of the Davis Equation

Variable	Value	Units
CN Cross-sectional Area, $A_{CN}$	170	ft <sup>2</sup>
CN Drag Term, $C_{CN}$	7.1	nondimensional
AAR Area Drag Coefficient, $C_{DA}$	39.6	nondimensional

the variation when calculating the percent difference between the modified equation and the other forms of the Davis Equation. For this reason, in this comparative analysis this first term has been adjusted in the modified Davis Equation to reflect the value used in the model it is being compared against. The second part of the  $A$  term remains constant for all forms of the Davis Equation. The largest difference between the models compared here occurs in the aerodynamic,  $C$  term.

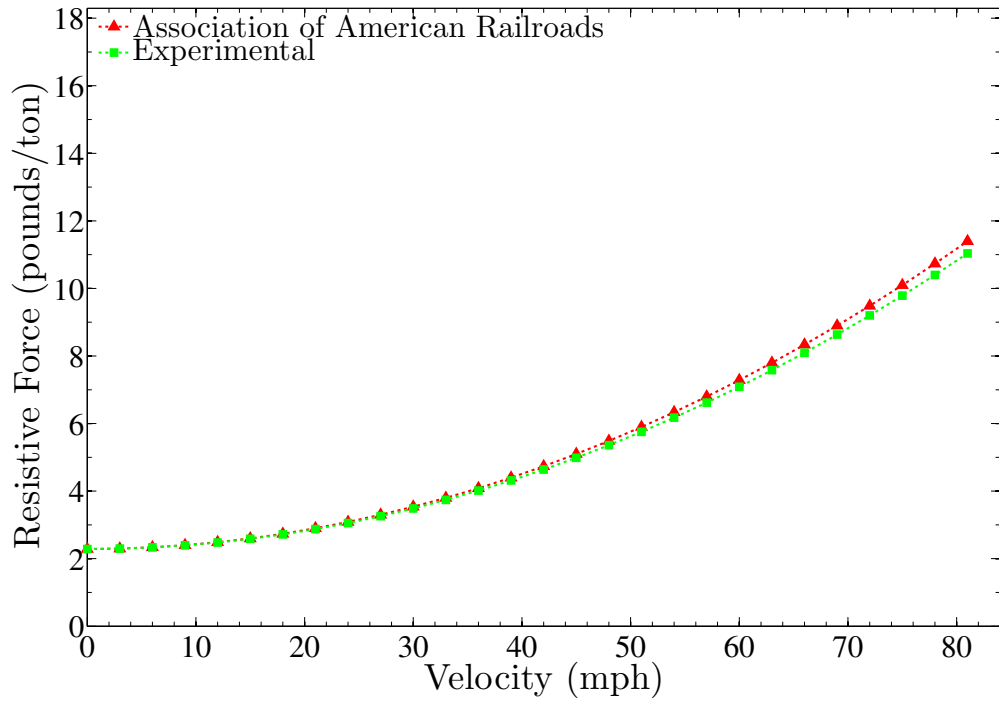
$$R_t = 1.3 + \frac{18}{w} + \frac{0.5 \rho C_{DA}}{w N} V^2 \quad (1.3)$$

$$R_t = 1.5 + \frac{18 N}{W} + 0.045 V + \frac{C_{CN} A_{c,CN}}{10000 W} V^2 \quad (1.4)$$

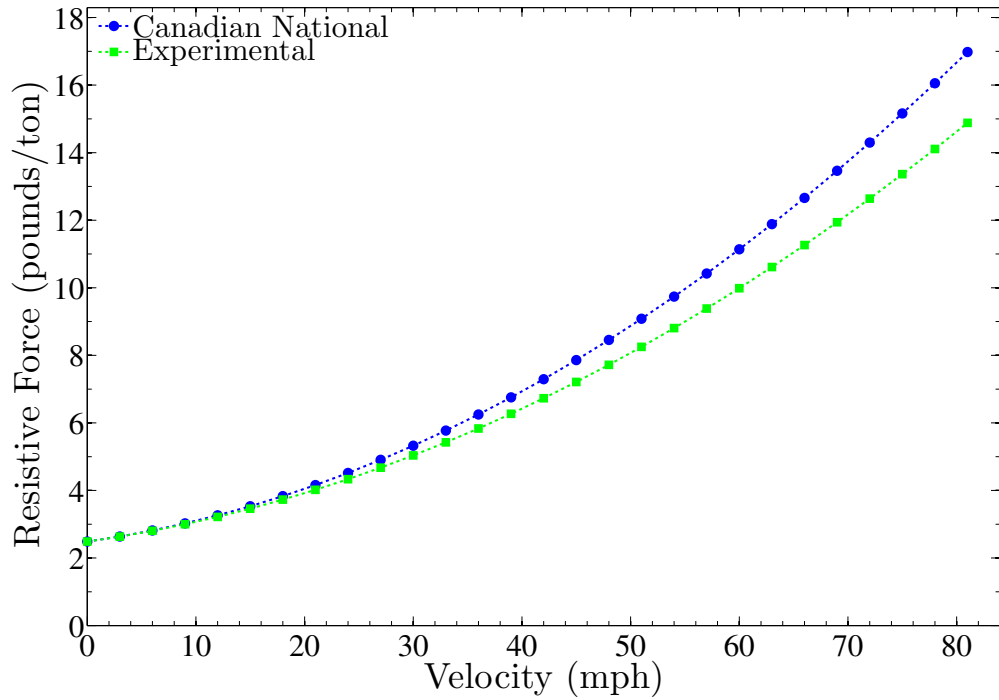
The general variable values used in Eq. 1.3 and Eq. 1.4 are those presented in Table 4.1. The values that are specific to each respective equation, namely those variables that appear in the aerodynamic  $C$  term, are given in Table 4.2. It should be noted that the cross-sectional area used in the modified form of the Davis Equation varies slightly from the CN model. Though the areas could have been set to the same value across all forms of the Davis Equation, the difference was maintained in this analysis so the drag terms were representative of the analyses actually presented in the literature [36].

The comparison between the modified, CN and AAR models of the Davis Equation are presented in Fig. 4.2. To reiterate, to compare these equations the modified form has been adjusted to emulate the assumptions and values that the CN and AAR models of the Davis Equation suggest, namely the neglect of the  $B$  term and the values in the first part of the  $A$  term.

Figure 4.2a shows the case when the modified form follows the same assumptions as the AAR model. The modified Davis Equation matches the AAR form quite well. Upon investigation, the two methods vary by nominally 1.8% over the velocity range 0 - 82 miles/hour. At the maximum value of 82 miles/hour the variation is 3.2%.



(a)



(b)

Figure 4.2: Comparison of the modified Davis Equation to the published analyses. (a) Comparison to the Association of American Railroads version of the Davis Equation and (b) comparison to the Canadian National Railway Company version of the Davis Equation.

The comparison between the modified Davis Equation and the CN model is presented in Fig. 4.2b and resulted in a larger difference. The average difference across the entire velocity range is 6.9% while a 12.4% difference was determined at 82 miles/hour. Although this difference is larger than the AAR comparison with the modified form, this difference is still acceptable. The difference in these analyses can be attributed to several factors. The cross-sectional area used in the modified form of the Davis Equation varied from the CN version. Furthermore, the actual railcars measured in these analyses are not perfectly identical. Overall profile is similar, but the drag coefficients in each study unsurprisingly varied. The general curves created by the data of the modified Davis Equation matched the trends of the AAR and CN forms when compared respectively. This suggests that the modified Davis Equation is a good approximation of the resistive force.

From this analysis, the difference between the AAR and CN forms of the Davis equation can also be noted. The major difference between these analyses is whether the  $B$  term is neglected or retained in the equation. From Fig. 4.1 and Fig. 4.2, the  $B$  appears to contribute a significant resistance to the train. However, this study makes no effort to determine whether  $B$  is negligible or otherwise, therefore both approaches will be used and the data presented during the energy analysis. By including the  $B$  term the resulting total resistive force is expected to be a more conservative approximation. Furthermore, the inclusion of the  $B$  term is anticipated to result in the studied  $C$  term having a more modest influence on train resistance and thus a smaller influence on the overall fuel reduction.

## 4.2 Davis Equation Analysis

Tractive force is a function of input torque, wheel diameter, tractive force coefficient and weight of the locomotive [49]. Knowledge about the tractive force of the locomotive is necessary for this method of making predictions about fuel conservation. The locomotive that is used in this study is the General Electric C44AC. The tractive force curve for a single GE C44AC is given in Fig. 4.3. This curve represents the amount of force that the locomotive is expected to output and has been plotted as a function of velocity. N1 - N8 represent the eight discrete notch settings on the throttle at which the locomotive is capable of running. A specific amount of fuel will be burned at each throttle setting. These values are given in Table 4.3.

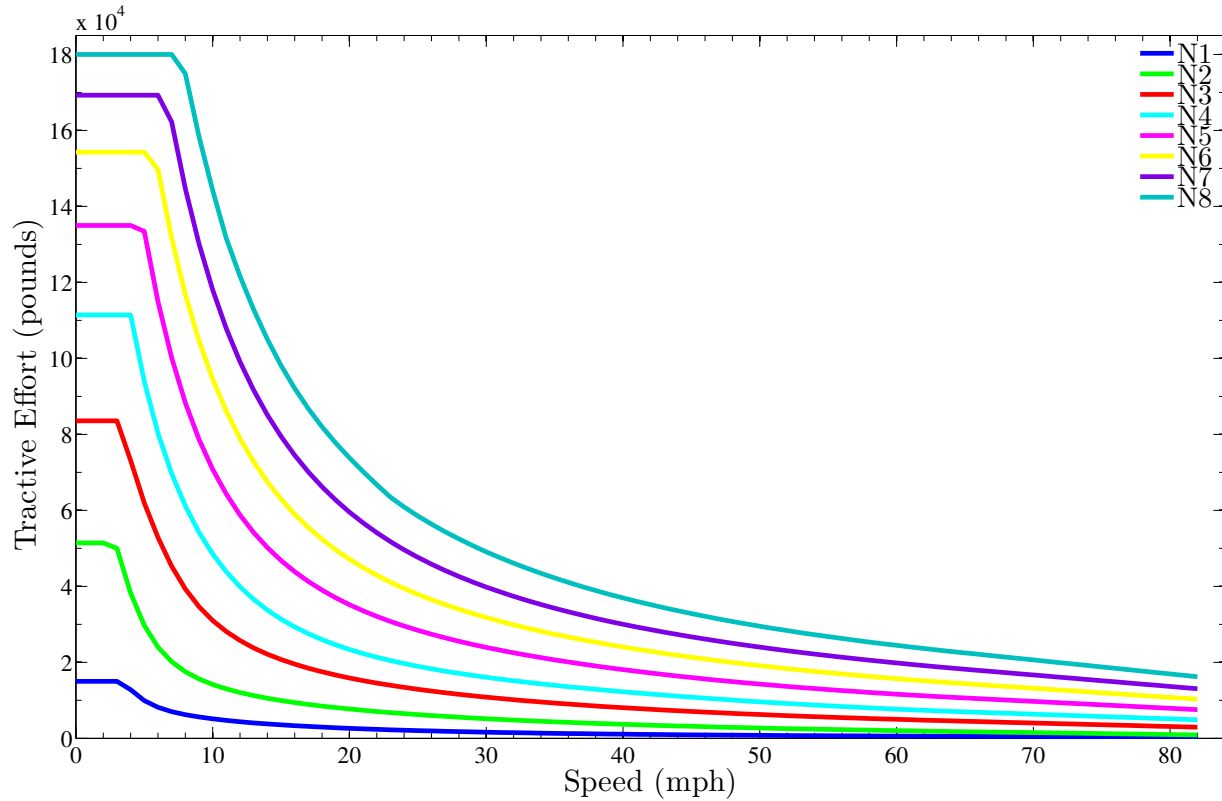


Figure 4.3: Tractive force curve for the GE C44AC locomotive.

The tractive force curve, knowledge of the fuel consumption at each setting and the results from the Davis Equation allow fuel consumption of a train to be approximated. The time spent at each throttle setting allows the fuel consumption to be determined for a specific train route. An example of these values is given in Table 4.3. These time values will vary depending on the needs of the train. Although the schedule and the terrain the train is traversing have large influences on these values, for the purpose of this study, these values will be assumed to be those values presented in Table 4.3. The method for determining the energy consumption of the train will be discussed later.

It has been assumed that the tractive curve will scale with the addition of locomotives, meaning having two locomotives will double the force output. This assumption allows different scenarios to be considered regarding the composition of a train. Before this can be done, the Davis Equation must be manipulated to calculate the resistive force for the entire train from known parameters.

Table 4.3: Locomotive Data for the General Electric C44AC

Throttle Setting	Idle	Dynamic Braking	N1	N2	N3	N4	N5	N6	N7	N8
Fuel Burned (gallons per hour), $h_{single}$	3	3	12	27	53	79	109	140	171	210
Time Percent	25.0%	12.0%	2.0%	4.0%	5.5%	5.5%	20.0%	5.0%	5.0%	16.0%

Table 4.4: Values for the Locomotive Variables Used in the Modified Davis Equation

Variable	Value	Units
Number of Locomotive Axles, $N_l$	6	axles
Weight of a Locomotive, $W_l$	220	tons
Cross-sectional Area, $A_{c,l}$	140.2	ft <sup>2</sup>
Drag Coefficient, $C_{d,l}$	1.0	nondimensional

To compare the railcar modifications tested in this study, clarification on the parameters used is necessary. To calculate the resistance of a single railcar (Eqn. 4.1a), the measured drag coefficients presented in Chap. 3 were used in the modified Davis Equation. Also, the density that was measured during testing was used. Other parameters used in Eqn. 4.1a are those specified in Table 4.1. The first coefficient in the  $A$  term was taken to be 1.3 lbs/ton. Equation 4.1b is used to calculate the resistance of a single locomotive. The parameters to do this are given in Table 4.4. The drag coefficient was determined through computational fluid dynamics software analysis by another research group at Brigham Young University. It was determined that a leading locomotive with five trailing railcars had a drag coefficient of 1.763. Through the author’s personal communication with the research group the drag coefficient on a single locomotive was determined to be 1.0 [50].

With the individual resistances of a single locomotive and single railcar calculated, it is necessary to develop an equation that will calculate the total resistance of the train. This is accomplished by taking the resistance of a single railcar and a single locomotive and multiplying each by the number and weight of the railcars and locomotives, respectively. Equation 4.3 shows this.

$$R = N_l W_l R_{t,l} + N_r W_r R_{t,r} \quad (4.3)$$

Table 4.5: Values for the Variables Used in the Total Train Resistance Analysis

Variable	Value	Units
Number of Locomotives, $M_l$	2	cars
Number of Railcars, $M_r$	65	cars
Weight of a Locomotive, $W_l$	220	tons
Weight of a Railcar, $W_r$	73	tons

The parameters used in Eqn. 4.3 are given in Table 4.5. Note that the weight,  $W_l$  and  $W_r$ , of these vehicles has been restated for the convenience of the reader. Using these values will yield a total resistive force equation that is a function of velocity. It should be noted that the drag coefficient of the leading and trailing railcars have been assumed to be the same as a railcar in the center of the train. Although the drag on the leading and trailing railcar is higher than those in the center of the train, this assumption was made due to an absence of information available about the leading and trailing regions. This assumption is supported by the fact that the leading and trailing railcars, when compared to the length of the train, will add only a small amount more resistive force. Also, the  $C_d$  for the locomotive was assumed constant regardless of the position of the locomotive in the train. This was done for similar reasons as the assumption involving leading and trailing railcars, namely a lack of information regarding these regions.

The resistive force and the tractive force can now be overlaid on the same plot as functions of velocity. An example of this is given in Fig. 4.4 where the tractive force plot has been scaled by a factor of two to represent the output of two locomotives. The resistive results from the modified Davis Equation have been plotted from 0 miles/hour to 82 miles/hour for the corrugated baseline, smooth roof with a leading and trailing lip and smooth roof without a leading and trailing lip cases. The restrictive nature of the discrete notch settings system on the throttle of the locomotive means that the locomotive can only be run at certain velocities under a given load. This made it necessary to assume that the velocity could be held constant. This constant velocity assumption is represented in Fig. 4.4 by vertical lines. These lines were taken at the intersections of the tractive force curves and the Davis Equation results for the baseline case. The intersection points of the Davis Equation results for the modified railcars and the constant velocity, vertical lines were then determined for each modified case. This method resulted in a force value at each intersection between the tractive



force curves for the eight notch setting for the baseline case and a force value for all the modified railcar cases at each constant velocity result.

The above analysis results in a matrix of force values that can now be used to determine fuel conservation. This is done by relating the amount of fuel used in the baseline case to a reduction factor that is proportional to the reduced force needed by the train to maintain the constant speed. It is necessary to calculate a ratio of the reduced force needed by a modified train to that of the baseline train. This is done using Eqn. 4.4. The ratio of the forces is defined as  $\alpha$ .

$$\alpha_i = \frac{F_{i,modified}}{F_{i,base}} \quad \text{where } i = 1, 2, \dots, n \quad (4.4)$$

Note that this ratio is taken at each throttle setting such that  $n = 8$ .

The fuel consumption needs to be adjusted for the number of locomotives used in the analysis. The total fuel consumed at a given throttle setting is simply the product of  $h_{i,single}$ , the fuel consumption of a single locomotive which is given in Table 4.3, and  $M_l$ , the number of locomotives, as shown in Eq. 4.5.

$$h_{i,base} = h_{i,single} M_l \quad \text{where } i = 1, 2, \dots, n \quad (4.5)$$

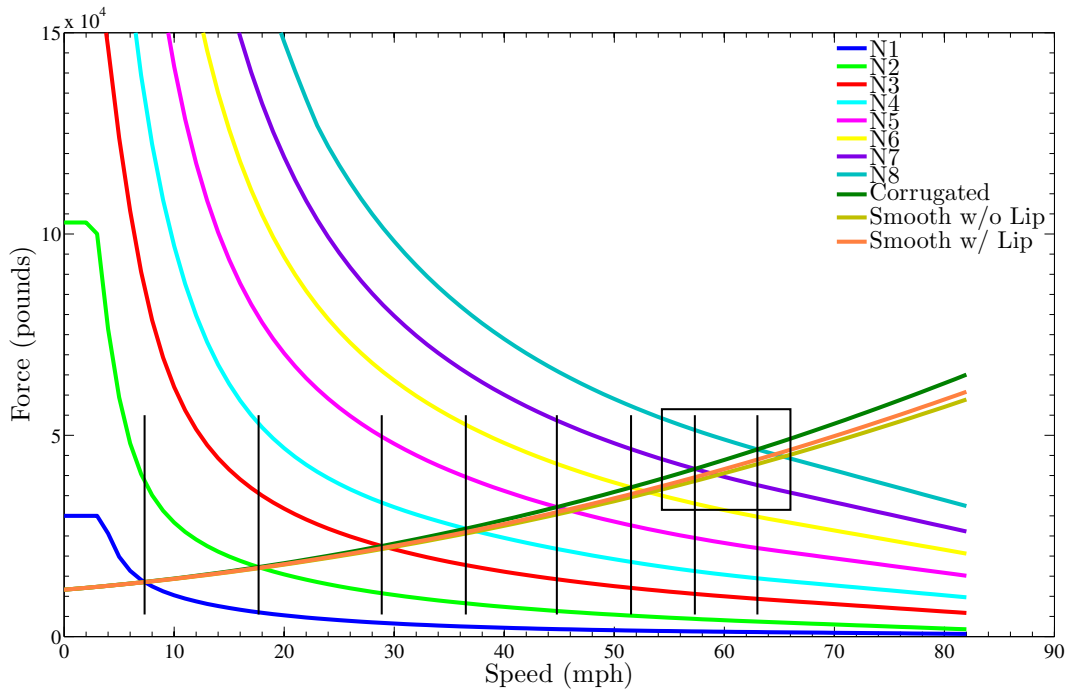
This ratio  $\alpha$  can now be used to determine the reduced fuel consumption of the modified train at each throttle setting. This is done using Eqn. 4.6 where  $h_{i,base}$  is the result of Eqn. 4.5.

$$h_{i,reduced} = \alpha_i h_{i,base} \quad \text{where } i = 1, 2, \dots, n \quad (4.6)$$

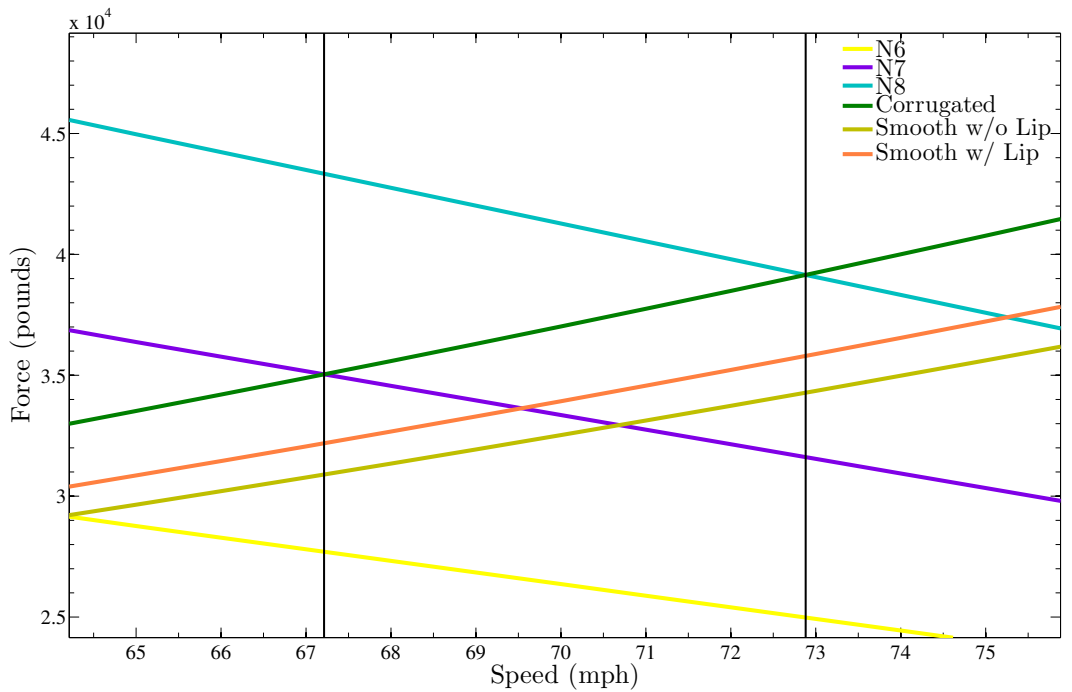
The value  $h_{i,reduced}$  is the fuel that is expected to be burned at a given throttle setting for a given modification. To find the percent fuel reduction,  $\psi_{i,reduced}$ , the fuel consumption array for  $n = 8$  can be compared to the baseline. Equation. 4.7 shows this approach.

$$\psi_{i,reduced} = \frac{h_{i,base} - h_{i,reduced}}{h_{i,base}} \quad \text{where } i = 1, 2, \dots, n \quad (4.7)$$

It is now possible to take the weighted average of these percent reduced fuel consumption values to determine an overall average fuel reduction,  $\bar{\psi}_{reduced}$ , based on the time fraction,  $t$  that



(a)



(b)

Figure 4.4: Tractive force curve for the locomotives and resistive force results of the corrugated and modified roof analyses, also showing vertical lines used when assuming constant velocity in the analysis (B Included). (a) Tractive and resistive force results and (b) tractive and resistive force results detail, zoomed in on the intersection point at the seventh and eighth throttle settings.

the train spends at each throttle notch setting. Again, the values for  $t$  used in this analysis are given in Table 4.3.

$$\bar{\Psi}_{reduced} = \frac{\sum_{i=1}^n \Psi_{i,reduced} t_i}{\sum_{i=1}^n t_i} \quad (4.8)$$

The fuel consumption analysis is sensitive to the time fraction input. The fuel usage is nearly linear as the notch settings are increased, although the force that is generated at each setting does not increase linearly. Due to the nonlinearity of this relation the more time the train spends at higher throttle settings, the larger the average fuel reduction will be, however the total fuel usage will also be higher. This fuel reduction variation can be as high as a few percent depending on the railcar modification being studied.

### 4.3 Davis Equation Results

The analysis of the data was done in MATLAB. The MATLAB code written for this analysis is given in Appendix C. The code compares the AAR and CN models of the Davis Equation against the modified form. The data from wind tunnel testing is loaded from an Excel workbook and averaged. The analysis using the modified Davis Equation and the energy analysis is also performed.

As part of this study, the percent force reduction was also determined. It was calculated using a similar method to the fuel reduction calculation, namely by finding the percent force reduction,  $\Phi_{i,reduced}$ , at each notch setting compared to the baseline case using Eqn. 4.9 and then calculating the weighted average force reduction,  $\bar{\Phi}_{reduced}$ , based on values of  $t$  using Eqn. 4.10.

$$\Phi_{i,reduced} = \frac{F_{i,base} - F_{i,modified}}{F_{i,base}} \quad \text{where } i = 1, 2, \dots, n \quad (4.9)$$

$$\bar{\Phi}_{reduced} = \frac{\sum_{i=1}^n \Phi_{i,reduced} t_i}{\sum_{i=1}^n t_i} \quad (4.10)$$

These force reduction values are presented with the results for the fuel reduction analysis. These values can be helpful in making design and maintenance decisions. Many designs for large equip-

Table 4.6: Force and Fuel Results for Auto-carrying Railcar Roof Modifications

Model Type	CN		AAR	
	Total Force Reduction, $\bar{\Phi}_{reduced}$	Fuel Reduction, $\bar{\Psi}_{reduced}$	Total Force Reduction, $\bar{\Phi}_{reduced}$	Fuel Reduction, $\bar{\Psi}_{reduced}$
Corrugated Roof (Baseline)	-	-	-	-
Smooth Roof without Lip	6.3%	5.7%	10.4%	9.6%
Smooth Roof with Lip	4.3%	3.9%	7.2%	6.6%

ment are based on structural requirements. The force reduction values represent less force being exerted on parts like locomotive and railcar connectors, which suggests that the longevity of such parts may increase.

The fuel reduction values from this analysis have already been noted to be dependent on the time fraction values. The number and weight of locomotives and railcars will also influence this analysis. The correlation between drag reduction and fuel reduction has been shown to be increasingly significant as the speed of train increases. There are many different facets that must be investigated to ensure accuracy; for this reason analyses that relate any resistive element reduction to an overall fuel reduction are sparse. One study suggested that 20% of the drag reduction can be expected in fuel savings [33].

The energy analysis for the corrugated roof baseline model and modifications is given in Table 4.6. The difference between retaining the  $B$  term and neglecting it resulted in quite different results. Including the  $B$  term results in 5.7% of the fuel being conserved when the smooth roof without leading and trailing lips is implemented. Fuel conservation increases by nearly a factor of two resulting in 9.6% if the  $B$  term is neglected. Referring to the drag coefficient comparison for these modifications in Table 3.1, the drag reduction was nominally 20.0% for the smooth roof without leading and trailing lips case. This means that including the  $B$  term predicts that 28.5% of the drag reduction can be expected in fuel savings. Similarly, by neglecting the  $B$  term 48.0% of the drag reduction could be anticipated in fuel savings. Including the  $B$  term appears to agree better with the claim that 20% of the drag reduction will be converted to fuel savings suggested by the study that was cited earlier [33].

Table 4.7: Force and Fuel Results for Auto-carrying Railcar Side Panels Modifications

Model Type	CN		AAR	
	Total Force Reduction, $\overline{\Phi}_{reduced}$	Fuel Reduction, $\overline{\Psi}_{reduced}$	Total Force Reduction, $\overline{\Phi}_{reduced}$	Fuel Reduction, $\overline{\Psi}_{reduced}$
Ribbed (No Holes)	2.9 %	2.6%	4.8%	4.4%
Smooth Panels	2.4 %	2.2%	4.1%	3.8%
Industry Replica	-	-	-	-
4x Larger, Blocked	0.9%	0.8%	1.5 %	1.4%
Slotted	-0.3%	-0.3%	-0.5%	-0.5%
4x Larger, Spaced	1.3%	1.2%	2.2%	2.1%

The results for the energy analysis for the side panel data is given in Table 4.7. Not surprisingly the fuel reduction percentages here are much less. This was expected due to the smaller drag reduction values presented in Table 3.2. While these values are smaller, the ability to implement these changes may also be easier. Although no return on investment or implementation analysis is done here, these are certainly topics that must be considered before implementing a design change.

Similar to the findings already presented, the results for the chassis modifications presented in Table 4.8 show that chassis modifications to auto-carrying railcars can have a positive influence on the fuel conservation of the train. Although this region of the railcar presents some larger challenges than other regions, largely because sections of the chassis need to be accessible, the large fuel reduction percentages suggests that working towards an aerodynamic solution could be beneficial.

In summary, the values presented have been based on values that vary from one train to the next. The time fraction values will depend on the route and needs of the train. The time values can have a significant effect on the fuel consumption values. If the train is operated mainly at the N1 throttle setting, aerodynamics will change the fuel consumption less than a percent or two even when multiple modifications are implemented. This result is not surprising considering the speed of the train is less than 8 miles/hour at N1 as seen in Fig. 4.4. However, as the speed of the train increases, higher throttle setting will be utilized, more fuel is expended and the aerodynamics will have a larger effect. For example if the train was run exclusively at the N8 throttle setting, the

Table 4.8: Force and Fuel Results for Auto-carrying Railcar Chassis Cover Modifications

Model Type	CN		AAR	
	Total Force Reduction, $\bar{\Phi}_{reduced}$	Fuel Reduction, $\bar{\Psi}_{reduced}$	Total Force Reduction, $\bar{\Phi}_{reduced}$	Fuel Reduction, $\bar{\Psi}_{reduced}$
Standard Chassis	-	-	-	-
Chassis Cover	2.1%	1.9%	3.4%	3.2%
Full Length Skirt	4.6 %	4.2%	7.7%	7.1%
Partial Skirt	4.6 %	4.2%	7.6%	7.0%

fuel reduction percentage ( $\bar{\Psi}_{reduced}$ ) would increase by nominally 35% of these stated values if the  $B$  term is included (CN method) or nominally 29% if the  $B$  term is excluded from the analysis (AAR method). These increases represent a maximum  $\bar{\Psi}_{reduced}$  expected for a given modification, however it is important to note that this means the locomotives running at N8 will be at peak pulling capacity and burning a maximum amount of fuel.

## CHAPTER 5. CONCLUSIONS

### 5.1 Conclusions

The results presented in this study confirm that much can be done to reduce the drag on auto-carrying railcars. Three regions were studied, namely the roof, side panels and chassis. Selected designs were tested on a composite model to determine an overall drag reduction.

The results from the auto carrying railcar tests show changing or covering the roof with flat material reduces the drag on the railcar by nominally 14%. The data also highlights the importance of avoiding aerodynamically inefficient or uncovered structure to the roof. For example, the lip on the model added 6% drag to the railcar. This was further supported by an investigation of the chassis.

The data suggested that modification to the chassis region could have a larger influence on the drag than the roof region, although the ability to modify the roof is easier. The chassis region of an auto-carrying railcar is normally exposed to the atmosphere. The modifications in this study suggest that by covering this region, the drag on the railcar can be reduced. By adding skirts, the drag was reduced by nominally 15%, however this type of fairing presents some difficulties regarding implementation and maintenance on mechanical parts underneath the railcar. However, the partial skirts reduce the invasive nature of a full skirt and still show potential if the difficulty of inspection of the chassis could be overcome.

Alternatively, the chassis cover reduces these difficulties, but at an aerodynamic penalty. This cover only exhibited a nominally 8% drag reduction. Although the chassis cover does not perform to the same level as the skirts, it may be the first step to finding a better aerodynamic solution than simply leaving the chassis exposed.

The side panel results suggested that the current designs used in industry could be improved by considering the size, shape and pattern of the holes on the side panels of the railcar. The most favorable result achieved, while still maintaining 5% void fraction, was nominally 5.1% drag

reduction by the side panels which had larger holes and preserved a pattern similar to the industry layout. The results also suggested that the holes can be too large or poorly oriented and cause an increase in drag, as seen in the case when slots were implemented. The case with the slotted side panel that exhibits a higher drag coefficient than that of the baseline industry replica case indicates that simply increasing the smooth surface area does not necessarily ensure the drag will be reduced. Care must be taken regarding the diameter and the pattern of the holes.

The testing of the composite model suggested that the combining modifications on the roof, side panel and chassis regions are not completely additive and may negatively interfere with one another. Modifications gave higher drag reductions when implemented individually than when the same modification was implemented with other modifications. Although the modifications were not perfectly additive, with each added modification, a drag reduction was observed. In conclusion, combining modifications still results in a higher drag reduction than single modification implementation.

The energy analysis outlined a method that allows changes in total resistance due to changes of resistance terms to be converted into reductions in fuel consumption. This analysis also yielded expected fuel reductions for the modifications tested in this study. As a general rule, if the  $B$  term from the Davis Equation is included in the analysis as done in the model presented by the Canadian National Railway Company, nominally 30% of the drag reduction can be expected in fuel reduction. If the  $B$  term is neglected as proposed by the Association of American Railroads, nominally 50% of the drag reduction will be seen in fuel reduction. Ultimately, these percentages are sensitive to the time fractions spent at each throttle setting as well as the modifications being implemented. In short, these energy analysis methods should be applied on a case by case basis, yet these percentages represent an average reduction for the modifications tested in this study.

## **5.2 Future Work**

There are still many options to be investigated regarding railcar aerodynamics and how to calculate energy usage of a train. The design modifications suggested in this study are in no way all inclusive. There are many ways to change or alter the aerodynamic profile of railcars. For example, hole size and pattern on the side panels could still be optimized. Although no design



with holes would be expected to exceed the smooth panel maximum of 9.2%, work can still be done to more closely approach this level of drag reduction.

The chassis cover can also be optimized. The mechanical and pneumatic components underneath the railcar will continue to pose design challenges, yet this study suggests even the simplest cover may yield an aerodynamic savings. Currently adding skirts to the railcars seem to be overly inconvenient, however when offering nominally 15% drag reduction the work of refining and testing a similar design may yield acceptable results.

The aerodynamic interaction between the three regions studied could also be better understood. The composite testing indicated smaller drag reductions for modifications when implemented with modifications in other regions than the independent modification testing proposed. Understanding the flow dynamics of how these regions are interacting may allow for designs that reduce this interaction. This would expectantly provide the larger drag reduction, similar to values seen during individual component testing.

There is also the question about the  $B$  term in the Davis equation. If the  $B$  term is included, nominally 30% of the drag reduction can be translated to fuel savings. If the  $B$  term is in fact negligible, then nominally 50% of the drag reduction can be translated to fuel savings. The importance of the contribution of the dynamics represented by the  $B$  term is a significant question to answer. Determining whether or not it can be neglected will help researchers identify which component of resistance is contributing the most and ultimately where to focus time and resources in an effort to reduce the resistance on the trains.

## REFERENCES

- [1] Bailey, M., 2005. “The history of tracks and trains: a lesson in joined-up thinking.” *Proceedings of the ICE - Civil Engineering*, **158**(3), pp. 134–142. 1
- [2] Paul, J., Johnson, R. W., and Yates, R. G., 2009. “Application of cfd to rail car and locomotive aerodynamics.” *Lecture Notes in Applied and Computational Mechanics*, **41**, pp. 259–297. 2
- [3] U.S. Energy Information Administration, 2014. Weekly u.s. no 2 diesel ultra low sulfur (0-15ppm) retail prices. vii, 2
- [4] Ahmed, S. R., Bayer, B. E., Callister, J. R., Deußen, N., Emmelmann, H.-J., Flegl, H., George, A. R., Gilhaus, A., Götz, H., Großmann, H., Hoffman, R., Hucho, W.-H., Hummel, D., Kohl, W. R., Necati, G. A., Piatek, R., Schlenz, D., Schmitt, J., Sebbecke, W., Singer, N., and Steinberg, P., 1998. *Aerodynamicis of Road Vehicles: From Fluid Mechanics to Vehicle Engineering.*, 4 ed. Society of Automotive Engineers,Inc., Warrendale, PA. 3, 5
- [5] Anderson Jr., J. D., 2012. *Introduction to Flight.*, 7 ed. McGraw-Hill, New York. 3
- [6] Irwin, P., 2008. “Bluff body aerodynamics in wind engineering.” *Journal of Wind Engineering and Industrial Aerodynamics*, **96**(6), pp. 701–712. 4
- [7] Roshko, A., 1993. “Perspective on bluff body aerodynamics.” *Journal of Wind Engineering and Industrial Aerodynamics*, **49**(1), pp. 79–100. 4
- [8] Bearman, P., 2009. “Bluff body flow research with application to road vehicles.” *Lecture Notes in Applied and Computational Mechanics*, **41**, pp. 3–13. 4
- [9] Choi, H., Lee, J., and Park, H., 2014. “Aerodynamics of heavy vehicles.” *Annual Review of Fluid Mechanics*, **46**, p. 441. 4
- [10] Hucho, W., and Sovran, G., 1993. “Aerodynamics of road vehicles.” *Annual Review of Fluid Mechanics*, **25**(1), pp. 485–537. 4
- [11] Baker, C., and Humphreys, N., 1996. “Assessment of the adequacy of various wind tunnel techniques to obtain aerodynamic data for ground vehicles in cross winds.” *Journal of Wind Engineering and Industrial Aerodynamics*, **60**, pp. 49–68. 4
- [12] Buil, R. M., and Herrer, L. C., 2009. “Aerodynamic analysis of a vehicle tanker.” *Journal of Fluids Engineering*, **131**(4), pp. 0412041–04120417. 4, 7
- [13] Garry, K. P., 1981. “Development of container-mounted devices for reducing the aerodynamic drag of commercial vehicles.” *Journal of Wind Engineering and Industrial Aerodynamics*, **9**(1), pp. 113–124. 4

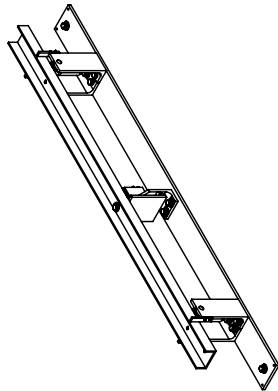
- [14] Wong, H. Y., Cox, R., and Rajan, A., 1980. “Drag reduction of trailer-tractor configuration by aerodynamic means.” *Journal of Wind Engineering and Industrial Aerodynamics*, **9**(1), pp. 101–111. 4
- [15] Modi, V. J., Hill, S. S., and Yokomizo, T., 1995. “Drag reduction of trucks through boundary-layer control.” *Journal of Wind Engineering and Industrial Aerodynamics*, **54**, pp. 583–594. 4, 5
- [16] Qi, X.-N., and qi Liu, Y., 2011. “Experimental and numerical studies of aerodynamic performance of trucks.” *Journal of Hydrodynamics*, **23**(6), pp. 752–758. 5
- [17] Sitlani, M., 2006. “Numerical simulations on aerodynamic drag of ground transport system (gts) model.” Master of engineering science, Lamar University. 5
- [18] Adams, J., Burr, J., Campbell, M., Jones, A., Peterson, E., Spear, M., Wells, K., and Maynes, D., 2011. Aerodynamic coal car covers Capstone summary, Brigham Young University. 5, 7
- [19] Spring, A., Taylor, B., Zollinger, C., Salmond, L., Henrie, S., and Maynes, D., 2012. Aerodynamic analysis of union pacific’s autoflex car Capstone summary, Brigham Young University. 5
- [20] Paul, J. C., Gielow, R. L., Gielow, M. A., and Polihonki, D. R., 1984. “Wind tunnel test of 3/10-scale skeletonized and well-type intermodal rail cars..” *Paper - American Society of Mechanical Engineers*. 6
- [21] Thacker, A., Aubrun, S., Leroy, A., and Devinant, R., 2012. “Effects of suppressing the 3d separation on the rear slant on the flow structures around an ahmed body.” *Journal of Wind Engineering and Industrial Aerodynamics*, **107**, pp. 237–243. 6
- [22] Ortega, J., and Salari, K., 2004. “An experimental study of drag reduction devices for a trailer underbody and base.” *34th AIAA Fluid Dynamics Conference and Exhibit*. 6
- [23] Hyams, D. G., Sreenivas, K., Pankajakshan, R., Nichols, D. S., Briley, W. R., and Whitfield, D. L., 2011. “Computational simulation of model and full scale class 8 trucks with drag reduction devices.” *Computers & Fluids*, **41**(1), pp. 27–40. 6
- [24] Tian, H.-Q., 2009. “Formation mechanism of aerodynamic drag of high-speed train and some reduction measures.” *Journal of Central South University of Technology*, **16**(1), pp. 166–171. 6, 7
- [25] Yang, X., Jin, J., and Shi, G., 2013. “Preliminary study on streamlined design of longitudinal profile of high-speed train head shape.” *Procedia - Social and Behavioral Sciences*. 6
- [26] Orellano, A., and Sperling, S., 2009. “Aerodynamic improvements and associated energy demand reduction of trains.” *Lecture Notes in Applied and Computational Mechanics*, **41**, pp. 219–231. 6
- [27] Raghunathan, R. S., Kim, H.-D., and Setoguchi, T., 2002. “Aerodynamics of high-speed railway train.” *Progress in Aerospace Sciences*, **38**(6), pp. 469–514. 6

- [28] Ido, A., Kondo, Y., Matsumura, T., Suzuki, M., and Maeda, T., 2001. “Wind tunnel tests to reduce aerodynamic drag of trains by smoothing the under-floor construction.” *Quarterly Report of RTRI*, **42**(2), pp. 94–97. 7
- [29] Yebo, L., and Zhiming, L., 2013. “Aerodynamic simulation of the air flow beneath the high speed train.” *Applied Mechanics and Materials*, **253-255**(1), pp. 2035–2040. 7
- [30] McCallen, R. C., Salari, K., Pointer, W. D., Browand, F., Ross, J., Slezak, L., Routbort, J., Ortega, J., Castellucci, P., Chang, J., Singh, S., Dringenberg, E., Radovich, C., Merzel, T., Plocher, D., Storms, B., Clarke, R. M., and Carrington, K., 2006. “Aerodynamic drag reduction.” *Annual Progress Report for Heavy Vehicle Systems Optimization Program*, **1**, pp. 1–59. 7
- [31] Lai, Y.-C., Barkan, C. P., and Önal, H., 2008. “Optimizing the aerodynamic efficiency of intermodal freight trains.” *Transportation research. Part E, Logistics and transportation review*, **44**(5), pp. 820–834. 7
- [32] Watkins, S., Saunders, J., and Kumar, H., 1992. “Aerodynamic drag reduction of goods trains.” *Journal of Wind Engineering and Industrial Aerodynamics*, **40**(2), pp. 147–178. 7
- [33] Saunders, J. W., Watkins, S., and Kumar, H., 1991. “Aerodynamics to save energy for unit-train freight wagons.” *National conference publication - Institute of Engineers. Australia*(91), pp. 98–102. 7, 64
- [34] American Railway Engineering and Maintenance-of-Way Association, 2003. *Practical Guide to Railway Engineering*. American Railway Engineering and Maintenance-of-Way Association. 8
- [35] Rochard, B. P., and Schmid, F., 2000. “Review of methods to measure and calculate train resistances.” *Proceedings of the Institution of Mechanical Engineers. Part F, Journal of rail and rapid transit*, **214**(4), pp. 185–199. 8
- [36] American Railway Engineering and Maintenance-of-Way Association, 2013. *Manual for Railway Engineering.*, Vol. 4. 9, 10, 11, 15, 51, 54, 55
- [37] Seedah, D., and Harrison, R., 2010. *Measuring the impact of intermodal rail movements in state transportation planning.*, Vol. 1. 9, 51
- [38] Gielow, M., and Furlong, C., 1988. Results of wind tunnel and full-scale tests conducted from 1983 to 1987 in support of the association of american railroad’s train energy program Final Report Report Number R-685, Association of American Railroads, December. 10, 11
- [39] Baker, C. J., and Brockie, N., 1991. “Wind tunnel tests to obtain train aerodynamic drag coefficients: Reynolds number and ground simulation effects.” *Journal of Wind Engineering and Industrial Aerodynamics*, **38**(1), pp. 23–28. 14
- [40] Willemsen, E., 1997. “High reynolds number wind tunnel experiments on trains.” *Journal of Wind Engineering and Industrial Aerodynamics*, **69**, pp. 437–447. 14

- [41] Willemsen, E., Pengel, K., Holthusen, H., Küpper, A., and Chiaberge, M., 2011. “Automotive testing in the german-dutch wind tunnels.” *New Trends and Developments in Automotive Industry*, pp. 17–32. 14
- [42] Lutz, T., and Sayers, A., 1999. “Wind tunnel boundary layer effects on the aerodynamic drag of model trucks.” *R&D Journal*, **15**(1), pp. 9–15. 14
- [43] Paradot, N., Talotte, C., Garem, H., Deville, J., and Bonnet, J. P., 2002. “A comparison of the numerical simulation and experimental investigation of the flow around a high speed train.” *American Society of Mechanical Engineers, Fluids Engineering Division*, **257**(1), pp. 1055–1060. 14
- [44] Munson, B. R., Young, D. F., Okiishi, T. H., and Huebsch, W. W., 2009. *Fundamentals of Fluid Mechanics.*, 6th edition. ed. John Wiley & Sons, Inc., Hoboken, NJ. 14
- [45] Baker, C., 2010. “The flow around high speed trains.” *Journal of Wind Engineering and Industrial Aerodynamics*, **98**(6), pp. 277–298. 15
- [46] Dunn, P., 2010. *Measurement and Data Analysis for Engineering and Science.*, 2 ed. CRC Press. 22, 23, 24
- [47] Figliola, R. S., and Beasley, D. E., 2006. *Theory and Design for Mechanical Measurements.*, 4 ed. Wiley. 22
- [48] Barlow, J. B., Guterres, R., and Ranzenbach, R., 2001. “Experimental parametric study of rectangular bodies with radiused edges in ground effect.” *Journal of Wind Engineering and Industrial Aerodynamics*, **89**(1415), pp. 1291 – 1309 Bluff Body Aerodynamics and Applications. 34
- [49] Kawamura, A., Takeuchi, K., Furuya, T., Cao, M., Takaoka, Y., and Yoshimoto, K., 2004. “Measurement of tractive force and the new maximum tractive force control by the newly developed tractive force measurement equipment.” *Electrical engineering in Japan*, **149**(2), pp. 49–59. 57
- [50] Brewer, S., Gillespie, M., Holden, J., Jarvis, J., Marsh, D., Pierce, L., and Truscott, T., 2013. Design of an aerodynamic freight locomotive Capstone summary, Brigham Young University. 59

## **APPENDIX A. TEST SETUP DESIGN**

ITEM NO.	PART NUMBER	DESCRIPTION	Default/ QTY.
1	TestSetup - Base	Setup Base	1
2	TestSetup - Tower - RT	Right Hand Support Tower	2
3	TestSetup - Shaft	Shaft	2
4	2337K807	Bearing	4
5	Track - Track Test Section	Track Test Selection	1
6	91081A129	Washer 1/4	16
7	91101A229	Lock Washer 1/4	12
8	92240A542	Hex Bolt 1/4-20 x1	4
9	92240A537	Hex Bolt 1/4-20 x 1/2	10
10	TestSetup - Sensor Mount Top	Sensor Top Mount	1
11	TestSetup - Sensor Mount Bottom ASSY	Bottom Mounting Bracket Assembly	1
12	Sensor	Interface MBP-5-19	1
13	92313A106	Set Screw 4-40 x 1/4	4
14	96659A103	Washer #8	6
15	91251A082	Socket Head Cap Screw 8-32 x 1 3/4	3
16	90631A009	Nyloc 8-32	3
17	90630A110	Nyloc 1/4-20	2
18	TestSetup - TrackAligner	Track Aligner	4
19	91251A112	Socket Head Cap Screw 4-40 X 0.625	8
20	TestSetup - Tower - LT	Left Hand Support Tower	2
21	Spacer	Spacer	4



	DESCRIPTION: <b>Test Setup Assembly</b>		SIZE DWG. NO. <b>A</b> TestSetup Assembly	
	MATERIAL FINISH			
DO NOT SCALE DRAWING		DRAWN BY Robert Condie		SCALE: 1:12 WEIGHT: 2 1
3		4		SHEET 1 OF 4

Figure A.1: Test setup assembly page 1.

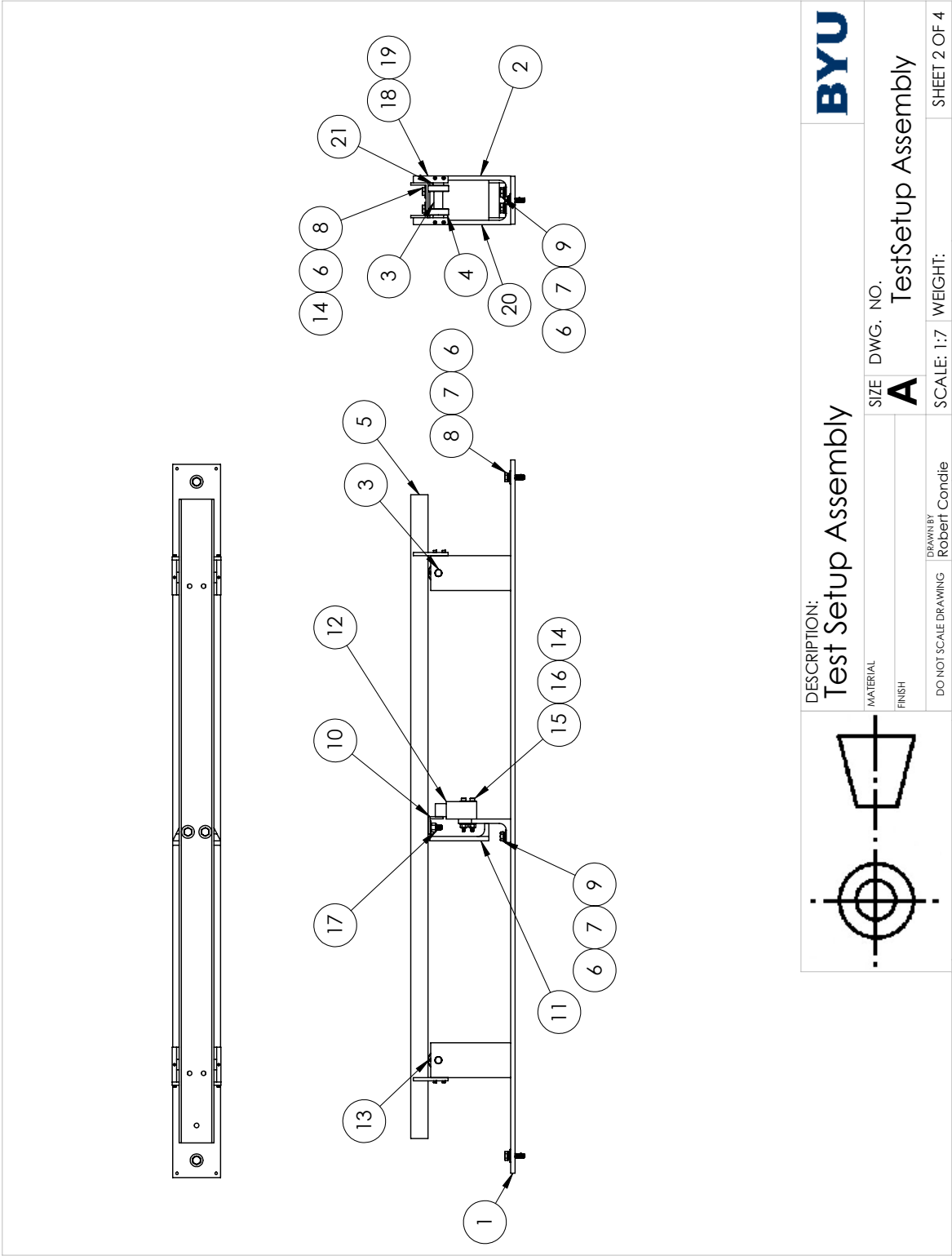
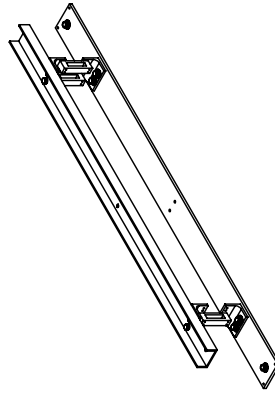


Figure A.2: Test setup assembly page 2.



ITEM NO.	PART NUMBER	DESCRIPTION	SENSOR SUPPORTED/QTY.
1	Track - Track Test Section	Track Test Selection	1
2	91081A129	Washer 1/4	6
3	91101A229	Lock Washer 1/4	10
4	92240A537	Hex Bolt 1/4-20 x 1/2	8
5	92240A542	Hex Bolt 1/4-20 x 1	2
6	TestSetup - Base	Setup Base	1
7	1 Cell ASSY	1 Load Cell Config	1
8	2 Cell ASSY	2 Load Cell Config	1



	DESCRIPTION: <b>Test Setup Assembly</b>		SIZE DWG. NO. <b>A</b> TestSetup Assembly	<b>BYU</b>
	MATERIAL FINISH	DO NOT SCALE DRAWING DRAWN BY Robert Condie		

Figure A.3: Test setup assembly page 3.

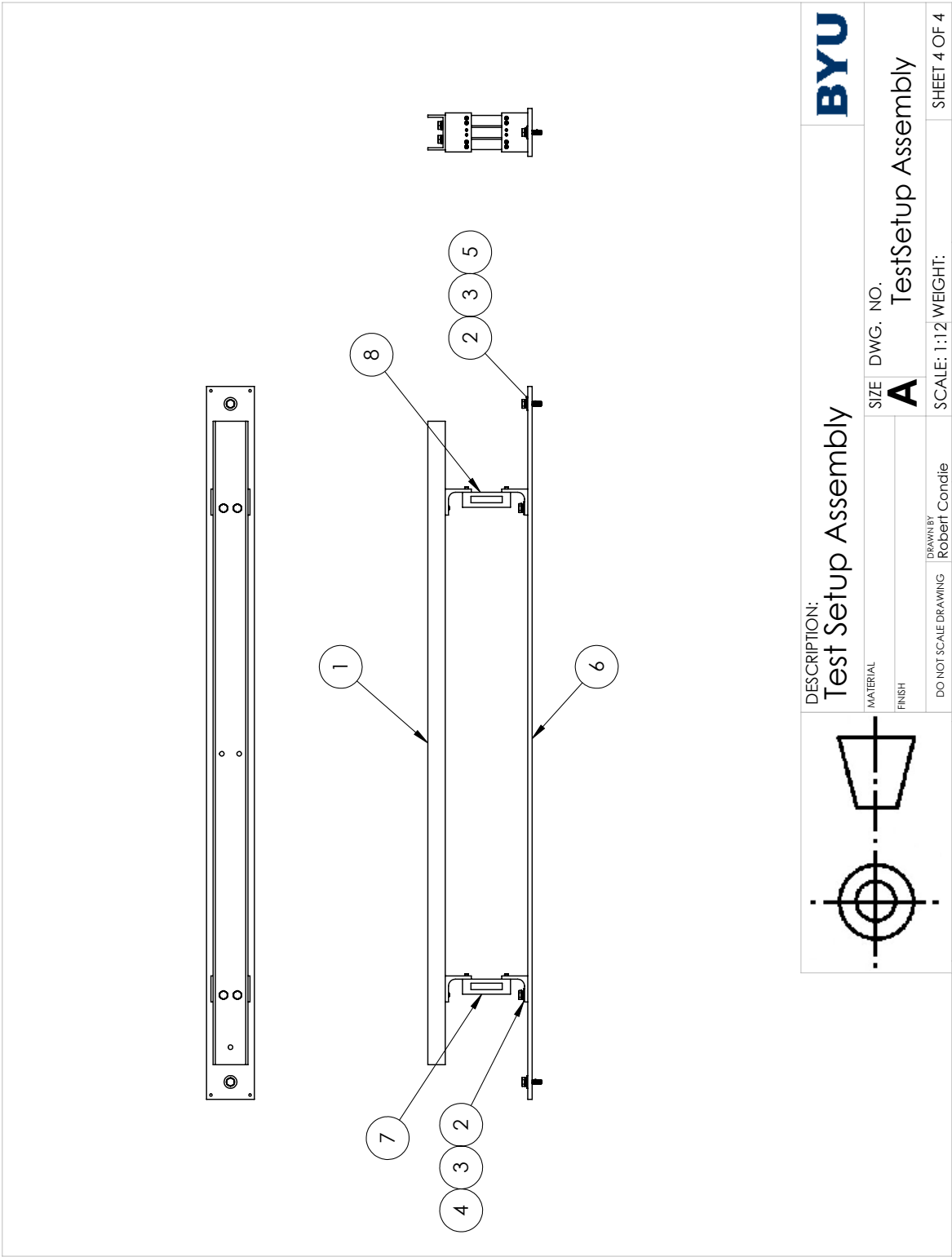


Figure A.4: Test setup assembly page 4.

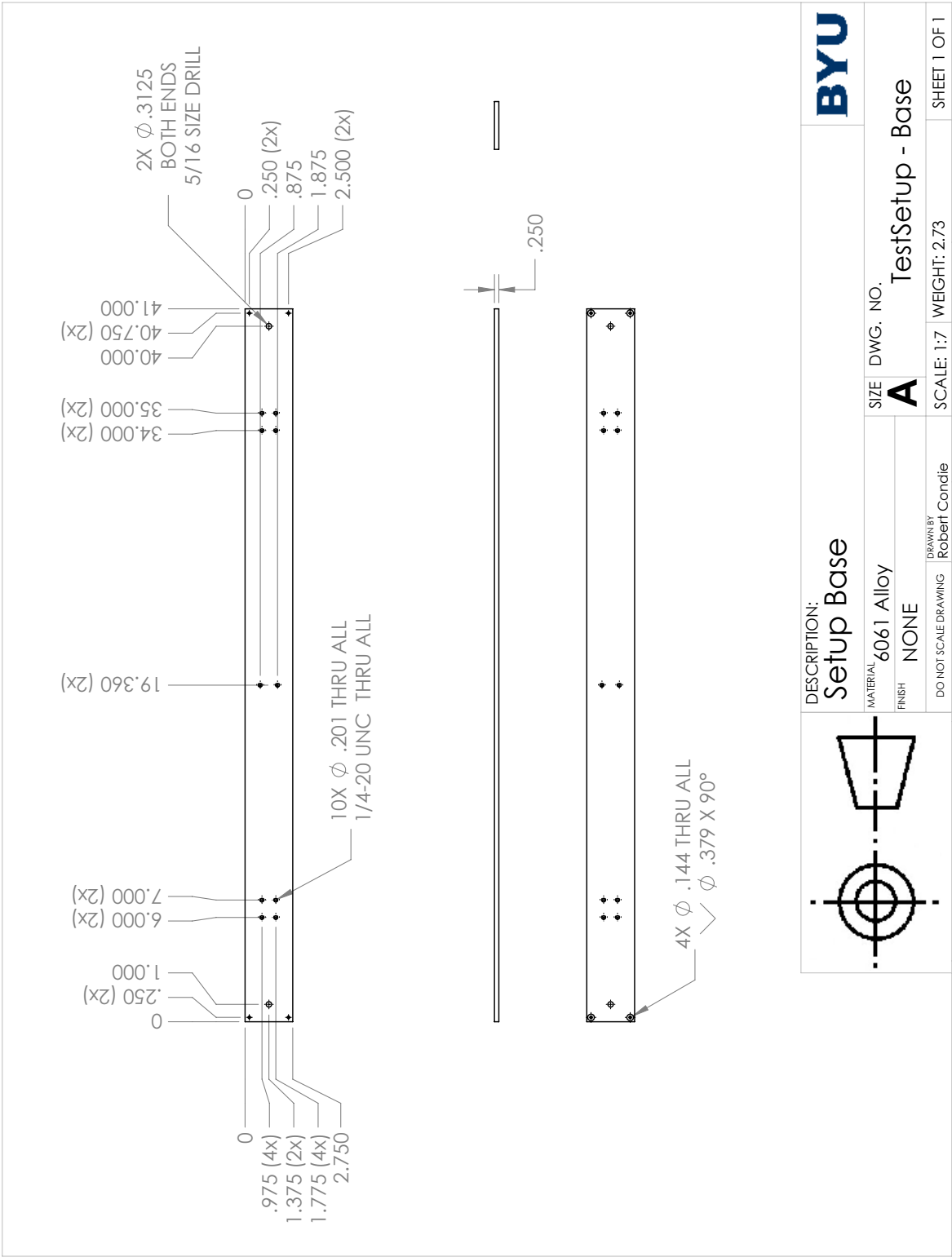


Figure A.5: Base plate assembly for the test setup assembly.

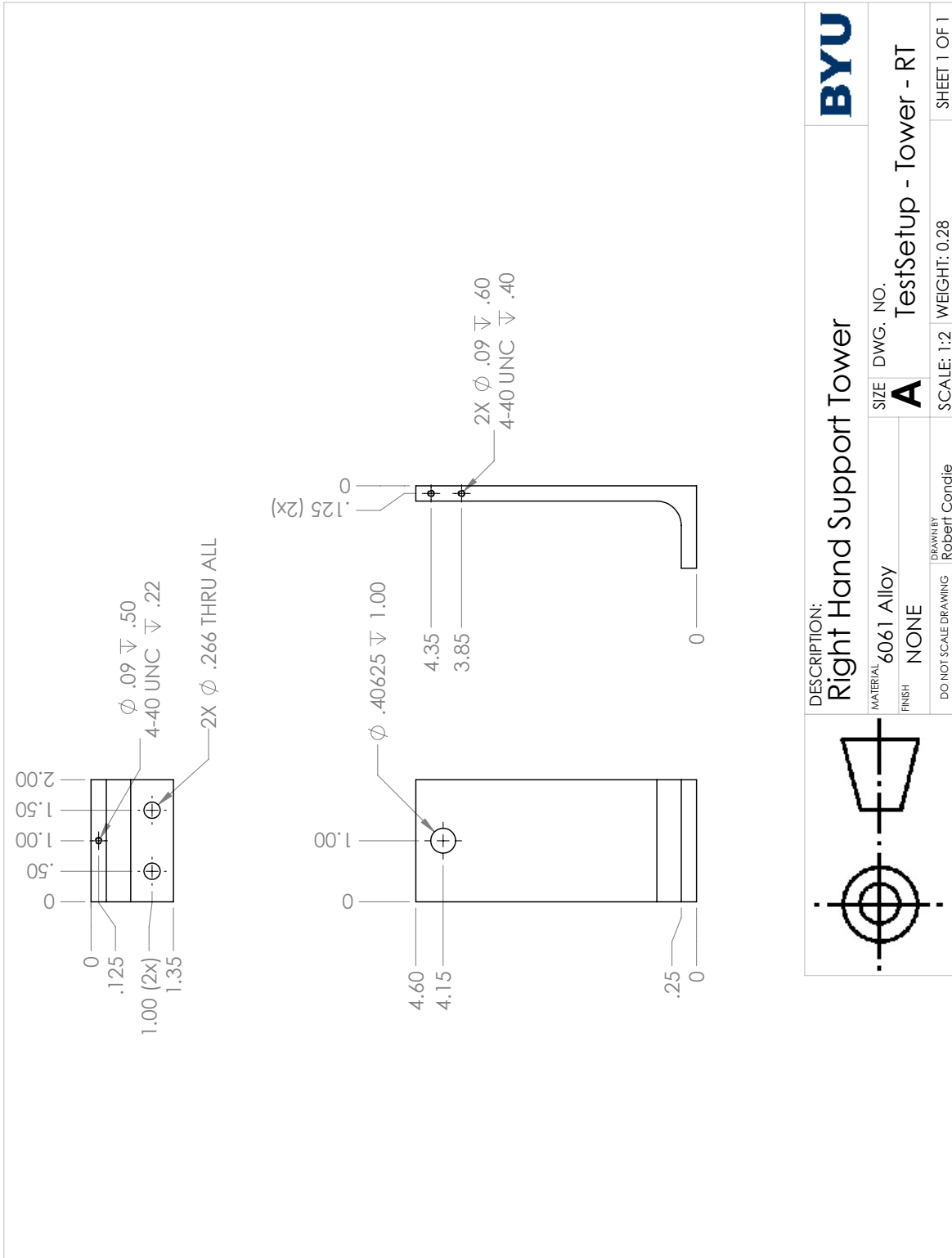


Figure A.6: Right-hand tower for the test setup assembly.

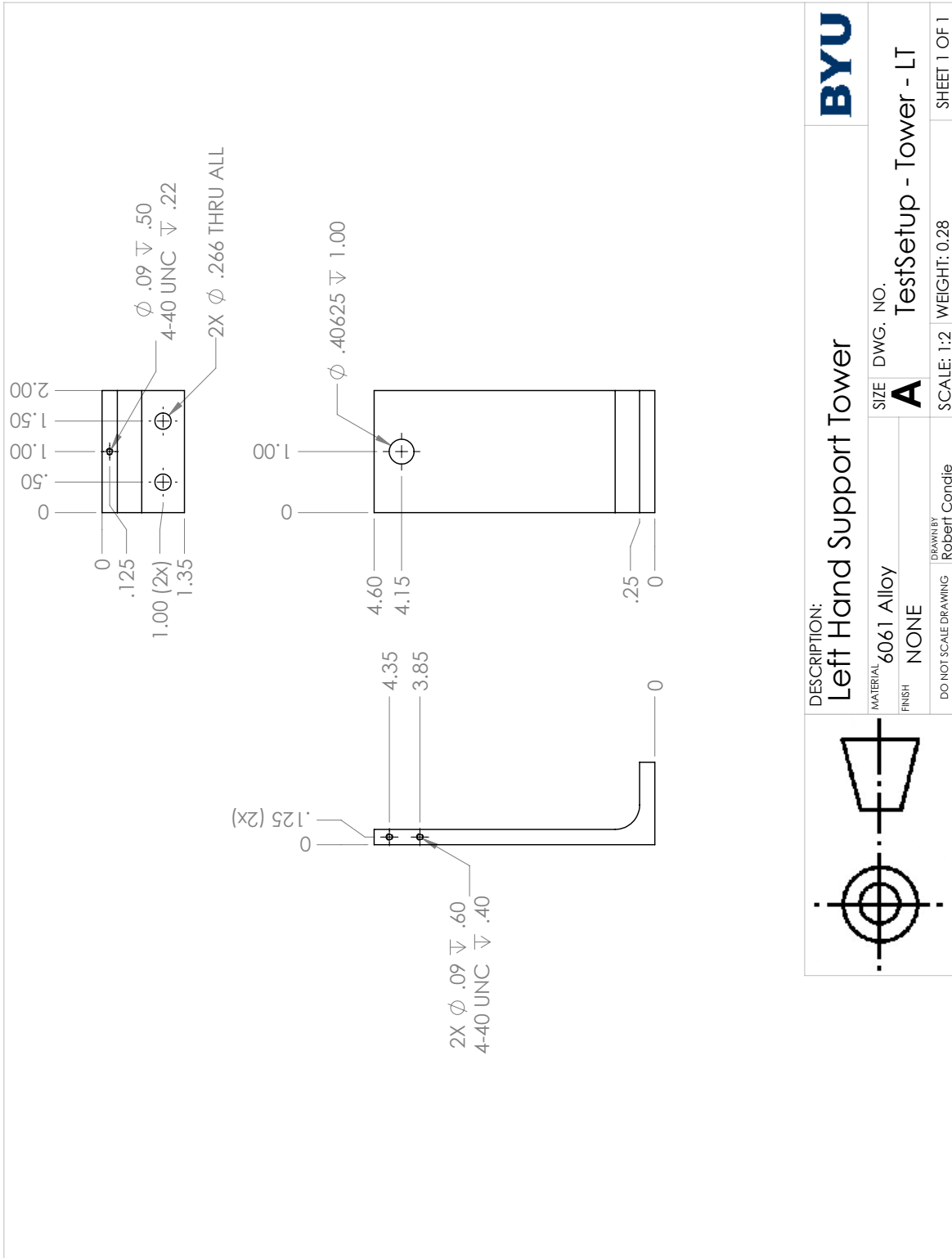


Figure A.7: Left-hand tower for the test setup assembly.

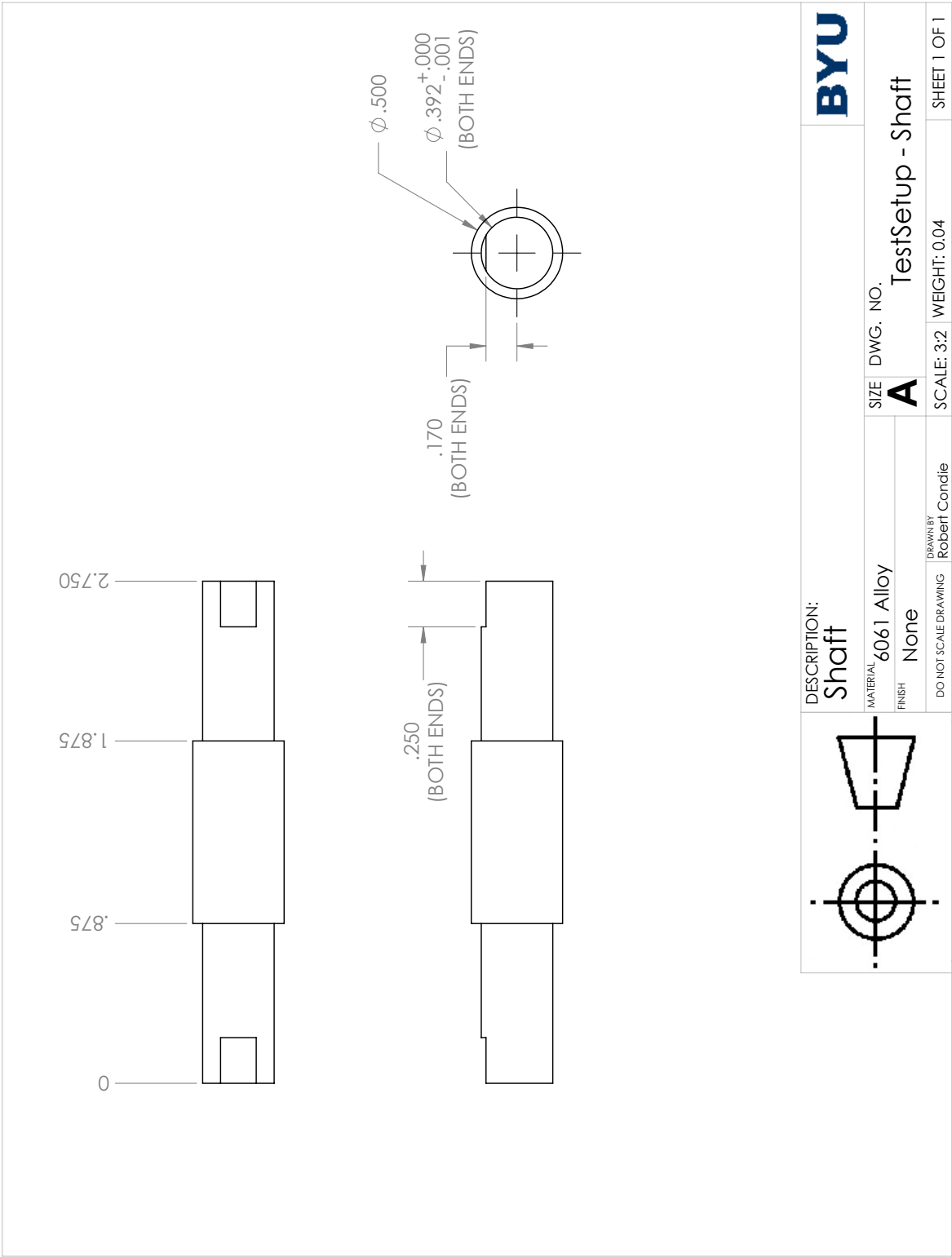


Figure A.8: Shaft used to carry the bearings for the test setup assembly.

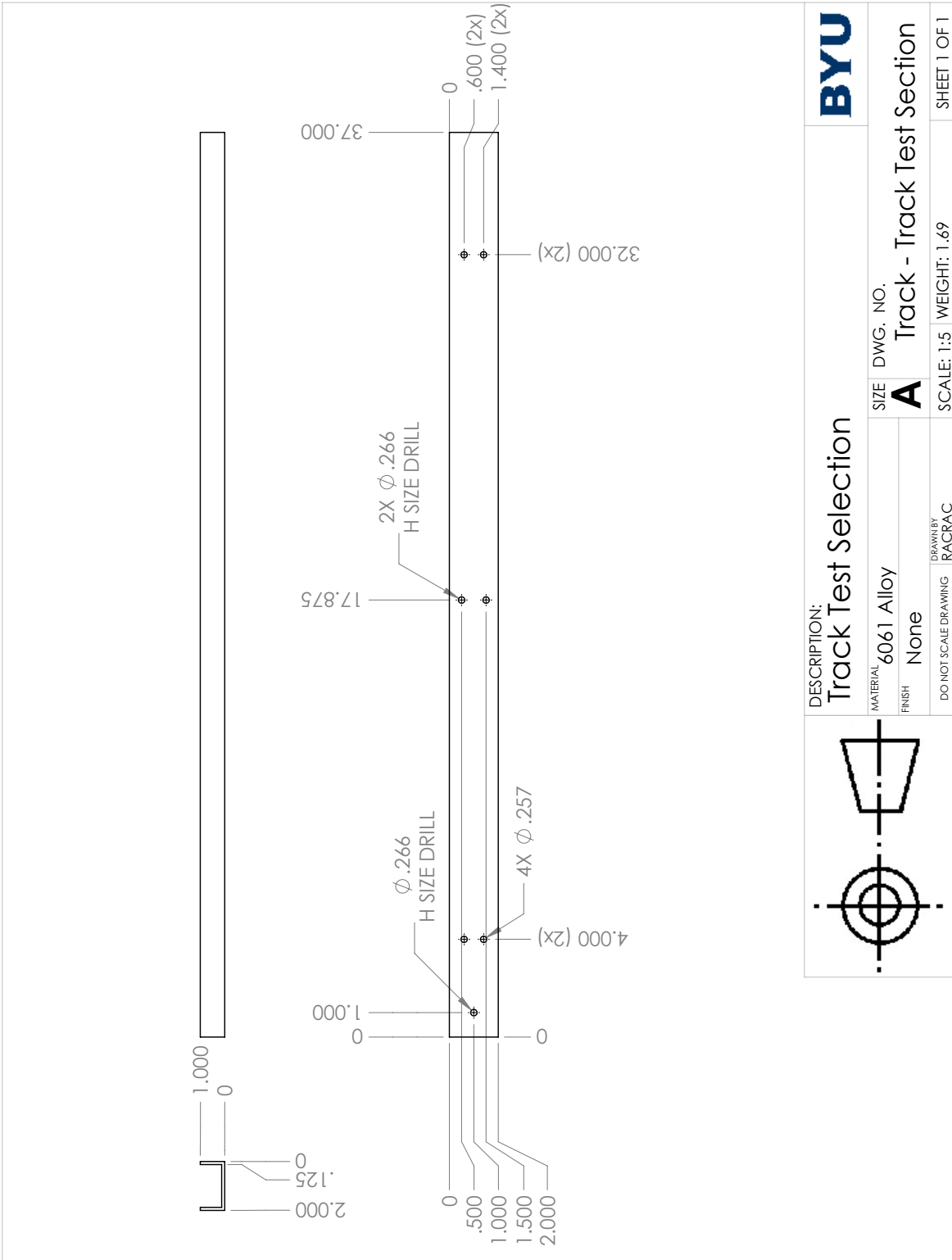


Figure A.9: Channel section used as the track for the test setup assembly.

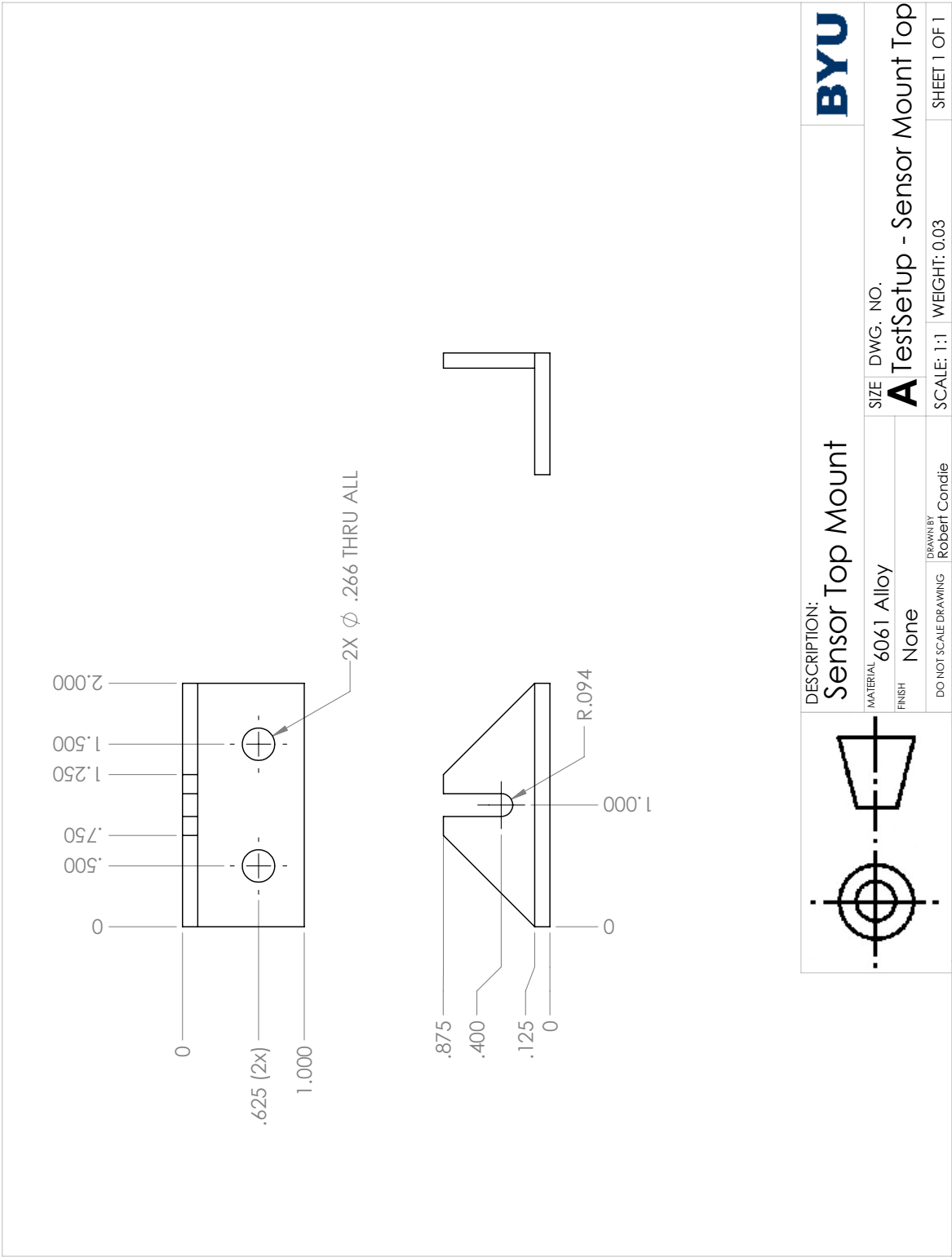


Figure A.10: Top mount for the single load cell configuration of the test setup assembly.



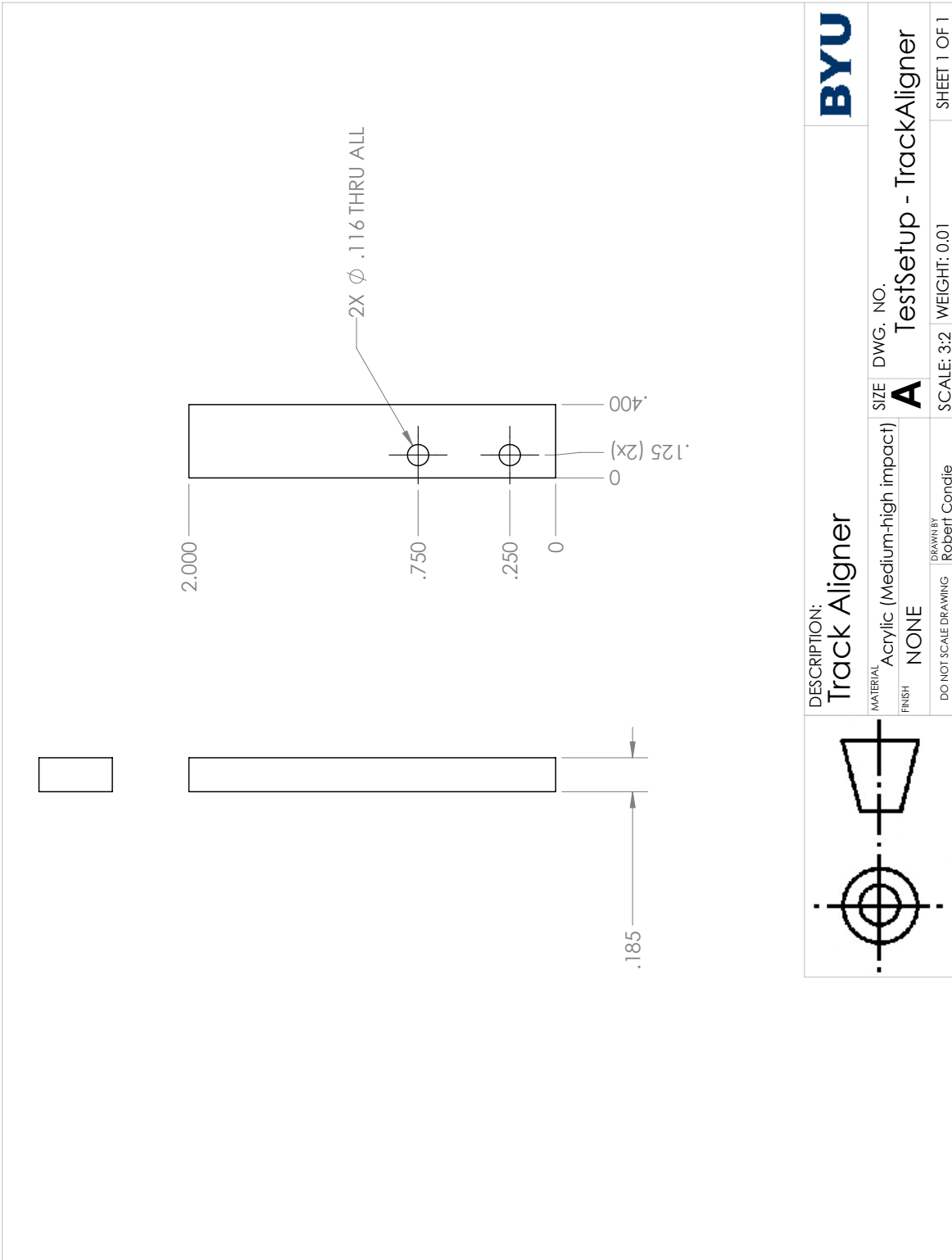


Figure A.11: Track aligner for the test setup assembly.

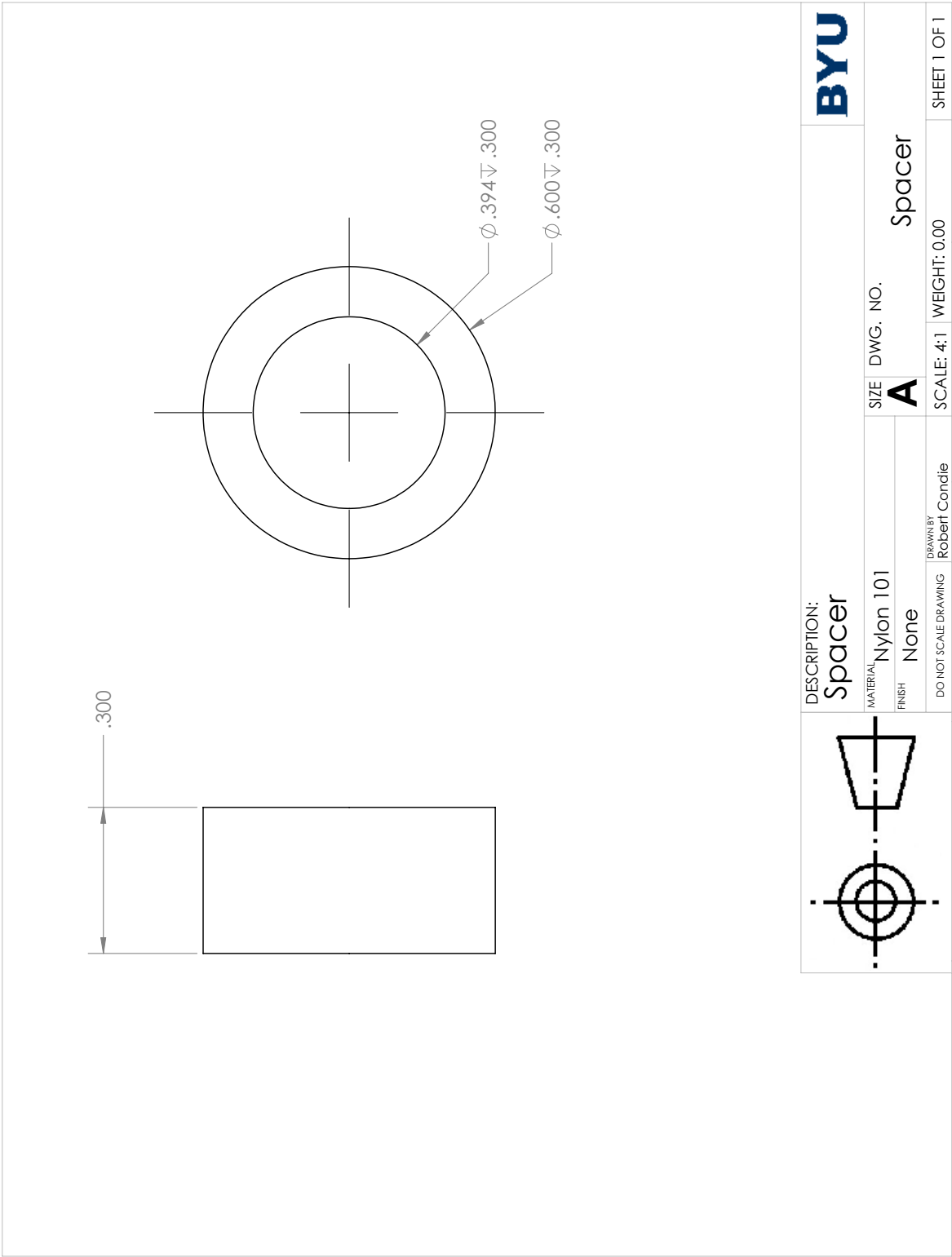


Figure A.12: Spacer used on the shaft to position the bearing for the test setup assembly.

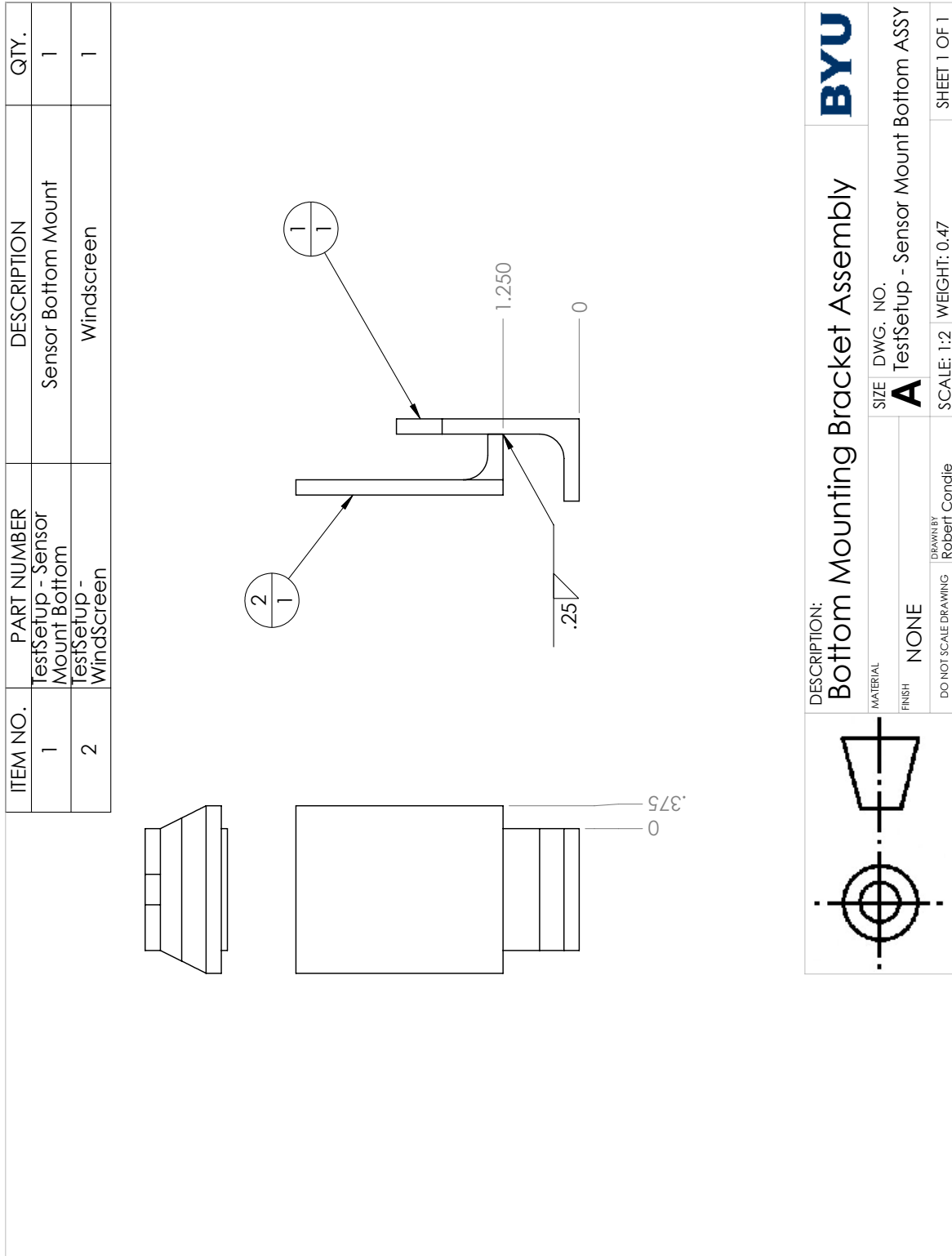


Figure A.13: Bottom mount weldment of the bottom mount for the test setup assembly.

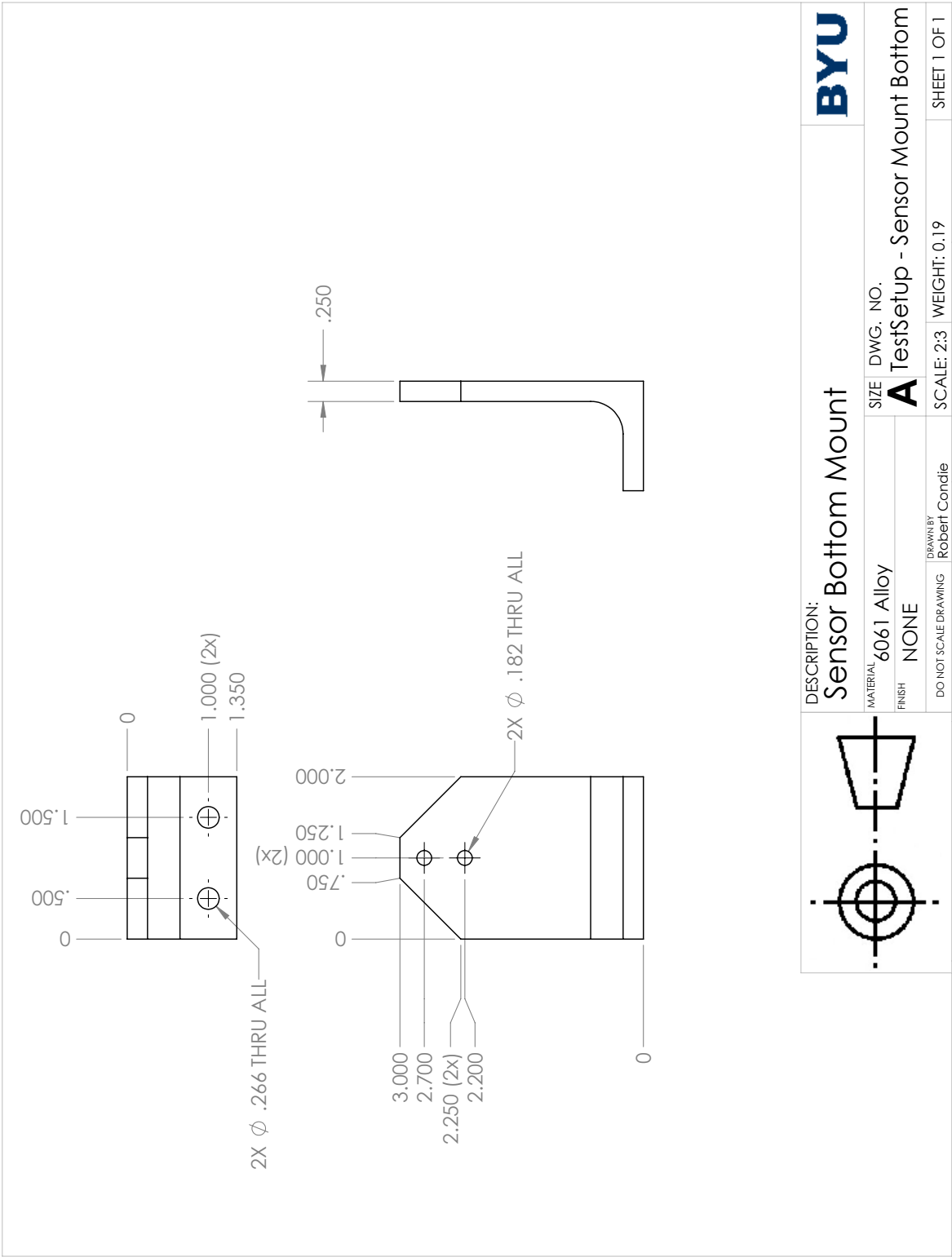


Figure A.14: Bracket section of the bottom mount for the test setup assembly.

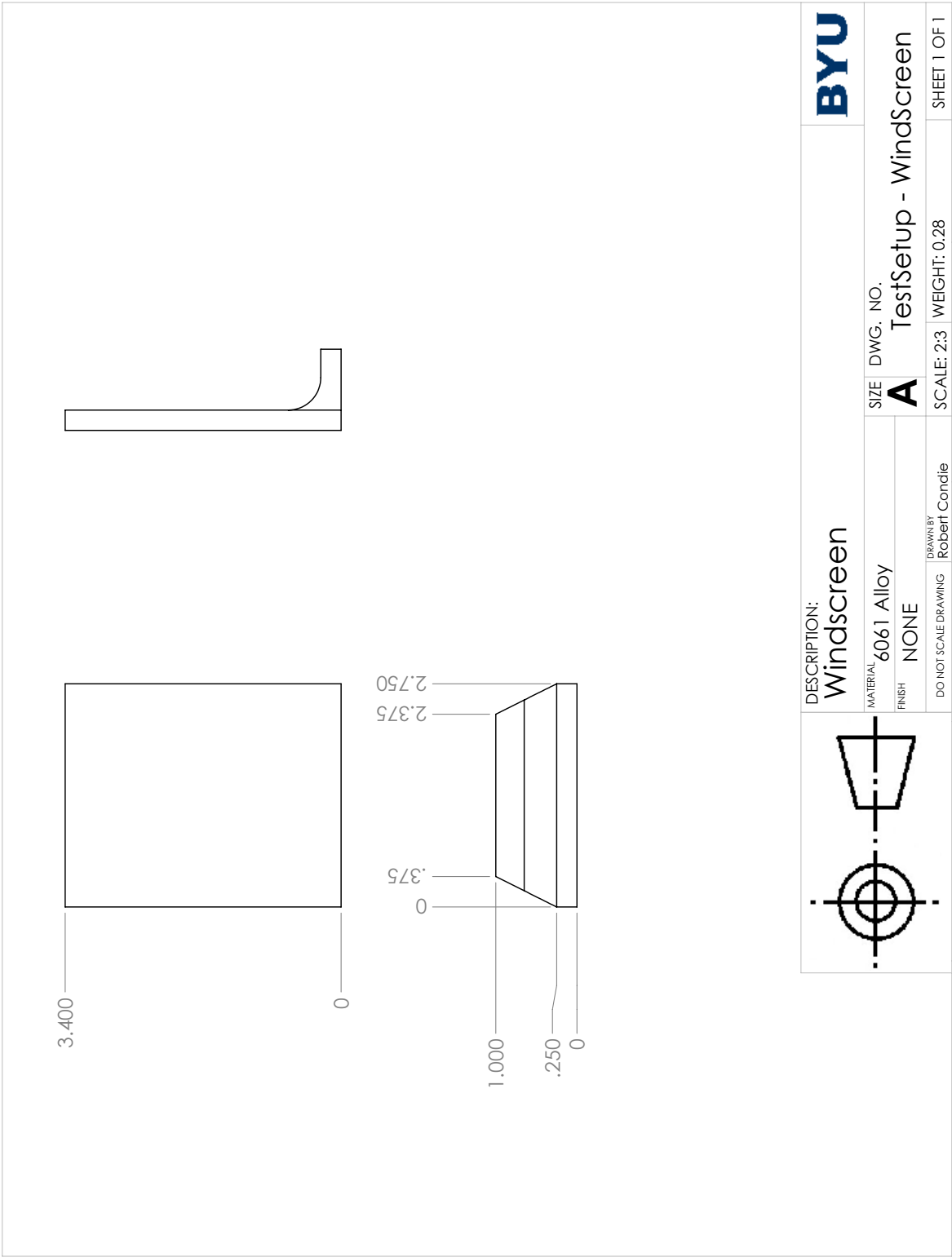


Figure A.15: Wind screen section of the bottom mount for the test setup assembly.

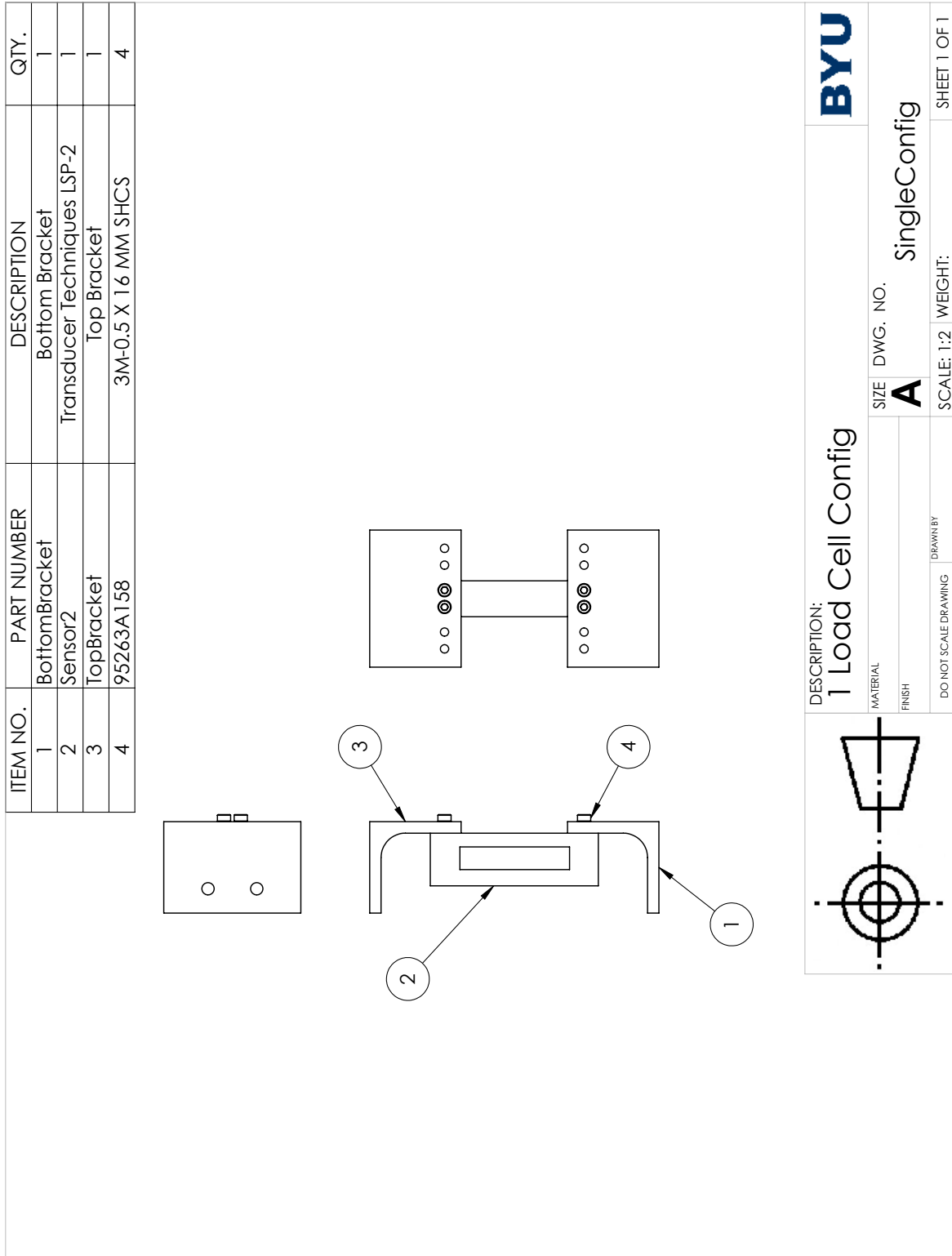


Figure A.16: Single load cell assembly used in the multi load cell test setup.

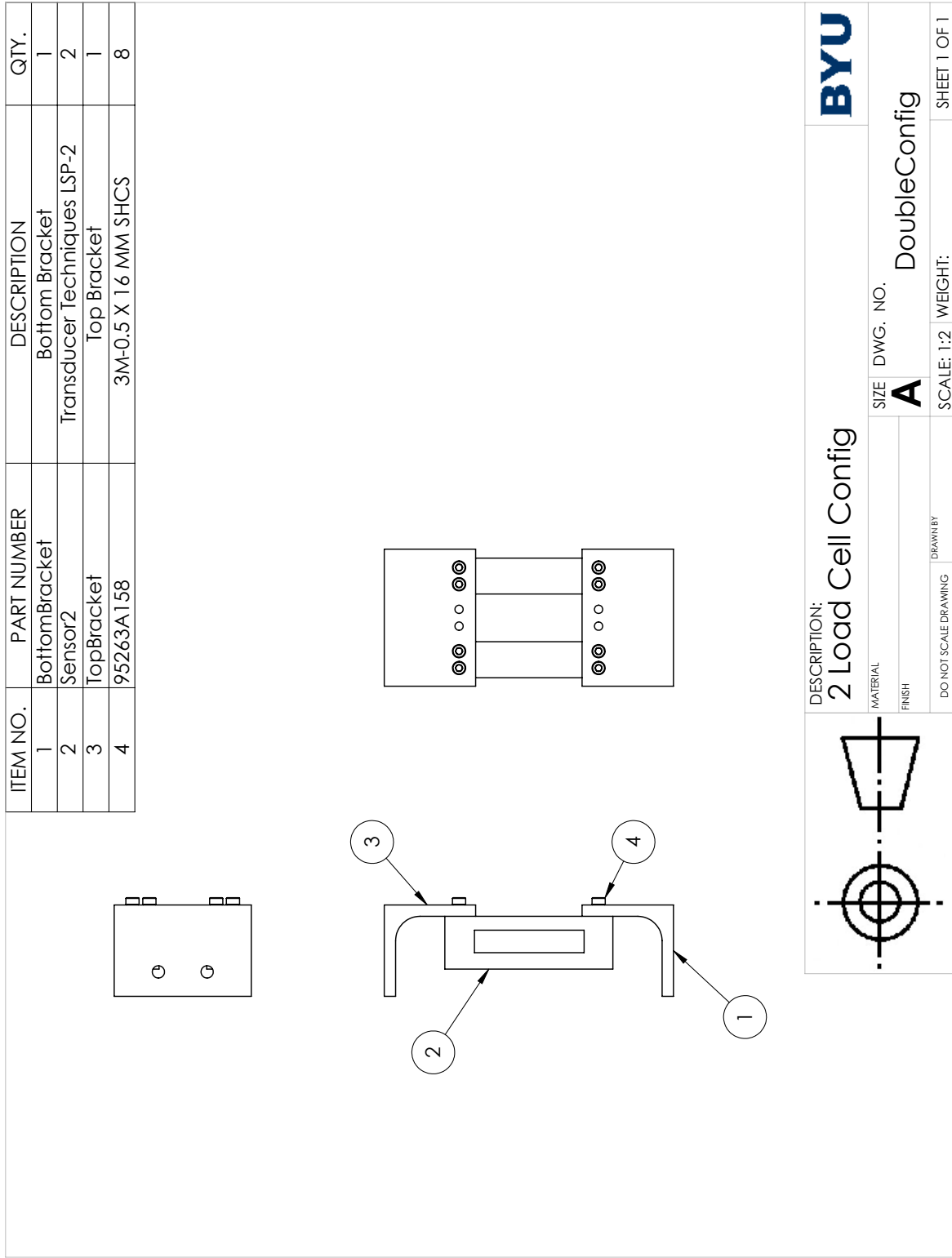


Figure A.17: Double load cell assembly used in the multi load cell test setup.

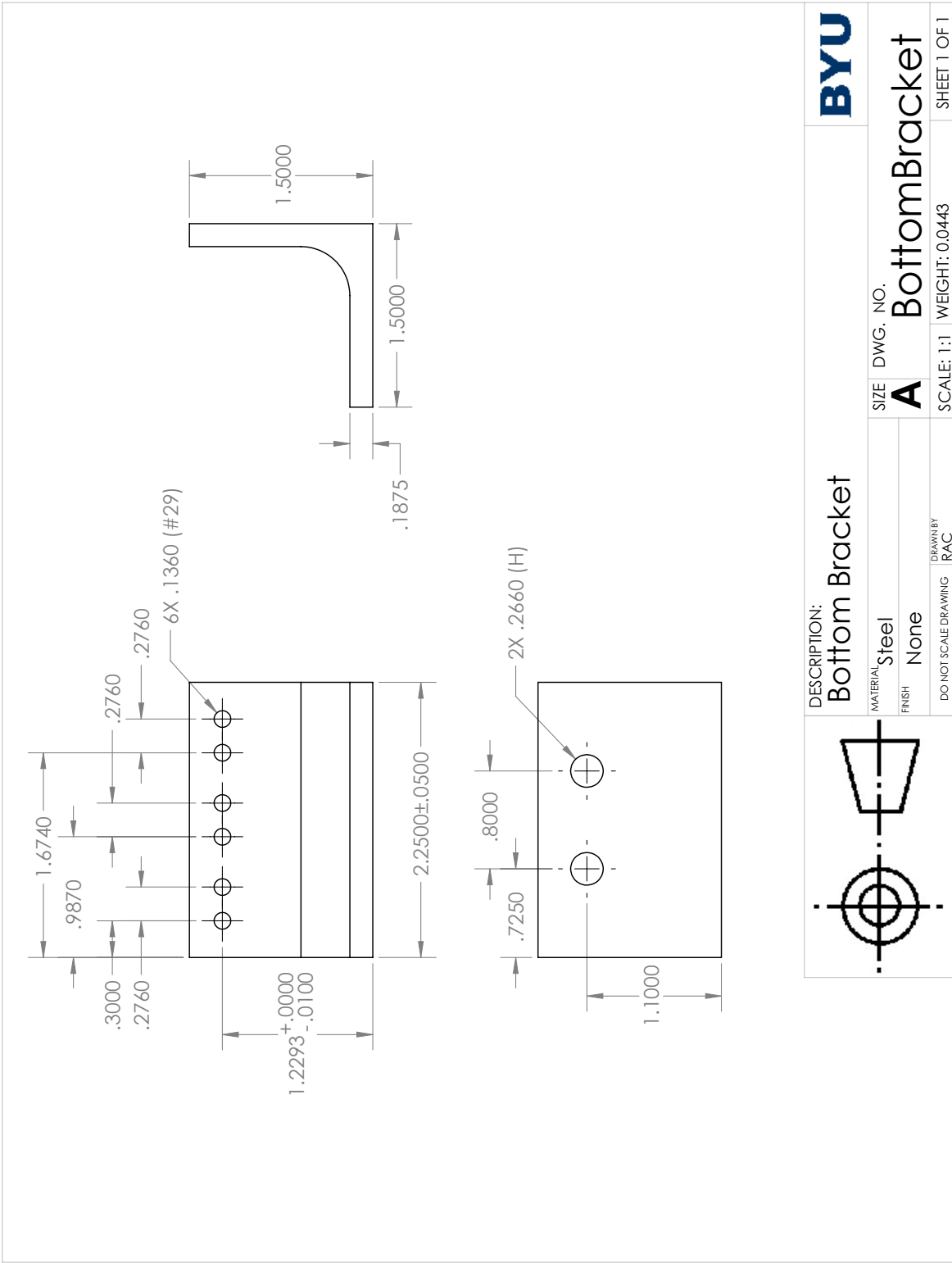


Figure A.18: Bottom bracket for the multi load cell test setup.



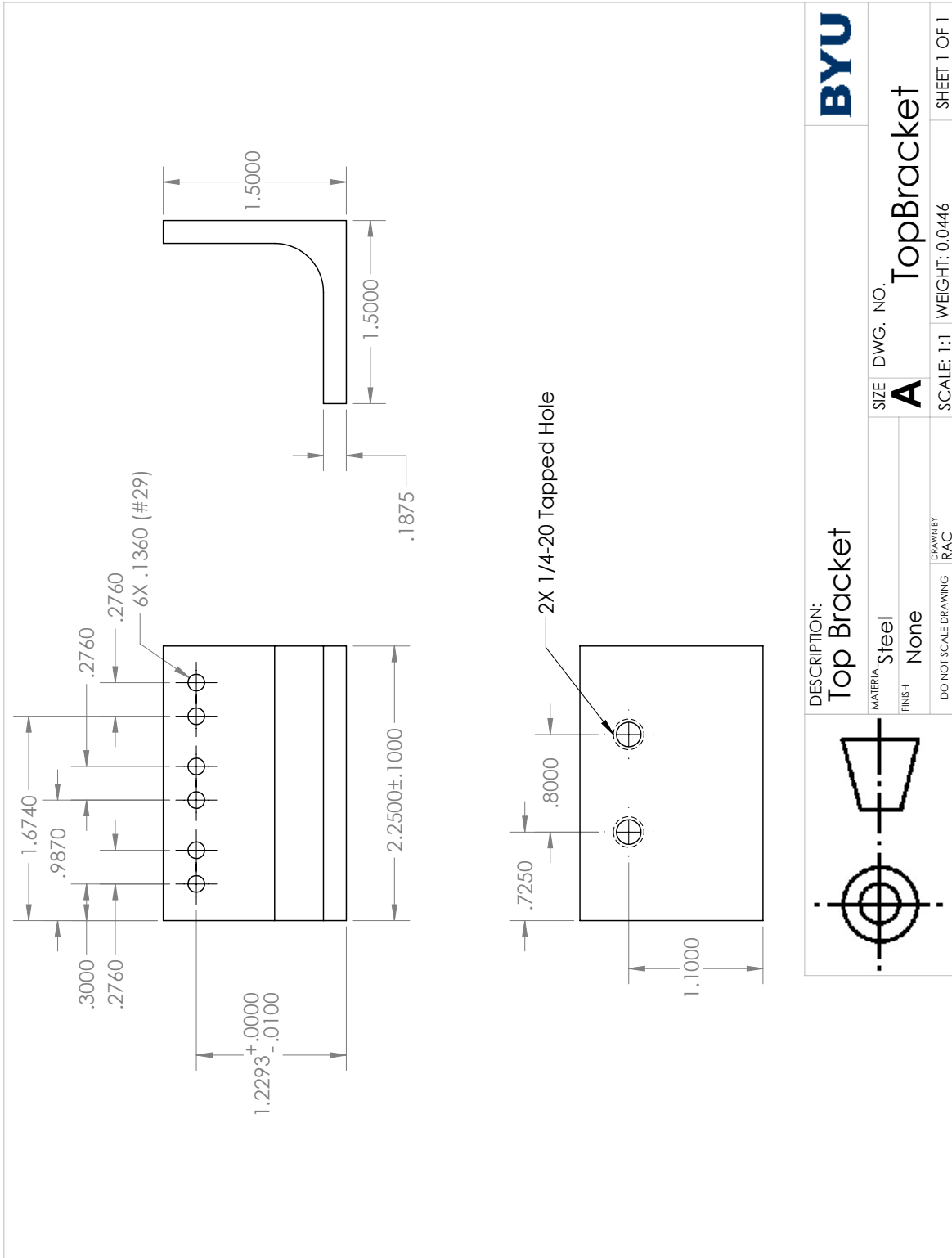


Figure A.19: Top bracket for the multi load cell test setup.

**APPENDIX B. SIDE PANEL DESIGNS**

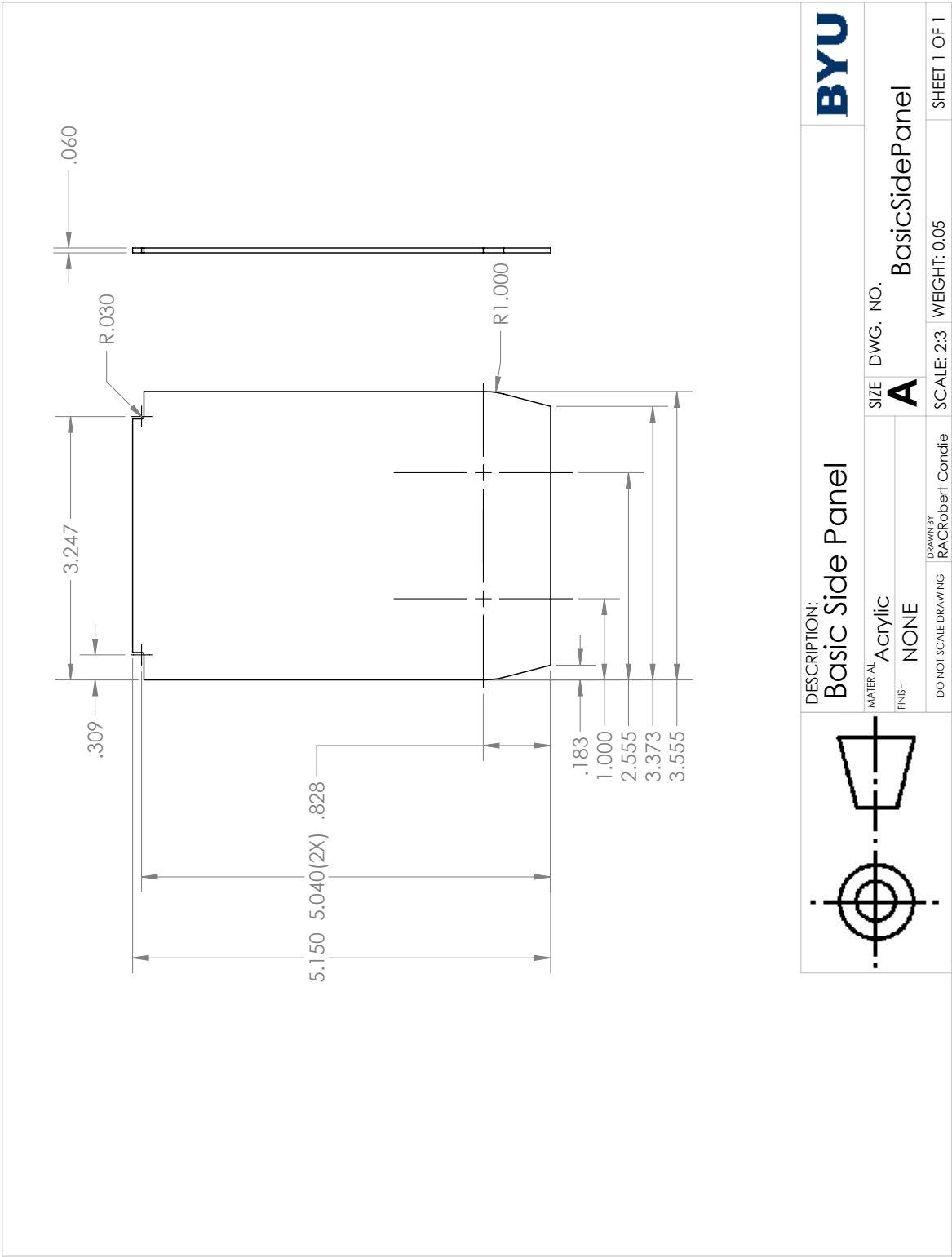


Figure B.1: Large smooth side panels

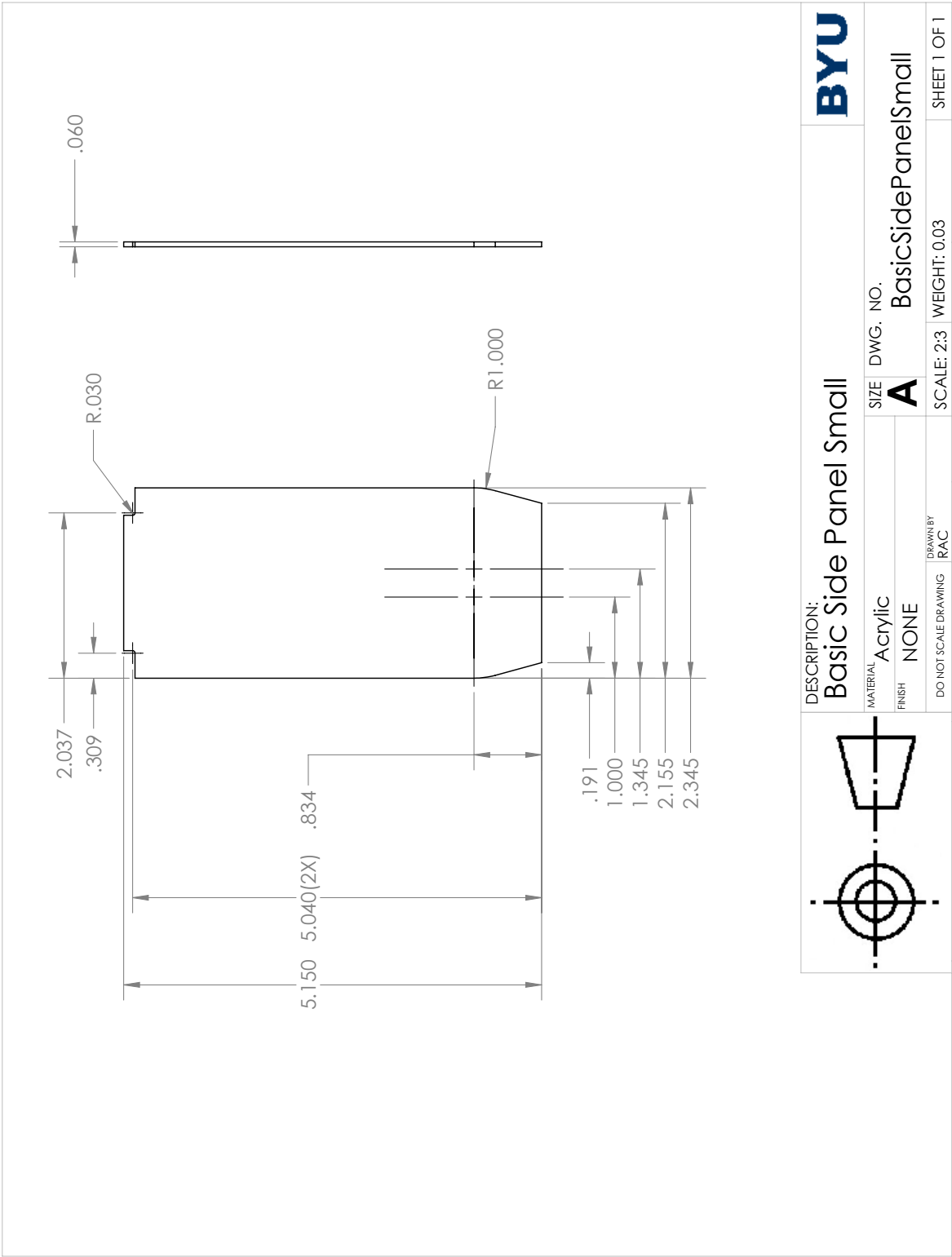


Figure B.2: Small smooth side panels

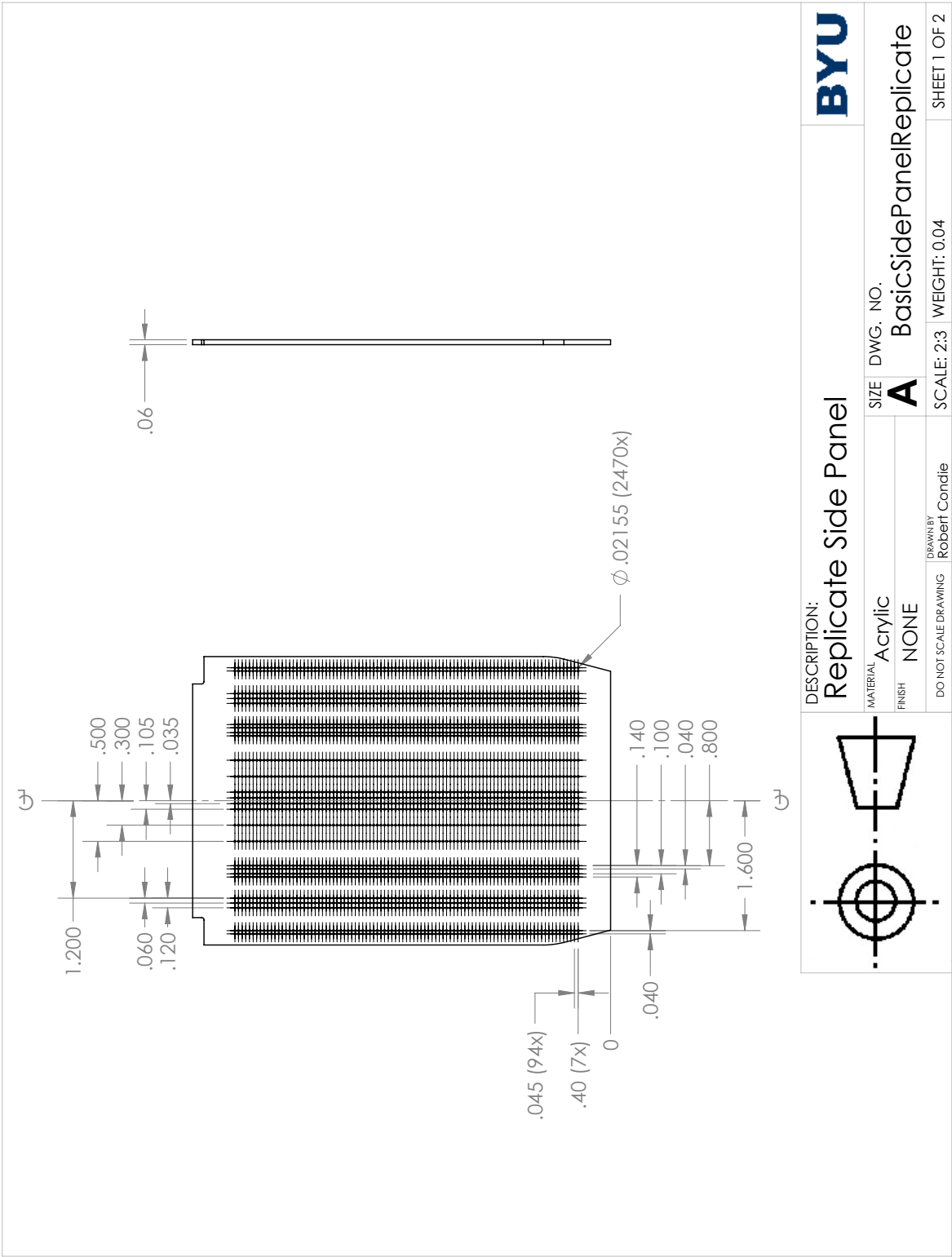


Figure B.3: Large replica side panels page 1

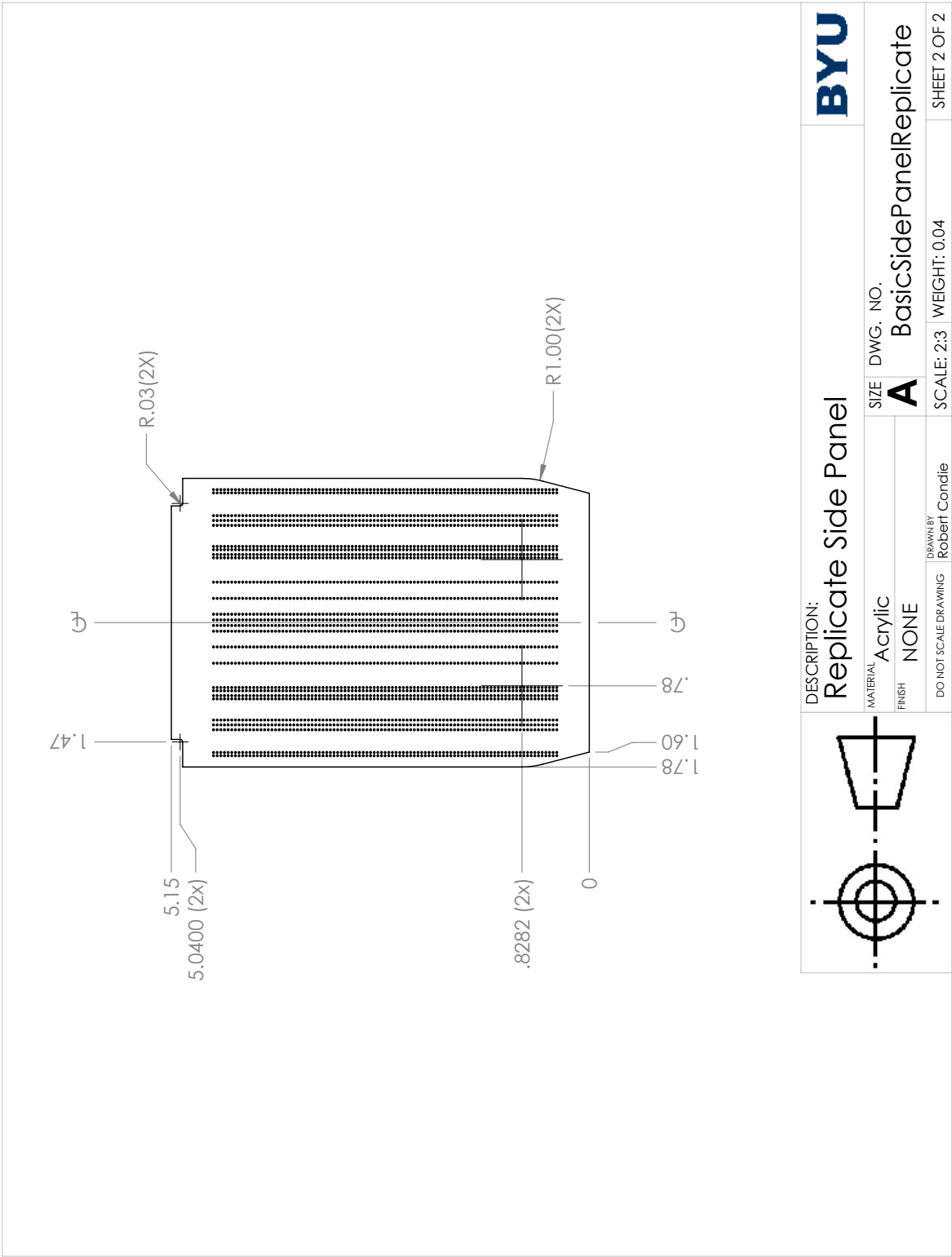


Figure B.4: Large replica side panels page 2

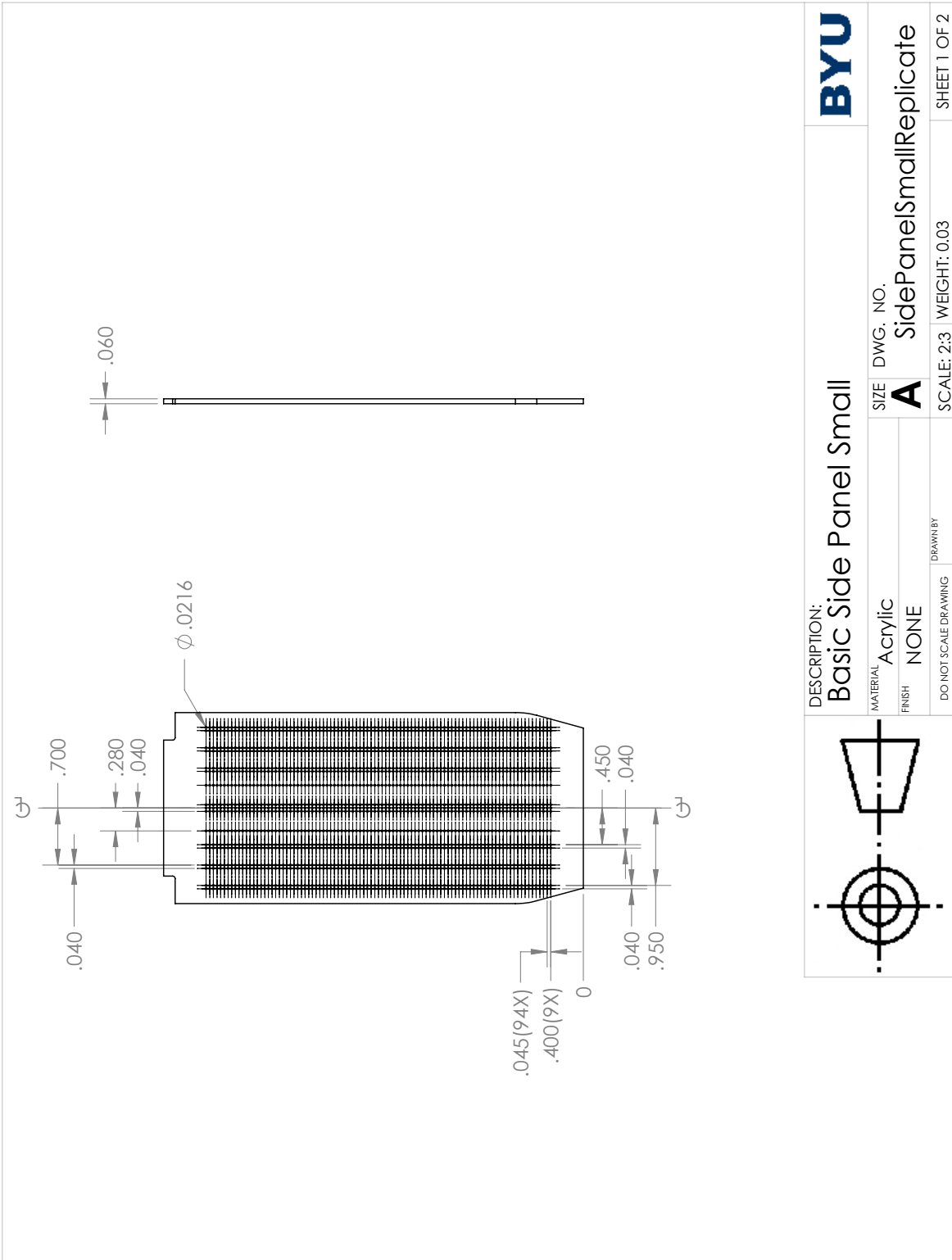


Figure B.5: Small replica side panels page 1

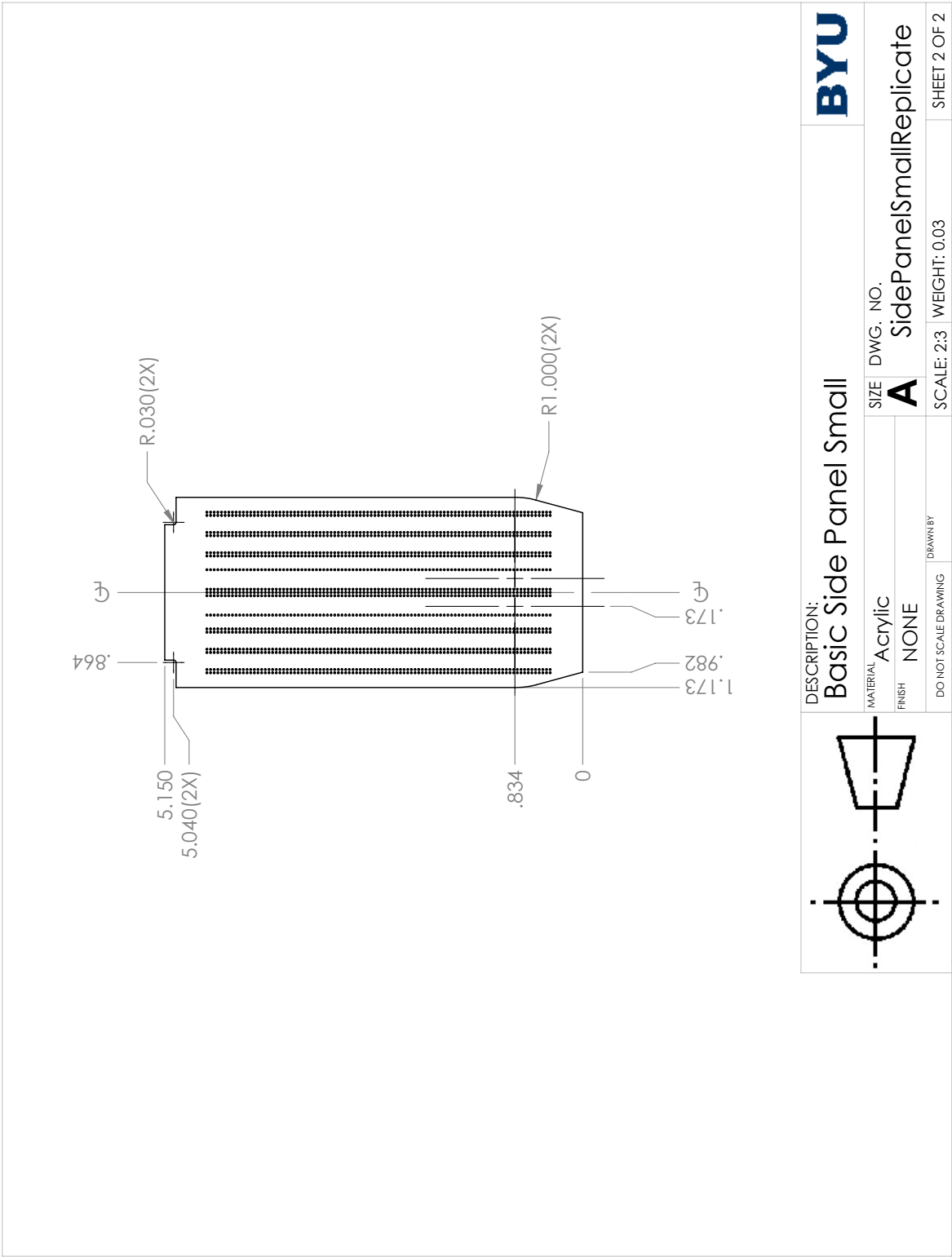


Figure B.6: Small replica side panels page 2



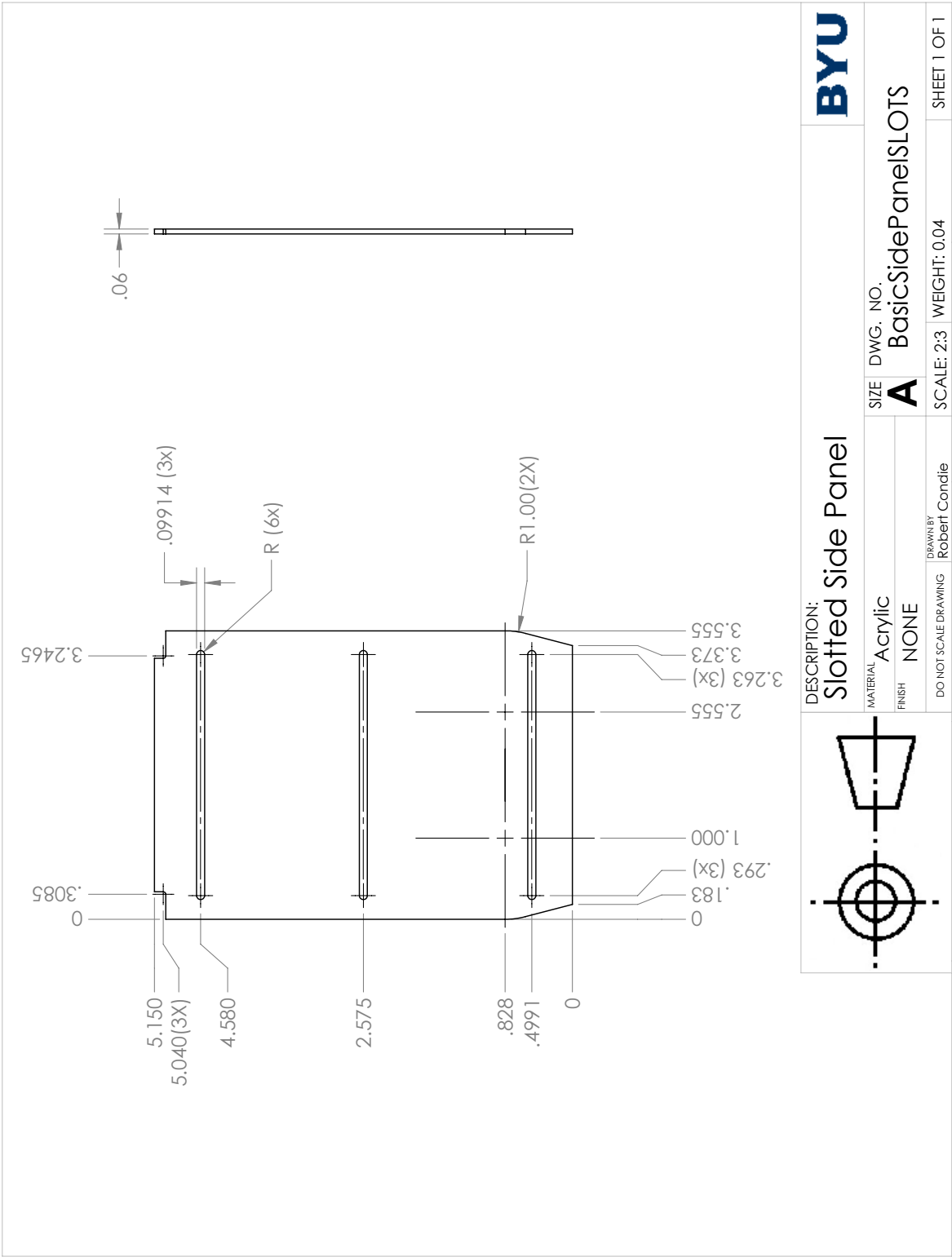


Figure B.7: Large slotted side panels

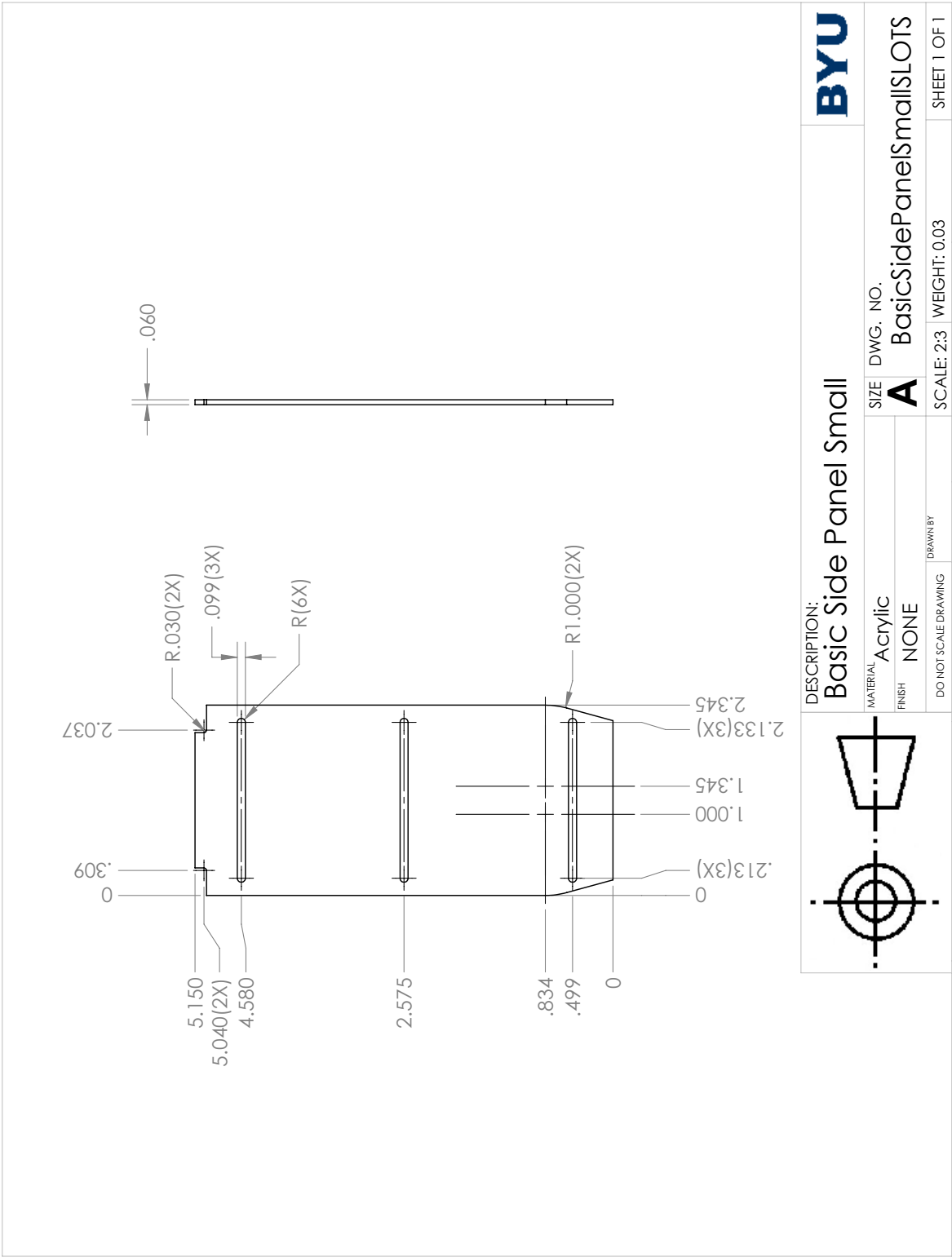


Figure B.8: Small slotted side panels

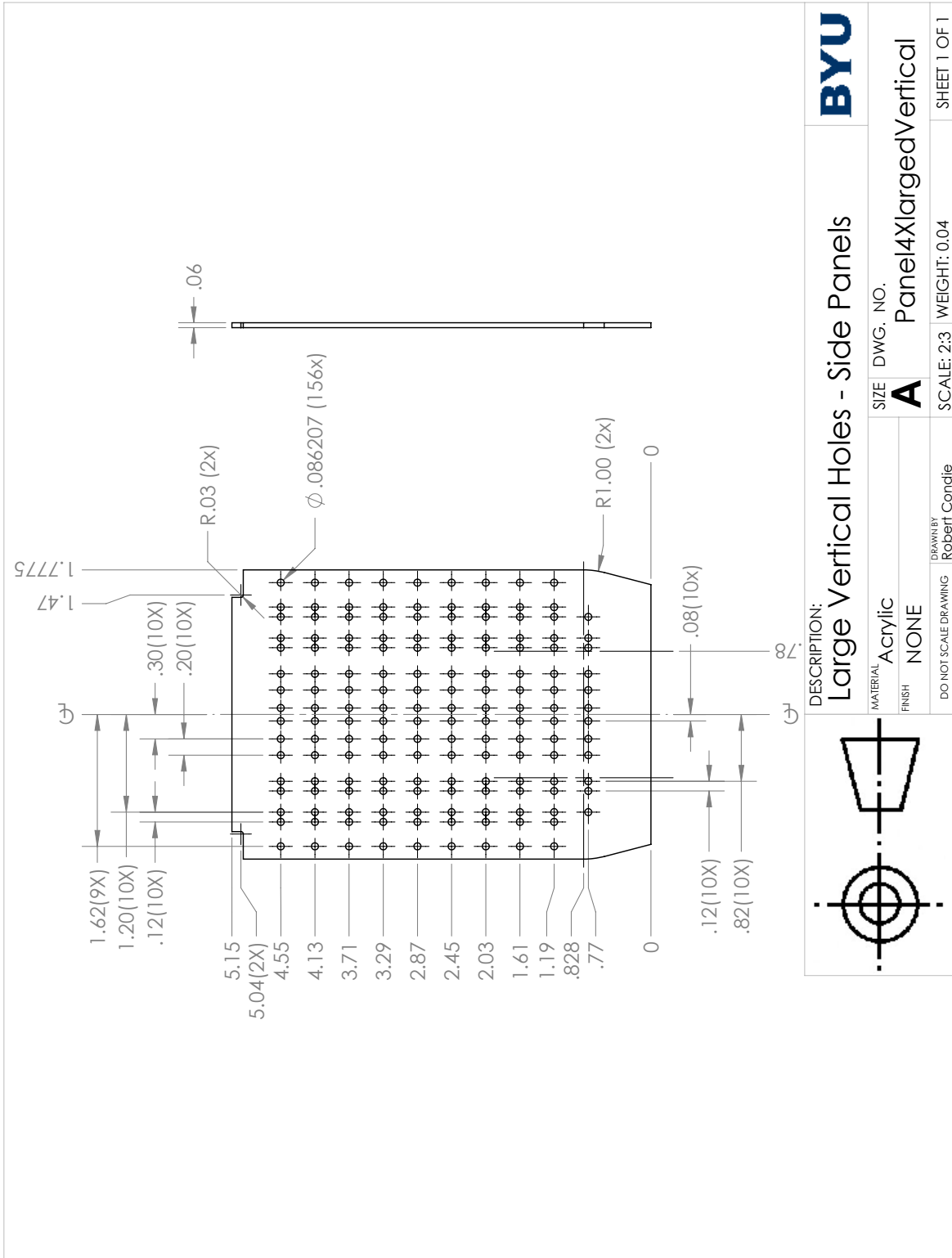


Figure B.9: Large spaced side panels with larger holes

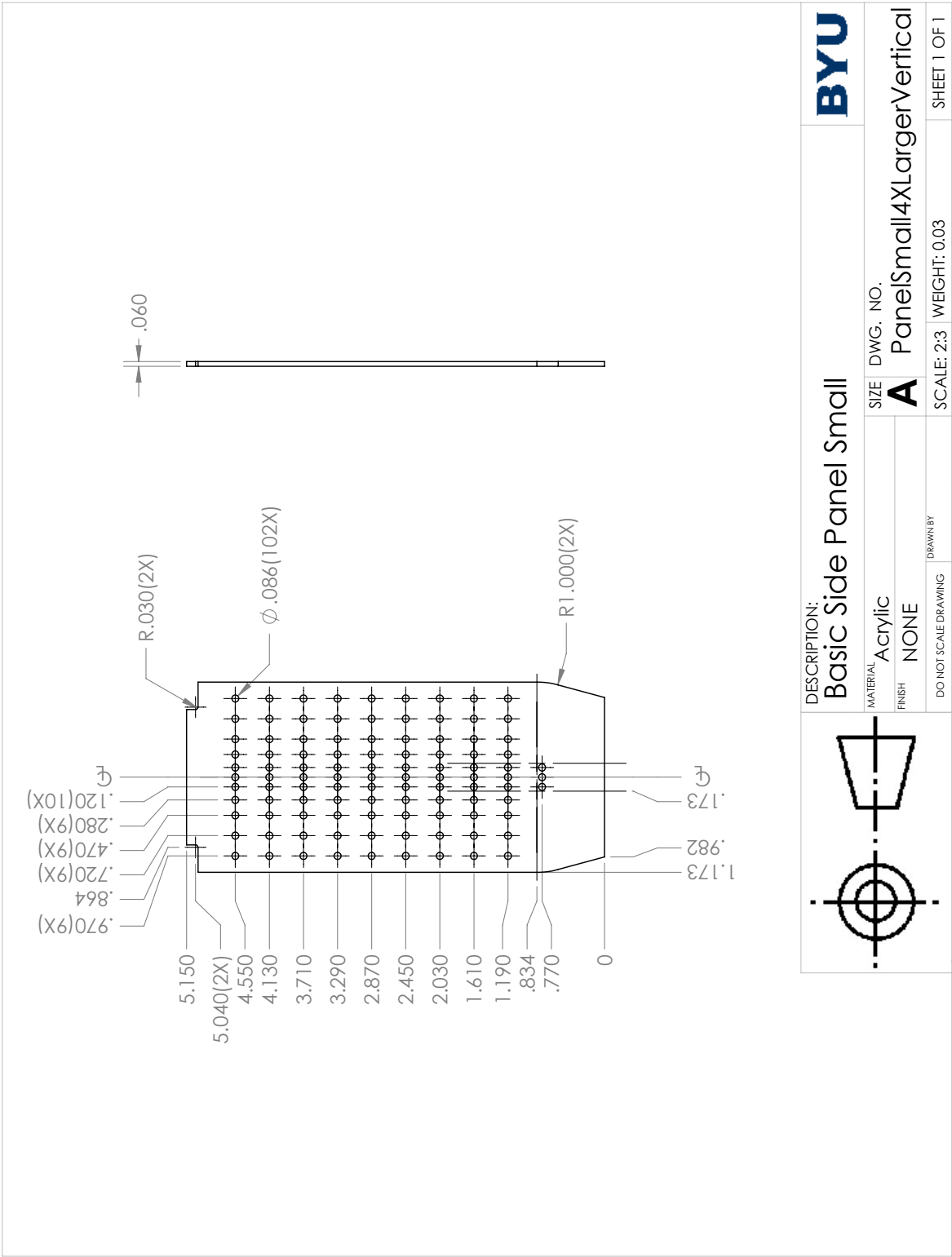


Figure B.10: Small spaced side panels with larger holes



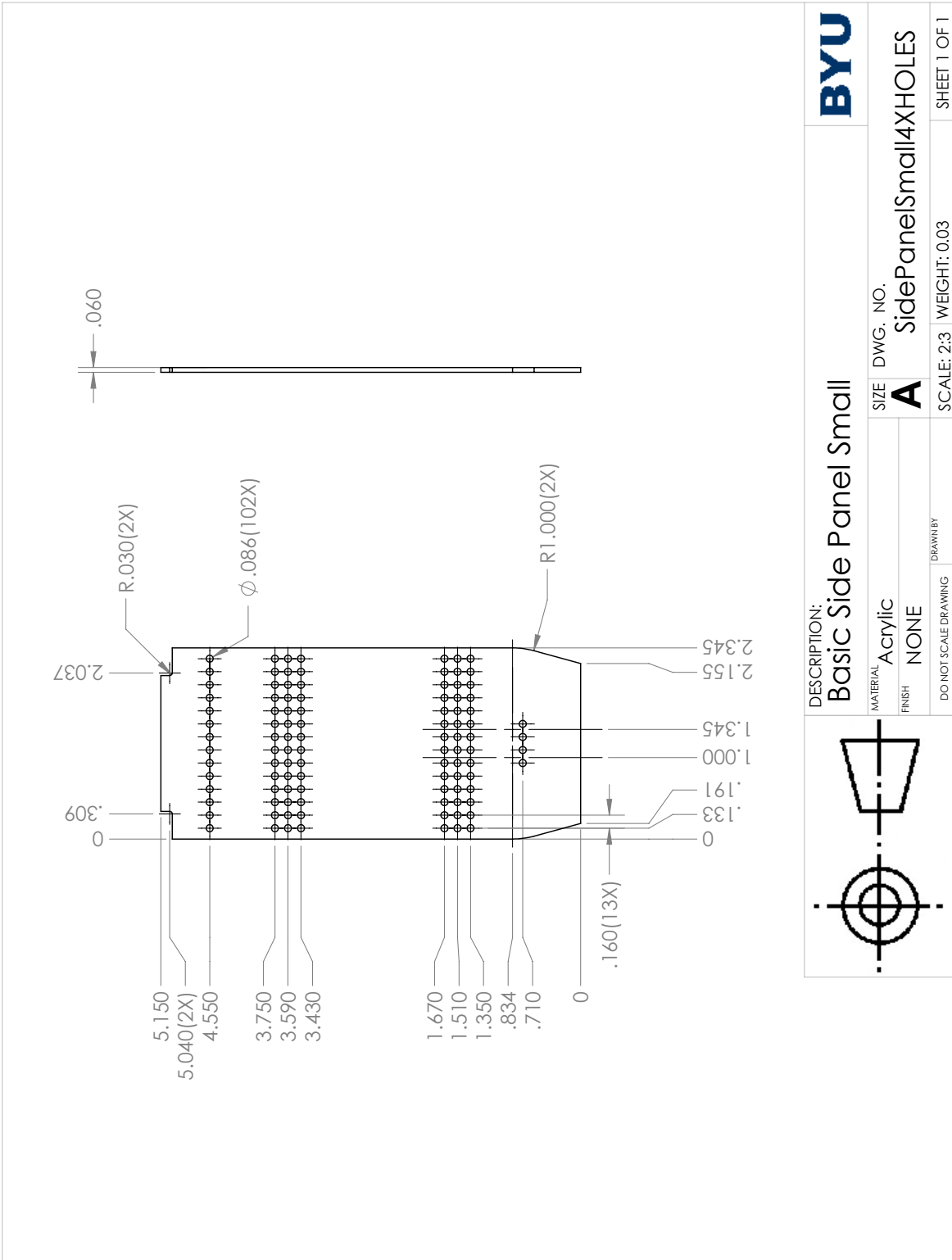


Figure B.12: Small grouped side panels with larger holes

## APPENDIX C. MATLAB ANALYSIS CODE

```
1 % Robert Condie
2 % Analysis for Master's Research: Aerodynamic Improvements on Auto-Carrying Railcars
3
4 % This code calculates the Resistance Force as determined by the Davis Equation for different
   Railcar Modifications.
5
6 % This code analyzes wind tunnel data and plots the results.
7
8 % Changable Parameters are a follows:
9 % ANALYSIS (Line 136) will indicate whether the analysis follows the Canadian National
   Approximation or the Association of American Railroads
10 % PLOT (Line 692) will toggle whether the results will be plotted or not
11 % Nloc (Line 256) sets the number of locomotives that will be used in the
12 % analysis
13 % Nauto (Line 257) sets the number of railcars used in the analysis
14 % User needs to add modification names to output array
15 %%%%%%%%%%%%%%%%%%%%%%%%%%%%%%%%%%%%%%%%%%%%%%%%%%%%%%%%%%%%%%%%%%%%%%%%%%
16
17 %Notes:
18 % Cover 0 is the corrugated roof = Data{1}
19 % Cover 1 is the smooth roof without a lip = Data{2}
20 % Cover 2 is the Belly Cover on the chassis = Data{3}
21 % Cover 3 is the smooth roof with a lip = Data{4}
22 % Cover 4 is the full length chassis skirt = Data{5}
23 % Num— 5 i2 the Average of the Smooth Roof w/ and w/o lip = Data{6}
24 % Cover 6 is the Partial chassis skirt (gaps around wheels) = Data{7}
25 % Cover 7 is the a replica of the current production side panels = Data{8}
26 % Cover 8 is the Smooth, no ribbed panels = Data{9}
27 % Cover 9 is the Light Corrugated Car with smooth ribbed panels = Data{10}
28 % Cover 10 is the 4x larger holes patterned panels aligned with the flow = Data{11}
29 % Cover 11 is the slotted side panels = Data{12}
30 % Cover 12 is the 4x larger vertically aligned holes side panels = Data{13}
31 % Cover 13 is the Replica Baseline = Data{14}
32 % Cover 14 is the Replica with belly cover, best tested side panels and smooth roof = Data{15}
33 % Cover 15 is the Replica with best side panels and smooth roof = Data{16}
34 % Cover 16 is the Replica with smooth top = Data{17}
35 % Cover 17 is the replica model with V-fairing and belly cover, best
```

```

36 % tested sides and smooth roof = Data{18}
37 % Cover 18 is the Replica with best sides only = Data{19}
38 % Cover 19 is the Replica with smooth top retest = Data{20}
39 %%
40 format long g
41 clear all;
42 clc;
43 close all;
44
45 % Add graphics handling files
46 addpath('C:\Users\Rob\Dropbox\export_fig')
47 % Support files for graphics handling
48 addpath('C:\Users\Rob\Dropbox\xpdfbin-win-3.03\xpdfbin-win-3.03\bin64')
49 % Add function file that find the intersect of two lines
50 addpath('C:\Users\Rob\Dropbox\intersections')
51
52 %%
53 tic
54 % Needed Constants
55 R = 287.04; %Ideal Gas Constant (J/kg*K)
56 Conv_v = 1.4666667; % Conversion mile/hour to ft/sec
57 Conv_rho = 0.001940320401227214; % Conversion metric to standard (kg/m^3 to slugs/ft^3)
58 Conv_f = 4.44822162; % Conversion Newtons to pounds
59 scale = 1/29; % G size Scaling factor
60 in2m = 0.0254; % Conversion inches to meters
61 in2ft = 1/12;
62 %%
63 % This block reads in the wind tunnel data that has been collected in a Spread sheet
64 CarH = (6+(5/8)); %Car Height (in)
65 CarW = (4+(1/16)); %Car Width (in)
66 %CarH = 7; %Car Height (in)
67 %CarW = 4; %Car Width (in)
68 CarL = 37; %Car Length (in)
69 CarHmetric = CarH * in2m; %Car height(m) converting from inches to meters
70 CarWmetric = CarW * in2m; %Car width(m) converting from inches to meters
71 CarLmetric = CarL * in2m; %Car Length(m)
72 Area = CarHmetric*CarWmetric; %Area (m^2)
73
74 % Set Baseline Models
75 Base1 = 1;
76 Base2 = 8;
77 Base3 = 14;
78
79 Data = struct([]); % Structure that holds wind tunnel data
80 Davis = struct([]); % Structure that holds Davis Equation variables

```



```

81 Analysis = struct([]); % Structure that holds variables for fuel consumption analysis
82 DataOut = struct([]); % Structure that holds data that is written out to an xlxs file.
83 % Most of the DataOut is important outputs from the analysis
84
85 % Read in experimental wind tunnel data
86 % Data comes in from the third sheet
87 Tunnel = xlsread('Master_File_CompositeData.xlsx',3);
88
89 for i = 1:9
90     TunnelData(:,i) = Tunnel(:,i);
91 end
92 % NumSet is the number of model configurations that have been tried
93 NumSet = max(TunnelData(:,5))+1;
94 TunnelData(:,1) = TunnelData(:,1)*(Conv_f); %Convert to Newtons from pounds
95
96 % Pull wind tunnel data into Matlab variables
97 for i = 1:NumSet
98     k=1;
99     for j = 1:length(TunnelData(:,5))
100         if(TunnelData(j,5)==i-1)
101             Data{i}.Drag(k,1) = TunnelData(j,1); %Drag Data (N)
102             Data{i}.Velocity(k,1) = TunnelData(j,4); %Speed Data (m/s)
103             Data{i}.Temperature(k,1) = TunnelData(j,3); %Temperature Data (K)
104             Data{i}.Pressure(k,1) = TunnelData(j,6); %Pressure Data (Pa)
105             Data{i}.Density(k,1) = TunnelData(j,6)/(R*TunnelData(j,3)); %Density (kg/m^3)
106             Data{i}.Viscosity(k,1) = -0.0000000001*TunnelData(j,3)^2+0.00000005*TunnelData(j,3)
                +0.000004;
107             % Correlation for dynamic viscosity taken from Munson, et. al. Text (kg/m*s)
108             Data{i}.ReNumber(k,1) = (Data{i}.Density(k,1)*Data{i}.Velocity(k,1)*CarWmetric)/Data{
                i}.Viscosity(k,1); %Calculate Reynolds Number (rho*v*1)/mu
109             Data{i}.Cd(k,1) = (2*Data{i}.Drag(k,1))/(Data{i}.Density(k,1)*Area*Data{i}.Velocity(k
                ,1)^2); %Calculate Cd (2*F)/(rho*A*V^2)
110             k=k+1;
111         end
112     end
113 end
114
115 for i = 1:NumSet
116     Data{i}.MeanCd = mean(Data{i}.Cd(:,1)); % Calculate mean Cd for orientation
117     Data{i}.MeanRe = mean(Data{i}.ReNumber(:,1)); % Calculate mean Re #
118     if i == 6
119         Data{6}.MeanCd = (Data{2}.MeanCd + Data{4}.MeanCd)/2;
120         Data{6}.MeanRe = (Data{2}.MeanRe + Data{4}.MeanRe)/2;
121     end
122 % Calculate Percent Reduction between Corrugated Roof and given orientation

```

```

123 end
124 for i = Base1:(Base2-1)
125     Data{i}.PercentReduc = abs((Data{Base1}.MeanCd - Data{i}.MeanCd)/Data{Base1}.MeanCd)*100;
126 end
127 for i = Base2:(Base3-1)
128     Data{i}.PercentReduc = abs((Data{Base2}.MeanCd - Data{i}.MeanCd)/Data{Base2}.MeanCd)*100;
129 end
130 for i = Base3:NumSet
131     Data{i}.PercentReduc = abs((Data{Base3}.MeanCd - Data{i}.MeanCd)/Data{Base3}.MeanCd)*100;
132 end
133 %%
134
135 ANALYSIS = 1;
136 % ANALYSIS = 1 -> follow Candian National (B term is used)
137 % ANALYSIS = 2 -> follow AAR (B term is assumed negligible)
138
139 % Read in TEvsV data
140 % This is the data specific to the locomotive
141 TracData = xlsread('C44AC speed v TE chart_analysis','DATA');
142 for i = 1:size(TracData,2)-1
143     N(:,i) = TracData(:,i+1);
144 end
145
146 V = TracData(:,1); % Velocity (mph)
147 V_ft = V*Conv_v; % Change velocity from mph to ft/s
148
149 % Formulation from Canadian National Train Resistance
150 % Analysis for Multi-level Auto Transporter (Auto)
151 % R = 1.5 + 18*N/W + 0.045V + C*A*V^2/(10000*W)
152 % Note: B = 0.03 for locomotives and 0.045 for railcars
153
154 % Canadian National Variables
155 W_can = 73; % Weight per car (tons)
156 N_can = 4; % Number of axles per car
157 w_can = W_can/N_can; % Weigth per axle (tons/axle)
158 bdyn_can = 0.045; % Flange Friction Coefficient
159 Cd_can = 7.1; % Gussed Drag Coefficient
160 Area_can = 170; % Full Scale Cross-sectional area
161 RollResist_can = 1.5; % Rolling Resistance term (lbf/ton)
162 Bearing_can = 18; % Bearing Resistanct (lbf/axle)
163
164 % Put values into Davis Equation Coefficients
165 A1_can = RollResist_can;
166 A2_can = (Bearing_can*N_can)/W_can;
167 B_can = bdyn_can;

```

```

168 C_can = Cd_can;
169 A_can = A1_can + A2_can;
170
171 for ii = 1:length(V)
172     AA_can(ii) = A_can;
173 end
174 BB_can = B_can*V';
175 CC_can = ((C_can*Area_can)/(10000*W_can))*V'.^2;
176 RR_can = AA_can+BB_can+CC_can;
177
178 % Formulation from Association of American Railroads
179 % R = 1.3 + 18/W + (Cav^2/WN)
180 % AAR Variables
181 W_aar = W_can;           % Weight per car (tons)
182 N_aar = N_can;         % Number of axles per car
183 w_aar = W_aar/N_aar;   % Weight per axle (tons/axle)
184 CDa_aar = 39.6;        % Drag Area
185 Area_aar = 157.2;      % Full Scale Cross-sectional area
186 RollResist_aar = 1.3;  % Rolling Resistance term (lbf/ton)
187 Bearing_aar = 18;      % Bearing Resistance (lbf/axle)
188 rho_aar = .00238;     % Density of air @ STP (slugs/ft^3)
189
190 % Put values into Davis Equation Coefficients
191 A1_aar = RollResist_aar;
192 A2_aar = (Bearing_aar)/w_aar;
193 A_aar = A1_aar + A2_aar;
194
195 for ii = 1:length(V)
196     AA_aar(ii) = A_aar;
197 end
198 % CC_aar = ((.5*rho_aar*Cd_aar*Area_aar*Conv_v^2*V'.^2)/(w_aar*N_aar));
199 CC_aar = ((0.5*rho_aar*CDa_aar)/(w_aar*N_aar))*V'.^2;
200 RR_aar = AA_aar+CC_aar;
201
202 % Experimental Data Approximation of the Davis Equation
203 % R = 1.3 + 18/w + BV + C*V^2/(wN)
204 % C = .5*rho*A*Cd*v^2
205 W_exp = W_can;         % Weight per car (tons)
206 N_exp = 4;            % Number of axles per car
207 w_exp = W_exp/N_exp;  % Weight per axle (tons/axle)
208 bdyn_exp = 0.0306818174845041; % Flange Friction Coefficient
209 Cd_exp = Data{1}.MeanCd; % Drag Coefficient
210 Area_exp = 170;       % Full Scale Cross-sectional area
211 RollResist_exp = 1.3; % Rolling Resistance term (lbf/ton)
212 Bearing_exp = 18;     % Bearing Resistance (lbf/axle)

```

```

213
214 rho_exp = rho_aar; % Density of air @ STP (slugs / ft^3)
215
216 % Put values into Davis Equation Coefficients
217 A1_exp = RollResist_exp;
218 A2_exp = (Bearing_exp/w_exp);
219 if ANALYSIS == 1
220     B_exp = bdyn_exp*Conv_v; % Approximates to the Canadian National equation
221     A_exp = A1_can + A2_can;
222 else
223     B_exp = 0*Conv_v; % Approximates to the ARR Davis equation
224     A_exp = A1_exp + A2_exp;
225 end
226 C_exp = (1/2)*rho_exp*Area_exp*Cd_exp*Conv_v^2;
227
228 for ii = 1:length(V)
229     AA_exp(ii) = A_exp;
230 end
231 BB_exp = B_exp*V';
232 CC_exp = (C_exp*V'.^2)/(w_exp*N_exp);
233 RR_exp = AA_exp+BB_exp+CC_exp;
234
235 % Drag Coefficient Analysis
236 AreaFull = 170;
237
238 % Find C term for all Train Orientations
239 for i=1:NumSet
240     Cd(i) = Data{i}.MeanCd;
241 end
242 C = (1/2)*mean(TunnelData(:,6)./(R*TunnelData(:,3)))*Conv_rho*AreaFull*Conv_v^2.*Cd;
243
244 for ii=1:length(C)
245     CC(:,ii) = C(ii)*V.^2/(w_exp*N_exp);
246 end
247
248 %=====
249 %%
250 % Using  $R = 1.3 + 18/w + BV + C*V^2/(wN)$  and the experimentally obtained
251 % data, the following analysis looks at forces for an entire train set
252
253 % Needed Train parameters
254 Nloc = 2; % Number of Locomotives
255 Nauto = 65; % Number of Autoflex cars
256 W_loc = 220; % Weight of Locomotive (tons)
257 W_auto = 73; % Weight of Autoflex cars (tons)

```

```

258 AxleL = 6; % Number of axles on a locomotive
259 AxleA = 4; % Number of axles on an autoflex
260 hi_loc = (6)*(1/scale)*in2ft; % Height of Locomotive (in to ft)
261 wi_loc = (4)*(1/scale)*in2ft; % Width of Locomotive (in to ft)
262 hi_auto = CarH*(1/scale)*in2ft; % Height of Autoflex (in to ft)
263 wi_auto = CarW*(1/scale)*in2ft; % Width of Autoflex (in to ft)
264
265 % Calculated Parameters
266 a_loc = hi_loc*wi_loc; % Area of Locomotive (ft^2)
267 a_auto = hi_auto*wi_auto; % Area of Autoflex (ft^2)
268 gvw = W_loc*Nloc + Nauto*W_auto; % Gross Vehicle Weight (tons)
269 w_loc = W_loc/AxleL; % Locomotive Weight per axle (tons/axle)
270 w_auto = W_auto/AxleA; % Autoflex Weight per axle (tons/axle)
271
272 for i = 1:NumSet
273     Davis{i}.CdL = 1; % Drag coefficient for locomotive
274     Davis{i}.CdA = Data{i}.MeanCd; % Drag coefficient for cars
275 end
276
277 % Davis Equation Parameters
278 bL = 0.03/Conv_v; % Coefficient of moving friction -
279 % locomotives -> .03/1.466667
280 bC = 0.045/Conv_v; % Coefficient of moving friction - freight
281 % cars -> 0.045/1.466667
282 for i = 1:NumSet
283
284     if ANALYSIS == 1
285 %         Davis{i}.AL = RollResist_can + (Bearing_can*AxleL)/W_loc;
286 %         Davis{i}.AA = RollResist_can + (Bearing_can*N_can)/W_can;
287         Davis{i}.BL = bL*Conv_v; % Approximates to the Canadian National equation
288     else
289 %         Davis{i}.AL = RollResist_exp + Bearing_exp/w_loc;
290 %         Davis{i}.AA = RollResist_exp + Bearing_exp/w_auto;
291         Davis{i}.BL = 0*Conv_v; % Approximates to the ARR Davis equation
292     end
293
294     Davis{i}.AL = RollResist_exp + Bearing_exp/w_loc;
295     Davis{i}.AA = RollResist_exp + Bearing_exp/w_auto;
296
297     Davis{i}.CL = (1/2)*mean(Data{i}.Density)*Conv_rho*a_loc*Davis{i}.CdL*Conv_v^2;
298
299     if ANALYSIS == 1
300         Davis{i}.BA = bC*Conv_v; % Approximates to the Canadian National equation
301     else
302         Davis{i}.BA = 0*Conv_v; % Approximates to the ARR Davis equation

```

```

303     end
304     Davis{i}.CA = (1/2)*mean(Data{i}.Density)*Conv_rho*a_auto*Davis{i}.CdA*Conv_v^2;
305
306     Davis{i}.BLTotal = Davis{i}.BL*V;
307     Davis{i}.CLTotal = Davis{i}.CL*V.^2/(w_loc*AxleL);
308
309     Davis{i}.BATotal = Davis{i}.BA*V;
310     Davis{i}.CATotal = Davis{i}.CA*V.^2/(w_auto*AxleA);
311
312     for j = 1:length(V)
313         Davis{i}.ALTotal(j,1) = Davis{i}.AL;
314         Davis{i}.AATotal(j,1) = Davis{i}.AA;
315     end
316 end
317
318 for i = 1:NumSet
319     Davis{i}.RL = Davis{i}.ALTotal + Davis{i}.BLTotal + Davis{i}.CLTotal;
320     Davis{i}.RA = Davis{i}.AATotal + Davis{i}.BATotal + Davis{i}.CATotal;
321
322     Davis{i}.RLlbs = (Davis{i}.RL)*Nloc*W_loc;
323     Davis{i}.RALbs = (Davis{i}.RA)*Nauto*W_auto;
324
325     Davis{i}.RTotallbs = Davis{i}.RLlbs + Davis{i}.RALbs;
326 end
327
328 for i = 1:NumSet
329     DataOut{1}.ALTotal(:,i) = Davis{i}.ALTotal;
330     DataOut{1}.AATotal(:,i) = Davis{i}.AATotal;
331     DataOut{1}.BLTotal(:,i) = Davis{i}.BLTotal;
332     DataOut{1}.BATotal(:,i) = Davis{i}.BATotal;
333     DataOut{1}.CLTotal(:,i) = Davis{i}.CLTotal;
334     DataOut{1}.CATotal(:,i) = Davis{i}.CATotal;
335     DataOut{1}.RL(:,i) = Davis{i}.RL;    % Total of the component parts
336     DataOut{1}.RA(:,i) = Davis{i}.RA;    % Total of the component parts
337     DataOut{1}.RLlbs(:,i) = Davis{i}.RLlbs;
338     DataOut{1}.RALbs(:,i) = Davis{i}.RALbs;
339     DataOut{1}.RTotallbs(:,i) = Davis{i}.RTotallbs;
340 end
341
342 Nana = N*Nloc;
343 %%
344 fuel = xlsread('FuelConsumption.xlsx','DavisAnalysis');
345 %%
346 % ThrottleSet is the number of throttle settings (N1-N8)
347 ThrottleSet = length(fuel(1,:))-1;

```

```

348 % Number of Speed settings used in the wind tunnel
349 TunnelSet = 7;
350 % Read in the Simulated data for the corrugated case
351 DataOut{1}.SimulatedCorr = fuel(4,2:end); % Data provided from AAR Simulation
352 DataOut{1}.NormalFuelConsump = fuel(2,2:end)*Nloc;
353 DataOut{1}.TimePercent = fuel(3,2:end)/100;
354 Davis{6}.RTotallbs = (Davis{2}.RTotallbs+ Davis{4}.RTotallbs)/2; % Calculate the Average of
    the Smooth Roof cases
355
356 % Finding intersections
357 for i =1:ThrottleSet
358     for j = Base1:(Base2-1)
359         % Find the each orientation intersection with tractive curve
360         [Data{j}.XIntercept(i),Data{j}.YIntercept(i)] = intersections(V,Nana(:,i),V,Davis{j}.
            RTotallbs);
361     end
362 end
363 for i =1:ThrottleSet
364     for j = Base2:(Base3-1)
365         % Find the each orientation intersection with tractive curve
366         [Data{j}.XIntercept(i),Data{j}.YIntercept(i)] = intersections(V,Nana(:,i),V,Davis{j}.
            RTotallbs);
367     end
368 end
369 for i =1:ThrottleSet
370     for j = Base3:NumSet
371         % Find the each orientation intersection with tractive curve
372         [Data{j}.XIntercept(i),Data{j}.YIntercept(i)] = intersections(V,Nana(:,i),V,Davis{j}.
            RTotallbs);
373     end
374 end
375
376 for i = 1:ThrottleSet
377     for j=1:10
378         % Create the vertical line arrays at the corrugated case intersect
379         Analysis{i}.V_Corr1(j) = Data{Base1}.XIntercept(i);
380         Analysis{i}.VerticalLine1(j) = j*5500;
381     end
382 end
383 for i = 1:ThrottleSet
384     for j=1:10
385         % Create the vertical line arrays at the corrugated case intersect
386         Analysis{i}.V_Corr2(j) = Data{Base2}.XIntercept(i);
387         Analysis{i}.VerticalLine2(j) = j*5500;
388     end

```

```

389 end
390 for i = 1:ThrottleSet
391     for j=1:10
392         % Create the vertical line arrays at the corrugated case intersect
393         Analysis{i}.V_Corr3(j) = Data{Base3}.XIntercept(i);
394         Analysis{i}.VerticalLine3(j) = j*5500;
395     end
396 end
397 %%
398 % Find the intersections of all the Orientation sets with the corrugated case
399 for i = 1:ThrottleSet
400     for j = Base1:(Base2-1)
401         [Data{j}.XBaseInt(i), Data{j}.YBaseInt(i)] = intersections(Analysis{i}.V_Corr1, Analysis{i}
402             }.VerticalLine1 ,V, Davis{j}.RTotallbs);
403     end
404     for i = 1:ThrottleSet
405         for j = Base2:(Base3-1)
406             [Data{j}.XBaseInt(i), Data{j}.YBaseInt(i)] = intersections(Analysis{i}.V_Corr2, Analysis{i}
407                 }.VerticalLine2 ,V, Davis{j}.RTotallbs);
408         end
409         for i = 1:ThrottleSet
410             for j = Base3:NumSet
411                 [Data{j}.XBaseInt(i), Data{j}.YBaseInt(i)] = intersections(Analysis{i}.V_Corr3, Analysis{i}
412                     }.VerticalLine3 ,V, Davis{j}.RTotallbs);
413             end
414         end
415     %%
416     PerFuel = fuel(3,:)/100;
417     % Calculate the Fraction Force Reduction at each car configuration
418     for i = 1:ThrottleSet
419         for j = 1:NumSet
420             Data{j}.FN(i) = Data{j}.YBaseInt(i)*PerFuel(i+1);
421         end
422     end
423     DataOut{1}.Nsum = sum(DataOut{1}.TimePercent);
424     for i = Base1:(Base2-1)
425         Data{i}.FNsum = sum(Data{i}.FN);
426         Data{i}.FBar = Data{i}.FNsum/DataOut{1}.Nsum;
427         Data{i}.ForceReduce = ((Data{Base1}.FBar-Data{i}.FBar)/Data{Base1}.FBar);
428         Data{i}.AvgPercentForceReduce = ((Data{Base1}.FBar-Data{i}.FBar)/Data{Base1}.FBar)*100;
429         Data{i}.PercentForceReduce = abs(Data{Base1}.YBaseInt-Data{i}.YBaseInt) ./ Data{Base1}.YBaseInt
430         ;

```



```

430 end
431 for i =Base2:(Base3-1)
432     Data{i}.FNsum = sum(Data{i}.FN);
433     Data{i}.FBar = Data{i}.FNsum/DataOut{1}.Nsum;
434     Data{i}.ForceReduce = ((Data{Base2}.FBar-Data{i}.FBar)/Data{Base2}.FBar);
435     Data{i}.AvgPercentForceReduce = ((Data{Base2}.FBar-Data{i}.FBar)/Data{Base2}.FBar)*100;
436     Data{i}.PercentForceReduce = abs(Data{Base2}.YBaseInt-Data{i}.YBaseInt) ./ Data{Base2}.YBaseInt
        ;
437 end
438 for i =Base3:NumSet
439     Data{i}.FNsum = sum(Data{i}.FN);
440     Data{i}.FBar = Data{i}.FNsum/DataOut{1}.Nsum;
441     Data{i}.ForceReduce = ((Data{Base3}.FBar-Data{i}.FBar)/Data{Base3}.FBar);
442     Data{i}.AvgPercentForceReduce = ((Data{Base3}.FBar-Data{i}.FBar)/Data{Base3}.FBar)*100;
443     Data{i}.PercentForceReduce = abs(Data{Base3}.YBaseInt-Data{i}.YBaseInt) ./ Data{Base3}.YBaseInt
        ;
444 end
445 %=====
446 %%
447 % Error Between the AAR Simulation Data and my Davis Equation
448 for i = 1:ThrottleSet
449     DataOut{1}.SimDiff(i) = (abs(DataOut{1}.SimulatedCorr(i)-Data{1}.XIntercept(i)))/Data{1}.
        XIntercept(i)*100;
450 end
451
452 AvgSimDiff = mean(DataOut{1}.SimDiff(1,2:end)); % Note the difference of N2 isn't great. If only
        N3-N8 are considered the average improves by almost 0.6 %.
453 %%
454 % Calculate the Percent Fuel Reduction
455 % The term-wise (N1-N8) force reduction is calculated above.
456 % Term-wise Ratio
457 for i = Base1:(Base2-1)
458     Data{i}.Ratio = Data{i}.FN./Data{Base1}.FN;
459     Data{i}.ReducedForce = Data{Base1}.YBaseInt.*Data{i}.Ratio;
460     Data{i}.ReducedFuelConsump = DataOut{1}.NormalFuelConsump.*Data{i}.Ratio;
461     Data{i}.PercentFuelReduce = abs(DataOut{1}.NormalFuelConsump - Data{i}.ReducedFuelConsump) ./
        DataOut{1}.NormalFuelConsump;
462     Data{i}.AvgFuelTopSum = sum(DataOut{1}.TimePercent.*Data{i}.PercentFuelReduce);
463 end
464 for i = Base2:(Base3-1)
465     Data{i}.Ratio = Data{i}.FN./Data{Base2}.FN;
466     Data{i}.ReducedForce = Data{Base2}.YBaseInt.*Data{i}.Ratio;
467     Data{i}.ReducedFuelConsump = DataOut{1}.NormalFuelConsump.*Data{i}.Ratio;
468     Data{i}.PercentFuelReduce = abs(DataOut{1}.NormalFuelConsump - Data{i}.ReducedFuelConsump) ./
        DataOut{1}.NormalFuelConsump;

```

```

469     Data{i}.AvgFuelTopSum = sum(DataOut{1}.TimePercent.*Data{i}.PercentFuelReduce);
470 end
471 for i = Base3:NumSet
472     Data{i}.Ratio = Data{i}.FN./Data{Base3}.FN;
473     Data{i}.ReducedForce = Data{Base3}.YBaseInt.*Data{i}.Ratio;
474     Data{i}.ReducedFuelConsump = DataOut{1}.NormalFuelConsump.*Data{i}.Ratio;
475     Data{i}.PercentFuelReduce = abs(DataOut{1}.NormalFuelConsump - Data{i}.ReducedFuelConsump)./
        DataOut{1}.NormalFuelConsump;
476     Data{i}.AvgFuelTopSum = sum(DataOut{1}.TimePercent.*Data{i}.PercentFuelReduce);
477 end
478 for i = Base1:(Base2-1)
479     DataOut{1}.AvgPercentFuelReduce{i} = ((Data{i}.AvgFuelTopSum)./DataOut{1}.Nsum)*100;
480 end
481 for i = Base2:(Base3-1)
482     DataOut{1}.AvgPercentFuelReduce{i} = ((Data{i}.AvgFuelTopSum)./DataOut{1}.Nsum)*100;
483 end
484 for i = Base3:NumSet
485     DataOut{1}.AvgPercentFuelReduce{i} = ((Data{i}.AvgFuelTopSum)./DataOut{1}.Nsum)*100;
486 end
487 %%
488 %Write data to a file
489 DataOut{1}.ColNames = {'N1','N2','N3','N4','N5','N6','N7','N8'};
490 DataOut{1}.RowNames = {'Corrugated Roof';'Smooth w/o lip';'Belly Cover';'Smooth w/ lip';'Full
        Skirt';'Average Smooth';'Partial Skirt';'Light Hole Pattern';'Light Smooth';'Light Corrugated
        ';'4x Larger Holes';'Slotted';'4x Vertical';'Replica Baseline';'Replica B/S/T';'Replica S/T';
        'Replica T';'Replica VFairing/B/S/T';'Replica S';'Replica Top Retest'};
491 for i =1:NumSet
492     DataOut{1}.XIntercept(i,:) = Data{i}.XIntercept;
493     DataOut{1}.YIntercept(i,:) = Data{i}.YIntercept;
494     DataOut{1}.XBaseInt(i,:) = Data{i}.XBaseInt;
495     DataOut{1}.YBaseInt(i,:) = Data{i}.YBaseInt;
496     DataOut{1}.ReducedFuelConsump(i,:) = Data{i}.ReducedFuelConsump;
497     DataOut{1}.AvgDragCoeffReduction{i} = Data{i}.PercentReduc;
498     DataOut{1}.MeanCd{i} = Data{i}.MeanCd;
499 end
500 for i = 1:NumSet
501     DataOut{1}.AvgPercentForceReduce{i} = Data{i}.AvgPercentForceReduce;
502 end
503 %%
504 % This block of code calculates the average Data
505 % Uncertainty Analysis
506 % Systematic Error Terms
507 usP = 135; % Pa
508 usF1 = .00801911; % kg
509 usF3 = .008829; % kg

```

```

510 usT = 2.2; % K
511 usdP = 6.158; % Pa
512 usAc = .0000035921; % m
513
514 for i=1:NumSet
515     DataSetCount(i) = ceil(length(Data{i}.Cd)/7);
516 end
517 for i=1:NumSet
518     if i==6
519
520     else
521         Data{i}.dP = (Data{i}.Velocity.^2.*Data{i}.Density)./2;
522     end
523 end
524
525 % Prepare individual run data for export to excel
526 % calculating the standard deviation of the Cd
527 for i=1:NumSet
528     if i==6
529         % DataOut{1}.stdCd(j,1) = 1;
530         % DataOut{1}.stdRe(j,1) = 1;
531     else
532         for j = 1:TunnelSet
533             if j == 1
534                 DataOut{1}.stdCd((j+TunnelSet*(i-1)),1) = std(Data{i}.Cd(1:DataSetCount(i)));
535                 DataOut{1}.stdRe((j+TunnelSet*(i-1)),1) = std(Data{i}.ReNumber(1:DataSetCount(i))
536                 );
537             else
538                 DataOut{1}.stdCd((j+TunnelSet*(i-1)),1) = std(Data{i}.Cd((((j-1)*DataSetCount(i)
539                 +1):j*DataSetCount(i))));
540                 DataOut{1}.stdRe((j+TunnelSet*(i-1)),1) = std(Data{i}.ReNumber((((j-1)*
541                 DataSetCount(i)+1):j*DataSetCount(i))));
542             end
543         end
544     end
545 end
546 for i=1:NumSet
547     if i==6
548         Data{i}.AvgCd = 1;
549     else
550         for j = 1:TunnelSet
551             if j == 1
552                 Data{i}.AvgCd(j) = mean(Data{i}.Cd(1:DataSetCount(i)));
553                 Data{i}.AvgReNumber(j) = mean(Data{i}.ReNumber(1:DataSetCount(i)));
554                 Data{i}.AvgF(j) = mean(Data{i}.Drag(1:DataSetCount(i)));

```

```

552         Data{i}.AvgdP(j) = mean(Data{i}.dP(1:DataSetCount(i)));
553         Data{i}.stdCd(j) = std(Data{i}.Cd(1:DataSetCount(i)));
554         Data{i}.stdRe(j) = std(Data{i}.ReNumber(1:DataSetCount(i)));
555     else
556         Data{i}.AvgCd(j) = mean(Data{i}.Cd((((j-1)*DataSetCount(i))+1):j*DataSetCount(i))
           );
557         Data{i}.AvgReNumber(j) = mean(Data{i}.ReNumber((((j-1)*DataSetCount(i))+1):j*
           DataSetCount(i)));
558         Data{i}.AvgF(j) = mean(Data{i}.Drag((((j-1)*DataSetCount(i))+1):j*DataSetCount(i)
           ));
559         Data{i}.AvgdP(j) = mean(Data{i}.dP((((j-1)*DataSetCount(i))+1):j*DataSetCount(i))
           );
560         Data{i}.stdCd(j) = std(Data{i}.Cd((((j-1)*DataSetCount(i))+1):j*DataSetCount(i))
           );
561         Data{i}.stdRe(j) = std(Data{i}.ReNumber((((j-1)*DataSetCount(i))+1):j*
           DataSetCount(i)));
562     end
563 end
564 end
565 end
566 % Set up the Student t values. Minimum number of data set taken was four and maximum was 10.
567 for i=1:NumSet
568     if i==6
569     else
570         if DataSetCount(i)-1 == 3
571             Data{i}.StudT = 3.192;
572         elseif DataSetCount(i)-1 == 4
573             Data{i}.StudT = 2.770;
574         elseif DataSetCount(i)-1 == 5
575             Data{i}.StudT = 2.571;
576         elseif DataSetCount(i)-1 == 6
577             Data{i}.StudT = 2.447;
578         elseif DataSetCount(i)-1 == 7
579             Data{i}.StudT = 2.365;
580         elseif DataSetCount(i)-1 == 8
581             Data{i}.StudT = 2.306;
582         elseif DataSetCount(i)-1 == 9
583             Data{i}.StudT = 2.262;
584         elseif DataSetCount(i)-1 == 10
585             Data{i}.StudT = 2.228;
586         else
587             Data{i}.StudT = 0;
588         end
589     end
590 end

```

```

591 for i=1:NumSet
592     if i==6
593     else
594         Data{i}.TF = 1./(Data{i}.AvgdP.*Area);
595         Data{i}.TdP = -(Data{i}.AvgF./((Data{i}.AvgdP.^2).*Area));
596         Data{i}.TAc = -(Data{i}.AvgF./((Data{i}.AvgdP).*Area^2));
597         Data{i}.usF1 = ((Data{i}.TF.*usF1).^2 + (Data{i}.TdP.*usdP).^2 + (Data{i}.TAc.*usAc).^2)
                    .^0.5;
598         Data{i}.usF3 = ((Data{i}.TF.*usF3).^2 + (Data{i}.TdP.*usdP).^2 + (Data{i}.TAc.*usAc).^2)
                    .^0.5;
599         Data{i}.stdCd2 = Data{i}.StudT*Data{i}.stdCd./(DataSetCount(i))^0.5;
600         Data{i}.utotal1 = (Data{i}.usF1.^2 + Data{i}.stdCd2.^2).^0.5;
601         Data{i}.utotal3 = (Data{i}.usF3.^2 + Data{i}.stdCd2.^2).^0.5;
602         Data{i}.utotal1per = Data{i}.utotal1./Data{i}.AvgCd*100;
603         Data{i}.utotal3per = Data{i}.utotal3./Data{i}.AvgCd*100;
604         Data{i}.uncertComp = [Data{i}.TF.*usF3; Data{i}.TdP.*usdP; Data{i}.TAc.*usAc; Data{i}.
                    usF3; Data{i}.stdCd2];
605     end
606 end
607
608 %%
609
610 DataOut{1}.CdMatrix = zeros(NumSet*7,max(DataSetCount));
611 Data{6}.uncertComp = zeros(5, TunnelSet);
612
613 for i=1:NumSet
614     if i==6
615
616     else
617         for j = 1:TunnelSet
618             if j == 1
619                 for k = 1:DataSetCount(i)
620                     DataOut{1}.CdMatrix((j+TunnelSet*(i-1)),k) = (Data{i}.Cd(k));
621                 end
622             else
623                 for k = 1:DataSetCount(i)
624                     DataOut{1}.CdMatrix((j+TunnelSet*(i-1)),k) = (Data{i}.Cd((k+DataSetCount(i))*(
                    j-1))));
625                 end
626             end
627         end
628         DataOut{1}.Uncertainty1(i,:) = Data{i}.utotal1per(1,:);
629         DataOut{1}.Uncertainty3(i,:) = Data{i}.utotal3per(1,:);
630     end
631     if i == 1

```

```

632         DataOut{1}.UncertComp(i:i+4,:) = Data{i}.uncertComp;
633     else
634         DataOut{1}.UncertComp((i*5)-4:(i*5) ,:) = Data{i}.uncertComp;
635     end
636 end
637
638 %%
639 xlswrite('dataoutfinal.xlsx', [DataOut{1}.CdMatrix], 'StandardDeviation', 'D2')
640 xlswrite('dataoutfinal.xlsx', [DataOut{1}.stdCd], 'StandardDeviation', 'Q2')
641 xlswrite('dataoutfinal.xlsx', [DataOut{1}.RowNames], 'Uncertainty', 'A12')
642 xlswrite('dataoutfinal.xlsx', [DataOut{1}.Uncertainty1], 'Uncertainty', 'B12')
643 xlswrite('dataoutfinal.xlsx', [DataOut{1}.Uncertainty3], 'Uncertainty', 'K12')
644 xlswrite('dataoutfinal.xlsx', [DataOut{1}.UncertComp], 'Uncertainty', 'B40')
645 %%
646 if ANALYSIS == 1
647     DataOut{1}.Analysis = {'CN'};
648 else
649     DataOut{1}.Analysis = {'AAR'};
650 end
651 %%
652 % Writing data to file
653 Time = 1;      % time in hours
654 xlswrite('dataoutfinal.xlsx', [DataOut{1}.Analysis], 'PercentReduction', 'A1');
655 xlswrite('dataoutfinal.xlsx', [DataOut{1}.ColNames], 'MatLabOutputAuto', 'A2');
656 xlswrite('dataoutfinal.xlsx', [DataOut{1}.NormalFuelConsump; DataOut{1}.TimePercent], '
        MatLabOutputAuto', 'B2');
657 xlswrite('dataoutfinal.xlsx', [DataOut{1}.XBaseInt; DataOut{1}.YBaseInt; DataOut{1}.
        ReducedFuelConsump], 'MatLabOutputAuto', 'B5');
658 [FuelFractionAway, FuelFractionReturn, DistanceAway, DistanceReturn, FuelTotals, DistanceTotals,
        GPMaway, GPMreturn] = FuelConsume(Data{1}.XBaseInt, Data{1}.XBaseInt, DataOut{1}.
        ReducedFuelConsump, DataOut{1}.ReducedFuelConsump, Time);
659 xlswrite('dataoutfinal.xlsx', [DataOut{1}.RowNames; DataOut{1}.RowNames; DataOut{1}.RowNames;
        DataOut{1}.RowNames], 'MatlabData', 'B2');
660 xlswrite('dataoutfinal.xlsx', DataOut{1}.ColNames, 'MatlabData', 'C1');
661 xlswrite('dataoutfinal.xlsx', [DataOut{1}.XIntercept; DataOut{1}.YIntercept; DataOut{1}.XBaseInt;
        DataOut{1}.YBaseInt], 'MatlabData', 'C2');
662 xlswrite('dataoutfinal.xlsx', [DataOut{1}.RowNames'; DataOut{1}.MeanCd; DataOut{1}.
        AvgDragCoeffReduction; DataOut{1}.AvgPercentForceReduce; DataOut{1}.AvgPercentFuelReduce], '
        PercentReduction', 'B1');
663 xlswrite('dataoutfinal.xlsx', DataOut{1}.ColNames, 'PercentReduction', 'B7');
664 xlswrite('dataoutfinal.xlsx', DataOut{1}.RowNames, 'PercentReduction', 'A8');
665 xlswrite('dataoutfinal.xlsx', DataOut{1}.ReducedFuelConsump, 'PercentReduction', 'B8');
666 xlswrite('dataoutfinal.xlsx', DataOut{1}.ColNames, 'SimCompare', 'B1');
667 xlswrite('dataoutfinal.xlsx', [DataOut{1}.SimulatedCorr; Data{1}.XBaseInt; DataOut{1}.SimDiff], '
        SimCompare', 'B2');

```

```

668 xlswrite('dataoutfinal.xlsx', [GPMaway;GPMreturn], 'GPMrates', 'B2');
669 xlswrite('dataoutfinal.xlsx', [FuelFractionAway; FuelFractionReturn; DistanceReturn; DistanceReturn
    ], 'FuelConsumptionDistance', 'B2');
670 if ANALYSIS == 1 % Canadian National
671     xlswrite('dataoutfinal.xlsx', DataOut{1}.RowNames, 'DavisEqnCN', 'C1');
672     xlswrite('dataoutfinal.xlsx', [DataOut{1}.ALTotal;DataOut{1}.AATotal;DataOut{1}.BLTotal;
        DataOut{1}.BATotal;DataOut{1}.CLTotal;DataOut{1}.CATotal;DataOut{1}.RL;DataOut{1}.RA;
        DataOut{1}.RLlbs;DataOut{1}.RALbs;DataOut{1}.RTotallbs], 'DavisEqnCN', 'C2');
673     xlswrite('dataoutfinal.xlsx', [V';AA_aar;CC_aar;RR_aar;AA_can;BB_can;CC_can;RR_can;AA_exp;
        BB_exp;CC_exp;RR_exp], 'ValidationCN', 'C2');
674 else % Association of American Railroads
675     xlswrite('dataoutfinal.xlsx', DataOut{1}.RowNames, 'DavisEqnAAR', 'C1');
676     xlswrite('dataoutfinal.xlsx', [DataOut{1}.ALTotal;DataOut{1}.AATotal;DataOut{1}.BLTotal;
        DataOut{1}.BATotal;DataOut{1}.CLTotal;DataOut{1}.CATotal;DataOut{1}.RL;DataOut{1}.RA;
        DataOut{1}.RLlbs;DataOut{1}.RALbs;DataOut{1}.RTotallbs], 'DavisEqnAAR', 'C2');
677     xlswrite('dataoutfinal.xlsx', [V';AA_aar;CC_aar;RR_aar;AA_can;BB_can;CC_can;RR_can;AA_exp;
        BB_exp;CC_exp;RR_exp], 'ValidationAAR', 'C2');
678 end
679 %% =====
680 % read in diesel price trend data for plotting
681 diesel = xlsread('FuelConsumption.xlsx', 'DieselPriceTrends');
682 % convert date serial to date string
683 dates1 = datestr(diesel(:,2)+693960,23);
684 dates = datenum(dates1, 'mm/dd/yyyy');
685 %dn=datenum(data(:,1), 'mmyy');
686 toc
687 %%
688
689 PLOT = 0;
690 % PLOT = 0 – Program doesn't output plots
691 % PLOT = 1 – Program plots all plots
692
693 % close all;
694
695 colors = ...
696 [ 0 0 1 % 1 BLUE
697   0 1 0 % 2 GREEN (pale)
698   1 0 0 % 3 RED
699   0 1 1 % 4 CYAN
700   1 0 1 % 5 MAGENTA (pale)
701   1 1 0 % 6 YELLOW (pale)
702   0.5 0 0.9 % 7 PURPLE
703   0 0.75 0.75 % 8 TURQUOISE
704   0 0.5 0 % 9 GREEN (dark)
705   0.75 0.75 0 % 10 YELLOW (dark)

```

```

706     1 0.50 0.25 % 11 ORANGE
707     0.75 0 0.75 % 12 MAGENTA (dark)
708     0.7 0.7 0.7 % 13 GREY
709     0.8 0.7 0.6 % 14 BROWN (pale)
710     0.6 0.5 0.4 ]; % 15 BROWN (dark)
711
712     xPixels = 1680;
713     yPixels = 1050;
714     NumLoc = num2str(Nloc);
715     NumAuto = num2str(Nauto);
716
717     Msize = 15;    % Marker Size
718     Tsize = 45;    % Title Font Size
719     Asize = 35;    % Axis Font Size
720     Fsize = 30;    % Other Font Size
721     Lwidth = 4;    % Line Width
722
723     set(0,'DefaultAxesColorOrder',colors,...
724         'DefaultAxesLineStyleOrder','-|--:'); % This line changes the order of the colors and
725         line type used for plotting
726
727     set(0,'DefaultAxesFontName', 'Times New Roman') % Change font style to New Times Roman
728     set(0,'defaultTextFontName', 'Times New Roman')
729     set(0, 'defaultTextInterpreter', 'latex')
730     % set(0,'DefaultAxesFontName', 'Calibri') % Change font style to New Times Roman
731     % set(0,'defaultTextFontName', 'Calibri')
732     % % % % % % set(0,'DefaultAxesFontName', 'factory') % To change it back to the
733     % % % % % % % factory settings
734     % Plot of the C44AC Tractive force data without any scaling
735
736     if PLOT == 1
737         %%
738         close all;
739
740         figure(99)
741         plot(dates, diesel(:,1), 'o', 'MarkerEdgeColor','b', 'MarkerFaceColor','b', 'MarkerSize',5)
742         datetick('x','kepticks','keplimits')
743         ylabel('Dollars per Gallon','fontsize', 26)
744
745         set(gca, 'FontSize',20)
746         set(gca, 'XMinorTick','on','YMinorTick','on')
747         set(gcf, 'Color', 'w');
748         set(gcf, 'Position', [100 160 xPixels yPixels]) %[pos-x pos-y length-x length-y]
749
750     export_fig Diesel -painters -jpg -eps

```



```

750 %%
751
752 %%
753 % Plots the tractive force curve for a single locomotive
754 figure(100)
755     plot(V,N(:,1),V,N(:,2),V,N(:,3),V,N(:,4),V,N(:,5),V,N(:,6),V,N(:,7),V,N(:,8),'MarkerSize',15,
           'LineWidth',4)
756     box on
757     h_legend = legend('N1','N2','N3','N4','N5','N6','N7','N8','Location','NorthEast');
758     legend boxoff
759 %     title('C44AC','FontSize',30)
760     xlabel('Speed (mph)','fontsize',26)
761     ylabel('Tractive Effort (pounds)','fontsize',26)
762     axis([0 V(length(V))+2 0 max(N(:,size(N,2)))+5000])
763     set(gca,'FontSize',20)
764     set(gca,'XMinorTick','on','YMinorTick','on')
765     set(h_legend,'FontSize',24)
766     set(gcf,'Color','w');
767     set(gcf,'Position',[100 160 xPixels yPixels]) %[pos-x pos-y length-x length-y]
768
769     export_fig C44ACdata -painters -jpg -eps
770 %%
771 figure(101) % Averaged Cd Data for Baseline and Roof Data
772
773     hold on
774     plot(Data{1}.AvgReNumber, Data{1}.AvgCd, 'o','MarkerEdgeColor','b','MarkerFaceColor','b','
           MarkerSize',Msize)
775     plot(Data{2}.AvgReNumber, Data{2}.AvgCd, 's','MarkerEdgeColor','r','MarkerFaceColor','r','
           MarkerSize',Msize)
776     plot(Data{4}.AvgReNumber, Data{4}.AvgCd, '^','MarkerEdgeColor','g','MarkerFaceColor','g','
           MarkerSize',Msize)
777 %     errorbar(Data{1}.AvgReNumber, Data{1}.AvgCd, Data{1}.utotal3, 'o','MarkerEdgeColor','b','
           MarkerFaceColor','b','MarkerSize',Msize)
778 %     errorbar(Data{2}.AvgReNumber, Data{2}.AvgCd, Data{2}.utotal3, 's','MarkerEdgeColor','r','
           MarkerFaceColor','r','MarkerSize',Msize)
779 %     errorbar(Data{4}.AvgReNumber, Data{4}.AvgCd, Data{4}.utotal3, '^','MarkerEdgeColor','g','
           MarkerFaceColor','g','MarkerSize',Msize)
780     hold off
781     box on
782 %     h_legend = legend('Corrugated roof (Baseline)',['Smooth roof without' char(10) 'leading and
           trailing lip'],['Smooth roof with' char(10) 'leading and trailing lip'],'Location','
           NorthEastOutside');
783     legend boxoff
784 %     title('Averaged Roof Data','FontSize',Tsize)
785     xlabel('$Re$', 'fontsize', Asize)

```

```

786     ylabel('$C_{d}$', 'fontSize', Asize)
787     xlim([200000 295000])
788
789     set(gca, 'FontSize', Fsize)
790     set(gca, 'XMinorTick', 'on', 'YMinorTick', 'on')
791     set(gcf, 'Color', 'w');
792     set(gcf, 'Position', [100 160 xPixels yPixels]) %[pos-x pos-y length-x length-y]
793
794     export_fig AutoRoof -painters -jpg -eps
795
796 %%
797 figure(102) % Averaged Cd Data for Baseline and Under Body Data
798
799     hold on
800     plot(Data{1}.AvgReNumber, Data{1}.AvgCd, '^', 'MarkerEdgeColor', 'r', 'MarkerFaceColor', 'r', '
      MarkerSize', Msize)
801     plot(Data{3}.AvgReNumber, Data{3}.AvgCd, 's', 'MarkerEdgeColor', 'g', 'MarkerFaceColor', 'g', '
      MarkerSize', Msize)
802     plot(Data{5}.AvgReNumber, Data{5}.AvgCd, 'v', 'MarkerEdgeColor', 'b', 'MarkerFaceColor', 'b', '
      MarkerSize', Msize)
803     plot(Data{7}.AvgReNumber, Data{7}.AvgCd, 'o', 'MarkerEdgeColor', 'm', 'MarkerFaceColor', 'm', '
      MarkerSize', Msize)
804     hold off
805     box on
806 %     h_legend = legend(['Standard chassis ', 'Chassis cover ', 'Full length skirts ', 'Partial length
      skirts '], 'Location', 'NorthEastOutside');
807     legend boxoff
808 %     title('Averaged Under Body Data', 'FontSize', Tsize)
809     xlabel('$Re$', 'fontSize', Asize)
810     ylabel('$C_{d}$', 'fontSize', Asize)
811     xlim([200000 295000])
812
813     set(gca, 'FontSize', Fsize)
814     set(gca, 'XMinorTick', 'on', 'YMinorTick', 'on')
815     set(gcf, 'Color', 'w');
816     set(gcf, 'Position', [120 140 xPixels yPixels]) %[pos-x pos-y length-x length-y]
817
818     export_fig AutoUnder -painters -jpg -eps
819 %%
820 figure(103) % Averaged Cd Data for Baseline and Panel Data
821     hold on
822     plot(Data{8}.AvgReNumber, Data{8}.AvgCd, 'o', 'MarkerEdgeColor', 'k', 'MarkerFaceColor', 'k', '
      MarkerSize', Msize)
823     plot(Data{9}.AvgReNumber, Data{9}.AvgCd, 's', 'MarkerEdgeColor', 'm', 'MarkerFaceColor', 'm', '
      MarkerSize', Msize)

```

```

824     plot(Data{10}.AvgReNumber, Data{10}.AvgCd, '^', 'MarkerEdgeColor', 'c', 'MarkerFaceColor', 'c', '
      MarkerSize', Msize)
825     plot(Data{11}.AvgReNumber, Data{11}.AvgCd, '<', 'MarkerEdgeColor', 'r', 'MarkerFaceColor', 'r', '
      MarkerSize', Msize)
826     plot(Data{12}.AvgReNumber, Data{12}.AvgCd, 'v', 'MarkerEdgeColor', 'b', 'MarkerFaceColor', 'b', '
      MarkerSize', Msize)
827     plot(Data{13}.AvgReNumber, Data{13}.AvgCd, '>', 'MarkerEdgeColor', 'g', 'MarkerFaceColor', 'g', '
      MarkerSize', Msize)
828 %Template Line     plot(Data{7}.AvgReNumber, Data{7}.AvgCd, 'o', 'MarkerEdgeColor', 'k', '
      MarkerFaceColor', 'k')
829     hold off
830     box on
831 %     h_legend = legend('Industry replica panel', 'Smooth panel', ['Ribbed panel (no holes)', ['
      Panels with 4X larger venting' char(10) 'holes in blocked configuration'], 'Slotted panel', ['
      Panels with 4X larger venting' char(10) 'holes in spaced configuration'], 'Location', '
      NorthEastOutside');
832     legend boxoff
833 %     title('Averaged Panel Data', 'FontSize', Tsize)
834     xlabel('$Re$', 'fontsize', Asize)
835     ylabel('$C_d$', 'fontsize', Asize)
836     xlim([200000 295000])
837
838     set(gca, 'FontSize', Fsize)
839     set(gca, 'XMinorTick', 'on', 'YMinorTick', 'on')
840     set(gcf, 'Color', 'w');
841     set(gcf, 'Position', [140 120 xPixels yPixels]) %[pos-x pos-y length-x length-y]
842
843     export_fig AutoPanel -painters -jpg -eps
844 %%
845 figure(104) % Averaged Cd Data for Baseline and Composite Data
846
847     hold on
848     plot(Data{14}.AvgReNumber, Data{14}.AvgCd, 'v', 'MarkerEdgeColor', 'c', 'MarkerFaceColor', 'c', '
      MarkerSize', Msize)
849     plot(Data{20}.AvgReNumber, Data{20}.AvgCd, 's', 'MarkerEdgeColor', 'g', 'MarkerFaceColor', 'g', '
      MarkerSize', Msize)
850     plot(Data{19}.AvgReNumber, Data{19}.AvgCd, '<', 'MarkerEdgeColor', 'r', 'MarkerFaceColor', 'r', '
      MarkerSize', Msize)
851     plot(Data{16}.AvgReNumber, Data{16}.AvgCd, '^', 'MarkerEdgeColor', 'm', 'MarkerFaceColor', 'm', '
      MarkerSize', Msize)
852     plot(Data{18}.AvgReNumber, Data{18}.AvgCd, 'o', 'MarkerEdgeColor', 'b', 'MarkerFaceColor', 'b', '
      MarkerSize', Msize)
853     plot(Data{15}.AvgReNumber, Data{15}.AvgCd, '>', 'MarkerEdgeColor', 'k', 'MarkerFaceColor', 'k', '
      MarkerSize', Msize)

```

```

854 %Template Line      plot(Data{7}.AvgReNumber, Data{7}.AvgCd, 'o', 'MarkerEdgeColor', 'k', '
      MarkerFaceColor', 'k')
855     hold off
856     box on
857 %     h_legend = legend('Baseline', 'Smooth Top', 'Side Panels', ['Side Panels and' char(10) 'Smooth
      Roof'], ['Bottom Cover w/ V-fairing', char(10) 'Side Panels and Smooth Roof'], ['Bottom Cover,
      Side Panels' char(10) 'and Smooth Roof'], 'Location', 'NorthEastOutside');
858     % h_legend = legend(['Bottom Cover w/ V-fairing', char(10) 'Side Panels and Smooth Roof']
      , ['Bottom Cover, Side Panels' char(10) 'and Smooth Roof'], ['Side Panels and' char(10) '
      Smooth Roof'], 'Smooth Top', 'Side Panels', 'Baseline', 'Location', 'NorthEastOutside');
859     legend boxoff
860 %     title('Averaged Panel Data', 'FontSize', Tsize)
861     xlabel('$Re$', 'fontSize', Asize)
862     ylabel('$C_{d}$', 'fontSize', Asize)
863     axis([200000 295000 .115 .25])
864
865     set(gca, 'FontSize', Fsize)
866     set(gca, 'XMinorTick', 'on', 'YMinorTick', 'on')
867     set(gcf, 'Color', 'w');
868     set(gcf, 'Position', [140 120 xPixels yPixels]) %[pos-x pos-y length-x length-y]
869
870     export_fig AutoComp -painters -jpg -eps
871 %%
872
873 figure(110) % Averaged Cd Data for Baseline and Roof Data
874
875     hold on
876     errorbar(Data{1}.AvgReNumber, Data{1}.AvgCd, Data{1}.utotal3, 'o', 'MarkerEdgeColor', 'b', '
      MarkerFaceColor', 'b', 'MarkerSize', Msize)
877     errorbar(Data{2}.AvgReNumber, Data{2}.AvgCd, Data{2}.utotal3, 's', 'MarkerEdgeColor', 'r', '
      MarkerFaceColor', 'r', 'MarkerSize', Msize)
878     errorbar(Data{4}.AvgReNumber, Data{4}.AvgCd, Data{4}.utotal3, '^', 'MarkerEdgeColor', 'g', '
      MarkerFaceColor', 'g', 'MarkerSize', Msize)
879     hold off
880     box on
881 %     h_legend = legend('Corrugated roof (Baseline)', ['Smooth roof without' char(10) 'leading and
      trailing lip'], ['Smooth roof with' char(10) 'leading and trailing lip'], 'Location', '
      NorthEastOutside');
882     legend boxoff
883 %     title('Averaged Roof Data', 'FontSize', Tsize)
884     xlabel('$Re$', 'fontSize', Asize)
885     ylabel('$C_{d}$', 'fontSize', Asize)
886     xlim([200000 295000])
887     ylim([0.16 0.235])
888     set(gca, 'FontSize', Fsize)

```

```

889     set(gca, 'XMinorTick', 'on', 'YMinorTick', 'on')
890     set(gcf, 'Color', 'w');
891     set(gcf, 'Position', [100 160 xPixels yPixels]) %[pos-x pos-y length-x length-y]
892
893     export_fig AutoRoofError -painters -jpg -eps
894
895 %%
896 figure(111) % Averaged Cd Data for Baseline and Under Body Data
897
898     hold on
899     errorbar(Data{1}.AvgReNumber, Data{1}.AvgCd, Data{1}.utotal3, '^', 'MarkerEdgeColor', 'r', '
          MarkerFaceColor', 'r', 'MarkerSize', Msize)
900     errorbar(Data{3}.AvgReNumber, Data{3}.AvgCd, Data{3}.utotal3, 's', 'MarkerEdgeColor', 'g', '
          MarkerFaceColor', 'g', 'MarkerSize', Msize)
901     errorbar(Data{5}.AvgReNumber, Data{5}.AvgCd, Data{5}.utotal3, 'v', 'MarkerEdgeColor', 'b', '
          MarkerFaceColor', 'b', 'MarkerSize', Msize)
902     errorbar(Data{7}.AvgReNumber, Data{7}.AvgCd, Data{7}.utotal3, 'o', 'MarkerEdgeColor', 'm', '
          MarkerFaceColor', 'm', 'MarkerSize', Msize)
903     hold off
904     box on
905 %     h_legend = legend(['Standard chassis', 'Chassis cover', 'Full length skirts', 'Partial length
          skirts'], 'Location', 'NorthEastOutside');
906     legend boxoff
907 %     title('Averaged Under Body Data', 'FontSize', Tsize)
908     xlabel('$Re$', 'fontSize', Asize)
909     ylabel('$SC_{d}$', 'fontSize', Asize)
910     xlim([200000 295000])
911     ylim([0.17 0.235])
912     set(gca, 'FontSize', Fsize)
913     set(gca, 'XMinorTick', 'on', 'YMinorTick', 'on')
914     set(gcf, 'Color', 'w');
915     set(gcf, 'Position', [120 140 xPixels yPixels]) %[pos-x pos-y length-x length-y]
916
917     export_fig AutoUnderError -painters -jpg -eps
918 %%
919 figure(112) % Averaged Cd Data for Baseline and Panel Data
920     hold on
921     errorbar(Data{8}.AvgReNumber, Data{8}.AvgCd, Data{8}.utotal3, 'o', 'MarkerEdgeColor', 'k', '
          MarkerFaceColor', 'k', 'MarkerSize', Msize)
922     errorbar(Data{9}.AvgReNumber, Data{9}.AvgCd, Data{9}.utotal3, 's', 'MarkerEdgeColor', 'm', '
          MarkerFaceColor', 'm', 'MarkerSize', Msize)
923     errorbar(Data{10}.AvgReNumber, Data{10}.AvgCd, Data{10}.utotal3, '^', 'MarkerEdgeColor', 'c', '
          MarkerFaceColor', 'c', 'MarkerSize', Msize)
924     errorbar(Data{11}.AvgReNumber, Data{11}.AvgCd, Data{11}.utotal3, '<', 'MarkerEdgeColor', 'r', '
          MarkerFaceColor', 'r', 'MarkerSize', Msize)

```

```

925     errorbar(Data{12}.AvgReNumber, Data{12}.AvgCd, Data{12}.utotal3, 'v', 'MarkerEdgeColor', 'b', '
        MarkerFaceColor', 'b', 'MarkerSize', Msize)
926     errorbar(Data{13}.AvgReNumber, Data{13}.AvgCd, Data{13}.utotal3, '>', 'MarkerEdgeColor', 'g', '
        MarkerFaceColor', 'g', 'MarkerSize', Msize)
927     hold off
928     box on
929 %     h_legend = legend('Industry replica panel', 'Smooth panel', ['Ribbed panel (no holes)', ['
        Panels with 4X larger venting' char(10) 'holes in blocked configuration'], 'Slotted panel', ['
        Panels with 4X larger venting' char(10) 'holes in spaced configuration'], 'Location', '
        NorthEastOutside');
930     legend boxoff
931 %     title('Averaged Panel Data', 'FontSize', Tsize)
932     xlabel('$Re$', 'fontSize', Asize)
933     ylabel('$C_d$', 'fontSize', Asize)
934     xlim([200000 295000])
935     ylim([0.18 0.2175])
936     set(gca, 'FontSize', Fsize)
937     set(gca, 'XMinorTick', 'on', 'YMinorTick', 'on')
938     set(gcf, 'Color', 'w');
939     set(gcf, 'Position', [140 120 xPixels yPixels]) %[pos-x pos-y length-x length-y]
940
941     export_fig AutoPanel -painters -jpg -eps
942 %%
943     figure(113)
944     hold on
945     errorbar(Data{14}.AvgReNumber, Data{14}.AvgCd, Data{14}.utotal3, 'v', 'MarkerEdgeColor', 'c', '
        MarkerFaceColor', 'c', 'MarkerSize', Msize)
946     errorbar(Data{20}.AvgReNumber, Data{20}.AvgCd, Data{20}.utotal3, 's', 'MarkerEdgeColor', 'g', '
        MarkerFaceColor', 'g', 'MarkerSize', Msize)
947     errorbar(Data{19}.AvgReNumber, Data{19}.AvgCd, Data{19}.utotal3, '<', 'MarkerEdgeColor', 'r', '
        MarkerFaceColor', 'r', 'MarkerSize', Msize)
948     errorbar(Data{16}.AvgReNumber, Data{16}.AvgCd, Data{16}.utotal3, '^', 'MarkerEdgeColor', 'm', '
        MarkerFaceColor', 'm', 'MarkerSize', Msize)
949     errorbar(Data{18}.AvgReNumber, Data{18}.AvgCd, Data{18}.utotal3, 'o', 'MarkerEdgeColor', 'b', '
        MarkerFaceColor', 'b', 'MarkerSize', Msize)
950     errorbar(Data{15}.AvgReNumber, Data{15}.AvgCd, Data{15}.utotal3, '>', 'MarkerEdgeColor', 'k', '
        MarkerFaceColor', 'k', 'MarkerSize', Msize)
951 %Template Line     plot(Data{7}.AvgReNumber, Data{7}.AvgCd, 'o', 'MarkerEdgeColor', 'k', '
        MarkerFaceColor', 'k')
952     hold off
953     box on
954 %     h_legend = legend('Baseline', 'Smooth Top', 'Side Panels', ['Side Panels and' char(10) 'Smooth
        Roof'], ['Bottom Cover w/ V-fairing', char(10) 'Side Panels and Smooth Roof'], ['Bottom Cover,
        Side Panels' char(10) 'and Smooth Roof'], 'Location', 'NorthEastOutside');

```

```

955     % h_legend = legend(['Bottom Cover w/ V-faifing ',' char(10) 'Side Panels and Smooth Roof']
          ,['Bottom Cover, Side Panels ' char(10) 'and Smooth Roof'],['Side Panels and' char(10) '
          Smooth Roof'],'Smooth Top','Side Panels ','Baseline ','Location ','NorthEastOutside ');
956 legend boxoff
957 % title('Averaged Panel Data', 'FontSize', Tsize)
958 xlabel('$Re$', 'fontSize', Asize)
959 ylabel('$C_{d}$', 'fontSize', Asize)
960 axis([200000 295000 .115 .25])
961
962 set(gca, 'FontSize', Fsize)
963 set(gca, 'XMinorTick', 'on', 'YMinorTick', 'on')
964 set(gcf, 'Color', 'w');
965 set(gcf, 'Position', [140 120 xPixels yPixels]) %[pos-x pos-y length-x length-y]
966
967 export_fig AutoCompError -painters -jpg -eps
968 %%
969 % ANALYSIS = 1 -> follow Candian National (B term is used)
970 % ANALYSIS = 2 -> follow AAR (B term is assumed negligible)
971 if ANALYSIS ==1
972     % This plot compares the results of the Canadian National, AAR and my
973     % experimental approximation of the Davis equation
974     figure(105)
975     hold on
976     plot(V(1:3:end),RR_can(1:3:end), ':ob', 'MarkerEdgeColor','b', 'MarkerFaceColor','b', 'MarkerSize
          ',8, 'LineWidth',Lwidth-2)
977 % plot(V(1:3:end),RR_aar(1:3:end), ':^r', 'MarkerEdgeColor','r', 'MarkerFaceColor','r', '
          MarkerSize',8, 'LineWidth',Lwidth-2)
978 plot(V(1:3:end),RR_exp(1:3:end), ':sg', 'MarkerEdgeColor','g', 'MarkerFaceColor','g', 'MarkerSize
          ',8, 'LineWidth',Lwidth-2)
979     hold off
980 % h_legend = legend('Canadian National','Association of American Railroads ','Experimental ','
          Location ','NorthWest ');
981 h_legend = legend('Canadian National','Experimental','Location','NorthWest');
982 box on
983 legend boxoff
984 % title('Davis Equation Approximation', 'FontSize', 30)
985 xlabel('Velocity (mph)', 'fontSize', Asize)
986 ylabel('Resistive Force (pounds/ton)', 'fontSize', Asize)
987 axis([0 V(length(V))+2 0 RR_can(length(RR_can))+1])
988
989 % set(gca, 'MarkerFaceColor', 'auto')
990 set(gca, 'FontSize', Fsize)
991 set(gca, 'XMinorTick', 'on', 'YMinorTick', 'on')
992 set(gcf, 'Color', 'w');
993 set(gcf, 'Position', [140 120 xPixels yPixels]) %[pos-x pos-y length-x length-y]

```

```

994
995     export_fig comparison_CN -painters -jpg -eps
996
997     % Plot of the Components of the Davis Equation
998     figure(106)
999     hold on
1000    plot(V(1:3:end),DataOut{1}.AATotal(1:3:end,1),'og','MarkerEdgeColor','g','MarkerFaceColor','
1001           g','MarkerSize',8,'LineWidth',Lwidth-2)
1002    plot(V(1:3:end),DataOut{1}.BATotal(1:3:end,1),'sr','MarkerEdgeColor','r','MarkerFaceColor','
1003           r','MarkerSize',8,'LineWidth',Lwidth-2)
1004    plot(V(1:3:end),DataOut{1}.CATotal(1:3:end,1),'^b','MarkerEdgeColor','b','MarkerFaceColor','
1005           b','MarkerSize',8,'LineWidth',Lwidth-2)
1006    plot(V(1:3:end),DataOut{1}.AATotal(1:3:end,1)+DataOut{1}.BATotal(1:3:end,1),'>m','
1007           MarkerEdgeColor','m','MarkerFaceColor','m','MarkerSize',8,'LineWidth',Lwidth-2)
1008    % plot(V(1:3:end),DataOut{1}.AATotal(1:3:end,1)+DataOut{1}.CATotal(1:3:end,1),'^b','
1009           MarkerEdgeColor','b','MarkerFaceColor','b','MarkerSize',8,'LineWidth',Lwidth-2)
1010    plot(V(1:3:end),DataOut{1}.BATotal(1:3:end,1)+DataOut{1}.CATotal(1:3:end,1),'vc','
1011           MarkerEdgeColor','c','MarkerFaceColor','c','MarkerSize',8,'LineWidth',Lwidth-2)
1012
1013    % h_legend = legend('A','B','C','A+B','A+C','B+C','Location','NorthWest');
1014    h_legend = legend('A','B','C','A+B','B+C','Location','NorthWest');
1015    legend boxoff
1016    box on
1017    hold off
1018    % title('Davis Equation Components','FontSize',30)
1019    xlabel('Velocity (mph)','fontSize',Asize)
1020    ylabel('Force (pounds/ton)','fontSize',Asize)
1021
1022    set(gca,'FontSize',Fsize)
1023    set(gca,'XMinorTick','on','YMinorTick','on')
1024    set(gcf,'Color','w');
1025    set(gcf,'Position',[140 120 xPixels yPixels]) %[pos-x pos-y length-x length-y]
1026
1027    export_fig DavisComponents -painters -jpg -eps
1028
1029    figure(109)
1030    hold on
1031    plot(V,DataOut{1}.AATotal(:,1)./DataOut{1}.RA(:,1),'og','MarkerEdgeColor','g','
1032           MarkerFaceColor','g','MarkerSize',8,'LineWidth',Lwidth-2)
1033    plot(V,DataOut{1}.BATotal(:,1)./DataOut{1}.RA(:,1),'ob','MarkerEdgeColor','b','
1034           MarkerFaceColor','b','MarkerSize',8,'LineWidth',Lwidth-2)
1035    plot(V,DataOut{1}.CATotal(:,1)./DataOut{1}.RA(:,1),'or','MarkerEdgeColor','r','
1036           MarkerFaceColor','r','MarkerSize',8,'LineWidth',Lwidth-2)
1037    % h_legend = legend('A','B','C','Location','NorthEast');
1038    legend boxoff

```



```

1030     box on
1031     hold off
1032     % title('Contribution of Aerodynamics to the Total Force', 'FontSize', 30)
1033     xlabel('Velocity (mph)', 'fontsize', Asize)
1034     ylabel('\% Total', 'fontsize', Asize)
1035
1036     set(gca, 'FontSize', Fsize)
1037     set(gca, 'XMinorTick', 'on', 'YMinorTick', 'on')
1038     set(gcf, 'Color', 'w');
1039     set(gcf, 'Position', [140 120 xPixels yPixels]) %[pos-x pos-y length-x length-y]
1040
1041     export_fig CvsTotal -painters -jpg -eps
1042
1043 else
1044     % This plot compares the results of the Canadian National, AAR and my
1045     % experimental approximation of the Davis equation
1046     figure(105)
1047     hold on
1048     % plot(V(1:3:end), RR_can(1:3:end), ':ob', 'MarkerEdgeColor', 'b', 'MarkerFaceColor', 'b', '
1049     % MarkerSize', 8, 'LineWidth', Lwidth-2)
1050     plot(V(1:3:end), RR_aar(1:3:end), '^r', 'MarkerEdgeColor', 'r', 'MarkerFaceColor', 'r', 'MarkerSize
1051     % ', 8, 'LineWidth', Lwidth-2)
1052     plot(V(1:3:end), RR_exp(1:3:end), ':sg', 'MarkerEdgeColor', 'g', 'MarkerFaceColor', 'g', 'MarkerSize
1053     % ', 8, 'LineWidth', Lwidth-2)
1054     hold off
1055     % h_legend = legend('Canadian National', 'Association of American Railroads', 'Experimental', '
1056     % Location', 'NorthWest');
1057     h_legend = legend('Association of American Railroads', 'Experimental', 'Location', 'NorthWest');
1058     box on
1059     legend boxoff
1060     % title('Davis Equation Approximation', 'FontSize', 30)
1061     xlabel('Velocity (mph)', 'fontsize', Asize)
1062     ylabel('Resistive Force (pounds/ton)', 'fontsize', Asize)
1063     axis([0 V(length(V))+2 0 RR_can(length(RR_can))+1])
1064
1065     set(gca, 'FontSize', Fsize)
1066     set(gca, 'XMinorTick', 'on', 'YMinorTick', 'on')
1067     set(gcf, 'Color', 'w');
1068     set(gcf, 'Position', [140 120 xPixels yPixels]) %[pos-x pos-y length-x length-y]
1069
1070     export_fig comparison_AAR -painters -jpg -eps
1071 end
1072
1073 %%
1074 % The plot is a zoomed in view of the N8 and N7 throttle settings, the

```

```

1071 % intersect with the davis equation and the vertical approximation line.
1072 figure(107)
1073 hold on
1074 plot(V,Nana(:,1),V,Nana(:,2),V,Nana(:,3),V,Nana(:,4),V,Nana(:,5),V,Nana(:,6),V,Nana(:,7),V,
      Nana(:,8),V, Davis{1}.RTotallbs,V, Davis{2}.RTotallbs,V, Davis{4}.RTotallbs,'MarkerSize'
      ,15,'LineWidth',4)
1075 h_legend = legend('N1','N2','N3','N4','N5','N6','N7','N8','Corrugated','Smooth w/o Lip','
      Smooth w/ Lip','Location','NorthEast');
1076 for i = 1:ThrottleSet
1077     plot(Analysis{i}.V_Corr1,Analysis{i}.VerticalLine1,'k','LineWidth',2)
1078 end
1079 box on
1080 legend boxoff
1081 % title('Tractive Force vs Pulling Resistance','FontSize',30)
1082 xlabel('Speed (mph)','fontSize',26)
1083 ylabel('Force (pounds)','fontSize',26)
1084 rectangle('Position',[Data{1}.XIntercept(7)-3,Data{1}.YIntercept(8)-15000,Data{1}.XIntercept
      (8)+3-Data{1}.XIntercept(7)+3,(Data{1}.YIntercept(8)+10000)-(Data{1}.YIntercept(8)
      -15000)],'LineWidth',2)
1085 axis([0 90 0 150000])
1086 set(gca,'FontSize',20)
1087 set(gca,'XMinorTick','on','YMinorTick','on')
1088 set(h_legend,'FontSize',24)
1089 set(gcf,'Color','w');
1090 set(gcf,'Position',[260 120 xPixels yPixels]) %[pos-x pos-y length-x length-y]
1091 hold off
1092
1093 export_fig fuelconsump -painters -jpg -eps
1094 %%
1095 % The plot is a zoomed in view of the N8 and N7 throttle settings, the
1096 % intersect with the davis equation and the vertical approximation line.
1097 figure(108)
1098 set(gcf,'DefaultAxesColorOrder',colors(6:end,:))
1099 hold on
1100 plot(V,Nana(:,6),V,Nana(:,7),V,Nana(:,8),V, Davis{1}.RTotallbs,V, Davis{2}.RTotallbs,V, Davis
      {4}.RTotallbs,'MarkerSize',15,'LineWidth',4)
1101 h_legend = legend('N6','N7','N8','Corrugated','Smooth w/o Lip','Smooth w/ Lip','Location','
      NorthEast');
1102 for i = 1:ThrottleSet
1103     plot(Analysis{i}.V_Corr1,Analysis{i}.VerticalLine1,'k','LineWidth',2)
1104 end
1105 box on
1106 legend boxoff
1107 % title('Tractive Force vs Pulling Resistance','FontSize',30)
1108 xlabel('Speed (mph)','fontSize',26)

```

```

1109 ylabel('Force (pounds)', 'fontsize', 26)
1110 axis([Data{1}.XIntercept(7)-3 Data{1}.XIntercept(8)+3 Data{1}.YIntercept(8)-15000 Data{1}.
      YIntercept(8)+10000])
1111 set(gca, 'FontSize', 20)
1112 set(gca, 'XMinorTick', 'on', 'YMinorTick', 'on')
1113 set(h_legend, 'FontSize', 24)
1114 set(gcf, 'Color', 'w');
1115 set(gcf, 'Position', [260 120 xPixels yPixels]) %[pos-x pos-y length-x length-y]
1116
1117 hold off
1118
1119 export_fig fuelconsumpzoom -painters -jpg -eps
1120
1121 %%
1122 % The plot shows the tractive curve vs. resistance curves of roof data
1123
1124 figure(108)
1125 hold on
1126 plot(V, Nana(:, 1), V, Nana(:, 2), V, Nana(:, 3), V, Nana(:, 4), V, Nana(:, 5), V, Nana(:, 6), V, Nana(:, 7), V,
      Nana(:, 8), V, Davis{1}.RTotallbs, V, Davis{2}.RTotallbs, V, Davis{4}.RTotallbs, 'MarkerSize'
      , 15, 'LineWidth', 4)
1127 h_legend = legend('N1', 'N2', 'N3', 'N4', 'N5', 'N6', 'N7', 'N8', 'Corrugated', 'Smooth w/o Lip', '
      Smooth w/ Lip', 'Location', 'NorthEast');
1128 for i = 1:ThrottleSet
1129     plot(Analysis{i}.V_Corr1, Analysis{i}.VerticalLine1, 'k', 'LineWidth', 2)
1130 end
1131 box on
1132 legend boxoff
1133 % title('Tractive Force vs Pulling Resistance', 'FontSize', 30)
1134 xlabel('Speed (mph)', 'fontsize', 26)
1135 ylabel('Force (pounds)', 'fontsize', 26)
1136 axis([0 85 0 150000])
1137 set(gca, 'FontSize', 20)
1138 set(gca, 'XMinorTick', 'on', 'YMinorTick', 'on')
1139 set(h_legend, 'FontSize', 24)
1140 set(gcf, 'Color', 'w');
1141 set(gcf, 'Position', [260 120 xPixels yPixels]) %[pos-x pos-y length-x length-y]
1142 hold off
1143
1144 export_fig fuelconsumpDefense -painters -jpg -eps
1145 end

```